CHEMICAL REVIEWS

Review

pubs.acs.org/CR

Doped Organic Transistors

Björn Lüssem,*[,†] Chang-Min Keum,[†] Daniel Kasemann,[‡] Ben Naab,[§,∥] Zhenan Bao,[§] and Karl Leo*[,‡]

[†]Department of Physics, Kent State University, Kent, Ohio 44242, United States

[‡]Institut für Angewandte Photophysik, TU Dresden, 01069 Dresden, Germany

[§]Department of Chemical Engineering, Stanford University, Stanford, California 94305, United States

ABSTRACT: Organic field-effect transistors hold the promise of enabling low-cost and flexible electronics. Following its success in organic optoelectronics, the organic doping technology is also used increasingly in organic field-effect transistors. Doping not only increases device performance, but it also provides a way to fine-control the transistor behavior, to develop new transistor concepts, and even improve the stability of organic transistors. This Review summarizes the latest progress made in the understanding of the doping technology and its application to organic transistors. It presents the most successful doping models and an overview of the wide variety of materials used as dopants. Further, the influence of doping on charge transport in the most relevant polycrystalline organic semiconductors is reviewed, and a concise overview on the influence of doping on transistor behavior and performance is given. In particular, recent progress in the understanding of contact doping and channel doping is summarized.

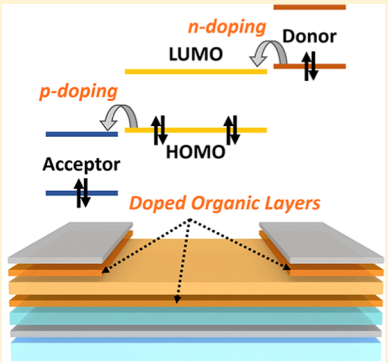

Downloaded via 63.147.34.5 on September 24, 2024 at 18:55:24 (UTC).
See https://pubs.acs.org/sharingguidelines for options on how to legitimately share published articles.

CONTENTS

1. Introduction 13714
2. Physics of Doping 13715
2.1. Thermal Activation of Organic Doping 13715
2.2. Charge Carrier Statistics in Doped Organic Layers 13716
2.3. Doping Efficiency 13718
3. Chemistry of Dopants 13718
3.1. p-Dopants 13718
3.1.1. Elemental Species 13719
3.1.2. Covalent Solids 13719
3.1.3. Brønsted and Lewis Acids 13719
3.1.4. Small Molecules 13719
3.2. n-Dopants 13720
3.2.1. Elemental Dopants 13720
3.2.2. Inorganic Salts 13720
3.2.3. Low Ionization Potential Donors 13720
3.2.4. Organic Salts 13720
3.2.5. Hydrides 13721
3.2.6. Anion Doping 13721
3.2.7. Dimers 13722
4. Doping of Polycrystalline Organic Semiconductors 13723
4.1. Doping of P3HT 13723
4.2. Doping of Pentacene 13724
4.2.1. p-Doping of Pentacene by Iodine 13724
4.2.2. p-Doping of Pentacene by Molecular Dopants 13725
4.2.3. p-Doping of Pentacene by Transition Metal Oxides 13726
4.2.4. n-Doping of Pentacene 13726
4.3. Doping of Fullerene C_{60} 13727
4.4. Doping Other Organic Semiconductors with High Charge Carrier Mobility 13728
5. Doped Organic Transistors 13728
5.1. Contact Doping 13729
5.1.1. Contact Resistance 13729
5.1.2. Quasi-Ohmic Contacts Realized by Doping 13732
5.1.3. Contact Doping for p-Type Transistors 13732
5.1.4. Contact Doping for n-Type Transistors 13734
5.2. Channel Doping 13735
5.2.1. Doped Organic MIS Junctions 13735
5.2.2. Doped Organic Transistors 13737
5.2.3. Majority and Minority Charge Carriers in Doped Transistors 13741
6. Outlook and Conclusions 13741
Author Information 13742
Corresponding Authors 13742
Present Address 13742
Notes 13742
Biographies 13742
Acknowledgments 13743
References 13743

1. INTRODUCTION

The advent of microelectronics has changed our everyday life. The key element is the field effect transistor, which was introduced in the early 1960s. In the city of Dresden, the largest microelectronics center in Europe, more than a million transistors are produced everyday, per human being on earth!

Received: May 25, 2016
Published: October 4, 2016

ACS Publications © 2016 American Chemical Society

DOI: 10.1021/acs.chemrev.6b00329
Chem. Rev. 2016, 116, 13714−13751

Pictiva EX2009
Samsung v Pictiva
IPR2026-00129

Current microelectronics technology is almost exclusively based on the technology of single crystalline silicon. While the technology has been scaled over many orders of magnitude to reach highest performance in speed, cost, and power reduction, there are many novel applications where this technology is less suited because properties like large-area, flexibility, and easy processing, for example, by printing, would be required.

Here, organic electronics might come into play as a new paradigm: Organic electronics is based almost entirely on carbon, can be deposited by simple fabrication at low temperatures on almost any substrate, including flexible and transparent materials, and offers a wide variety of functions, from switching over memory, light emission and absorption, to sensorics. The main drawback is that organic semiconductors are characterized by much lower mobilities than silicon and other crystalline inorganic semiconductors, thus limiting speed and current driving possibilities. Because of these properties, organic electronics will not compete with, but complement, silicon-based electronics in the future.

The key devices like organic field-effect transistor (OFET), organic light-emitting diode (OLED), and organic solar cell (OSC) were all first presented in the 1900s. At the time when this Review was written, OLEDs have already reached a multibillion US$ market as small displays, mainly used in smart phone displays, and are rapidly entering the TV market. Lighting based on white OLED and OSC is making the first steps into markets, while organic transistors have so far not reached the performance required for broad application in products, although they might have the highest market potential of all organic electronics devices.

When comparing the development of organic electronics with classical silicon electronics, one surprising observation is that doping, that is, the addition of impurities to control the Fermi level and raise the conductivity, was initially almost completely disregarded in organics. Typically, organic materials have rather large impurity concentrations, which, in association with usually larger gaps on the order of 2 eV, make it highly unlikely that they are intrinsic and that the Fermi level is positioned in the center of the gap. Nevertheless, there are only a few publications that consider the doping of organics from the early days of organic electronics. For instance, Yamamoto et al. used oxidizing gases such as iodine or bromine vapor to dope phthalocyanines.[1] Although this leads to a doping effect, the films such prepared are not stable.

The same material was also doped with organic acceptor molecules such as *ortho*-chloranil,[2] tetracyano-quinodimethane (TCNQ), or dicyano-dichloro-quinone (DDQ),[3,4] which produces more stable doping. Covalently bound stacked phthalocyanines[5] and oligothiophenes[6] were doped by DDQ, which is a rather effective dopant but has low thermal stability.

The importance of doping became obvious when highly efficient and stable doping was reported,[7] combined with the application in OLEDs,[8] where the p-doped hole transport layers led to significantly reduced operating voltages. Since then, the technique has been widely extended and refined and is today in broad commercial application as almost all commercially available OLED displays contain transport layers, which employ controlled doping. Similarly, dopants are applied in highly efficient white OLEDs for lighting applications[9] and OSCs, where the most efficient devices presented so far use doping techniques.[10,11]

The main effects that have made doping successful in organic devices are 2-fold:

First, doped layers have much higher conductivity, which reduces bulk Ohmic losses and allows thicker transport layers important for optical optimization and shortcut avoidance.

Second, doped layers create thin space charge layers at contacts, allowing efficient contacts even in case of electronic barriers due to work function mismatch.[12]

Naturally, one might ask whether the positive effects of doping also apply to the organic device class, which showed the least impact so far, organic transistors. Indeed, it has been shown that doping is improving the performance of organic transistors (see, e.g., refs 13−20), can be used to fine-tune transistor behavior,[21−24] and increases the stability of OFETs.[25,26]

In this Review, we discuss the recent progress of the application of doping in organic transistors in detail. After a short summary of different doping models, we discuss the chemistry and synthesis of dopants. Furthermore, we address the doping of polycrystalline materials with higher mobility and finally the device application in doped organic transistors.

2. PHYSICS OF DOPING

Organic doping resembles doping in inorganic semiconductors in many aspects. An impurity is added to a host material, which either donates an electron to the host (n-doping) or accepts an electron from the host, leaving a hole behind (p-doping).

Doped organic films can be processed either by coevaporation of host and dopant in a vacuum,[7] by adding a defined impurity into a solution of the host semiconductor and process the film wet-chemically, for example, by spin-coating,[27] or by exposing the semiconducting film or crystal to a gas of the dopant.[1]

Despite the ease of processing, the details of the organic doping process are surprisingly complex and still not understood in its entirety. Only recently has significant progress been made that allowed one to describe doping consistently over a wide range of doping concentrations. In the following, this progress is summarized, which will provide a starting point for the discussion of doping in organic transistors.

2.1. Thermal Activation of Organic Doping

In the most intuitive understanding of doping, an integer number of electrons is transferred from the host to the dopant (p-doping) or from the dopant to the host (n-doping).[7,28−33] To make this transfer efficient, the electron affinity (EA) of the dopant has to exceed the ionization potential (IP) of the host (p-doping), or the IP of the dopant has to be smaller than the EA of the host (n-doping) (see Figure 1). It has to be noted that the IE and EA have to be measured in the solid state, which are usually smaller than the energy levels in the gas phase.

However, this simplified understanding of doping does not fully capture the doping process. For example, although the EA of the popular p-dopant 2,2′-(perfluoronaphthalene-2,6-diylidene)dimalononitrile (F_6-TCNNQ) (EA ≈ 5.07 eV) and the IP of the hole transport material *N*,*N*,*N*′,*N*′-tetrakis(4-methoxyphenyl)-benzidine (MeO-TPD) (IP ≈ 5 eV) almost match, electron transfer between host and dopant is not spontaneous, but shows a significant activation energy of $E_A \approx 0.46$ eV;[35] that is, additional energy has to be supplied to generate a free hole in the Meo-TPD matrix.

Several explanations have been put forward to explain the origin of the activation energy. Often, it is argued that the activation energy reflects the low permittivity of the organic

DOI: 10.1021/acs.chemrev.6b00329
Chem. Rev. 2016, 116, 13714−13751

Pictiva EX2009
Samsung v Pictiva
IPR2026-00129

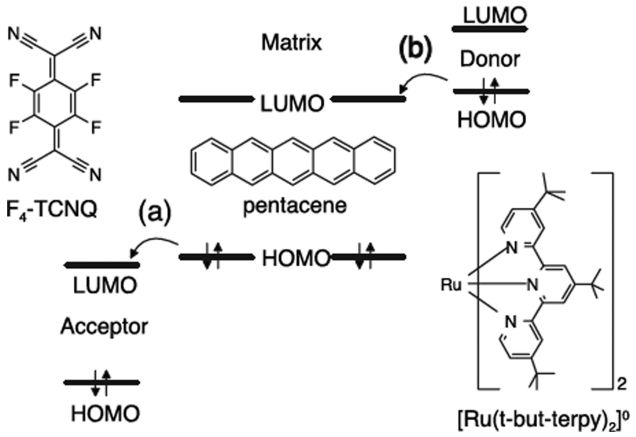

Figure 1. Simplified model of the organic doping process exemplified by the organic semiconductor pentacene doped with F_4-TCNQ (p-doping) or $[Ru(t\text{-but-terpy})_2]^0$ (n-doping). Free charge carriers are generated by an electron transfer between dopant and matrix molecule. To facilitate electron transfer, the LUMO of the p-dopant has to be lower than the HOMO of the matrix molecule (for p-doping, left), or the HOMO of the n-dopant has to exceed the LUMO of the matrix molecule (for n-doping, right). Reprinted with permission from ref 34. Copyright 2008 American Physical Society.

semiconductors, which leads to large Coulomb interactions between charge carriers and ionized dopant molecules.[36,37] Even if electron transfer between host and dopant is efficient, the transferred charge carrier still experiences a strong electrostatic attraction to the ionized dopant molecule. A charge transfer complex is formed between the host and the dopant, which has to be dissociated before a free electron or a free hole is generated. In fact, this understanding of the doping process is corroborated by scanning tunneling microscopy (STM) studies of Ha et al.,[38] who studied doping of pentacene by the p-dopant tetrafluoro-tetracyano-quinodimethane (F_4-TCNQ). They observe a cloud of positive charge around ionized dopant molecules, which they interpret in terms of a localization of the donated hole by the Coulomb potential of the ionized dopant.

The electrostatic attraction between the ionized dopant molecule and the hole or electron transferred to a neighboring molecule can be significant. Mityashin et al. even argued that in perfect organic crystals, the binding energy of this charge pair is too large to be overcome by thermal excitation, which means that it is highly improbable that free charge carriers are generated at all.[36] To explain doping observed at room temperature, they showed that the dissociation probability of the charge pair is increased due to increased disorder in the energy landscape at higher doping concentrations. Because of increasing disorder, more percolation paths are opened along which the hole on the matrix can escape the Coulomb attraction of the dopant.

A slightly different approach to explain doping was proposed recently by the Koch group.[39−41] It is argued that the simplified model of doping shown in Figure 1 implies that an integer number of charges is transferred between dopant and matrix, which might not be the case for all host and dopant combinations. In fact, charge transfer complexes formed during doping can be held together by both ionic and covalent contributions.[42] Integer charge transfer is assumed to take place if charge transfer complexes have mostly ionic character, which is often observed if the donor highest occupied molecular orbital (HOMO) is substantially higher in energy than the acceptor lowest unoccupied molecular orbital (LUMO).[43,44]

In contrast, charge transfer states arising from interactions where the donor HOMO is near or lower in energy than the acceptor LUMO will have a more covalent character and will involve significant hybridization of the donor and acceptor orbitals.[41] Salzmann et al.[39] proposed that these hybrid states formed by coupling the HOMO of the matrix and the LUMO of the dopant (for p-doping) are dominating doping. A bonding and an antibonding state are formed (see Figure 2). While the

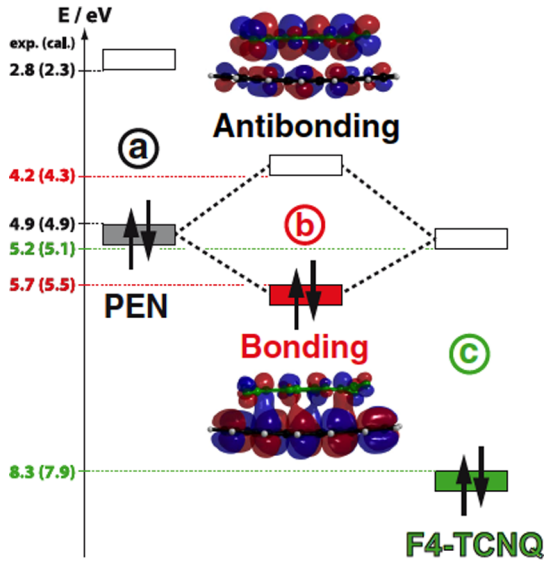

Figure 2. Doping via hybrid states. Instead of assuming an integer charge transfer between dopant and matrix, some authors argue that a hybrid state is formed by coupling the HOMO of the matrix and the LUMO of the dopant. The activation energy observed in experiments is reflected by the difference between the antibonding orbital of the hybrid state and the HOMO state of the host. In the figure, the model is sketched for the example of doping pentacene by F_4-TCNQ. Reprinted with permission from ref 39. Copyright 2012 American Physical Society.

bonding state of the hybrid is fully occupied by electrons, the antibonding state is located in the energy gap of the matrix and almost empty. However, due to thermal excitation, some electrons can be excited from the HOMO of the matrix to the antibonding state of the hybrid, leaving behind a hole on the matrix.[45]

Assuming partial charge transfer and the formation of a hybrid dopant/matrix complex, the activation energy for the doping process is given by the difference between the antibonding state of the hybrid and the HOMO of the matrix (for p-doping). This activation energy E_A can be approximated as[40,41]

$$E_A = \frac{H_M - L_D}{2}\left[1 + \sqrt{1 + \frac{4\beta^2}{(H_M - L_D)^2}}\right] \quad (1)$$

where H_M is the HOMO energy of the matrix, L_D is the LUMO energy of the dopant, and β is the resonance integral between the HOMO of the matrix and the LUMO of the dopant.

2.2. Charge Carrier Statistics in Doped Organic Layers

Regardless of the microscopic details of the doping process and the origin of its activation energy, a straightforward statistical

DOI: 10.1021/acs.chemrev.6b00329
Chem. Rev. 2016, 116, 13714−13751

Pictiva EX2009
Samsung v Pictiva
IPR2026-00129

model capable of describing the doping process over a wide range of doping concentrations and for different host/matrix was proposed recently.[35,46,47]

In the model, the charge neutrality equation for a p-doped semiconductor is solved self-consistently. To obtain a good agreement with experiments, trap states had to be included. The charge neutrality equation reads:

$$p + N_T^+ = n + N_A^- \approx N_A^- \tag{2}$$

where p is the density of free holes, N_T^+ is the density of positively charged traps, n is the density of electrons, and N_A^- is the density of ionized dopant molecules.

The density of free holes, p, and the density of charged trap states, N_T^+, obey the Fermi−Dirac integrals:

$$p = \int_{-\infty}^{\infty} \mathrm{d}E\, g_{\mathrm{DOS}}(E)[1 - f(E)] \tag{3}$$

$$N_T^+ = \int_{-\infty}^{\infty} \mathrm{d}E\, g_T(E)[1 - f(E)] \tag{4}$$

Here, $f(E)$ is the Fermi−Dirac distribution, $g_{\mathrm{DOS}}(E)$ is the density of mobile states in the HOMO of the matrix, and $g_T(E)$ is the density of trap states. A Gaussian distribution g_{DOS} is assumed, sometimes modified by an exponential tail.[35,46]

Finally, the doping process itself is described by thermal activation of the doped charge carrier from a discrete doping level at E_A toward an effective transport level in the HOMO density of states (DOS). The density of ionized dopants N_A^- thus reads:

$$N_A^- = \frac{N_A}{1 + \exp[(E_A - E_F)/k_B T]} \tag{5}$$

where N_A is the density of dopant molecules in the film, E_F is the Fermi level, k_B is the Boltzmann constant, and T is the temperature.

Representative results of this model are shown as solid lines in Figure 3. The model is used to determine the Fermi level position in the amorphous organic semiconductor MeO-TPD, which is a standard hole transport material,[48] doped by the p-dopant fluorinated fullerene $C_{60}F_{36}$[49,50] at various doping concentrations.

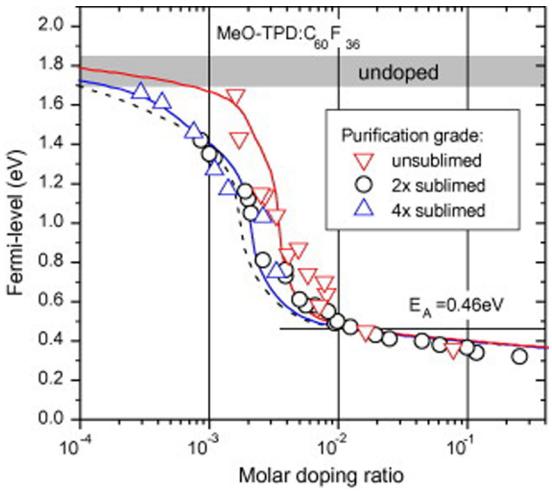

Figure 3. Shift of the Fermi level in the hole transport material MeO-TPD upon doping by $C_{60}F_{36}$. Different grades of MeO-TPD are compared (used as received, purified by two sublimation cycles, purified by four sublimation cycles). The model calculations (lines) fit the measurements (open symbols) well. Reprinted with permission from ref 46. Copyright 2013 Elsevier.

In Figure 3 is compared the calculated Fermi level position to the experimental Fermi level position obtained by photoelectron spectroscopy[35,46] (symbols). The Fermi level is plotted with respect to the HOMO position of MeO-TPD; that is, the HOMO position is set to 0 eV. Different purities of MeO-TPD are used: as received (red), purified twice (black), or purified four times (blue) by sublimation. Overall, an excellent agreement between the model and experimental data is found. Similar calculations were as well reported by Salzman et al. in 2015 for quaterthiophene doped by F_4-TCNQ.[45]

The numerical model can be used to study the details of the doping process. The results of these studies are sketched in Figure 4. At low doping concentrations, doping only fills trap states in the organic semiconductor, and no free charge carriers are generated[35,51,52] (see Figure 4 for $N_A < N_T$). Consequently, the Fermi level is pinned at the trap level. Once the doping concentration exceeds the trap density (see Figure 4 for $N_A > N_T$), free holes are generated in the HOMO of MeO-TPD, and the Fermi level shifts rapidly toward the HOMO at 0 eV. As expected, complete filling of all traps and the rapid shift of the Fermi level toward the HOMO occur earlier for highly purified materials (blue and black lines in Figure 3) as in materials with a lower purity (red line), indicating the lower trap density in purified MeO-TPD.

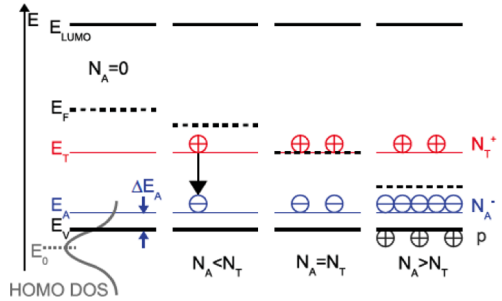

Figure 4. Simplified model to explain the complex shift of Fermi level position in MeO-TPD observed in Figure 3. At low concentrations, all donated holes are trapped by charge traps in MeO-TPD, and no free charge carriers are generated. Once all traps are filled, the Fermi level shifts rapidly toward the HOMO. Reprinted with permission from ref 35. Copyright 2012 American Physical Society.

Finally, the shift of the Fermi level saturates at high doping concentrations. Again, this behavior can be understood by the detailed charge carrier statistics as described by the above equations. The HOMO of the organic matrix material is approximated by a Gaussian DOS. Therefore, there is a significant DOS tailing into the gap of the matrix material, which pins the Fermi level close to the transport states in the HOMO.

The same model can be used to study doping in polycrystalline materials as well. For example, in Figure 5 is plotted the Fermi level shift in the polycrystalline material ZnPc doped by F_6-TCNNQ (p-doping) or tetrakis(1,3,4,6,7,8-hexahydro-2*H*-pyrimido[1,2-*a*]pyrimidinato)ditungsten(II) ($W_2(hpp)_4$) (n-doping) versus the doping concentration. Furthermore, the shift of the Fermi level in pentacene upon p-doping by $C_{60}F_{36}$ and n-type doping by $W_2(hpp)_4$ is shown in Figure 6. In both cases, the experimental data obtained by

DOI: 10.1021/acs.chemrev.6b00329
Chem. Rev. 2016, 116, 13714−13751
Pictiva EX2009
Samsung v Pictiva
IPR2026-00129

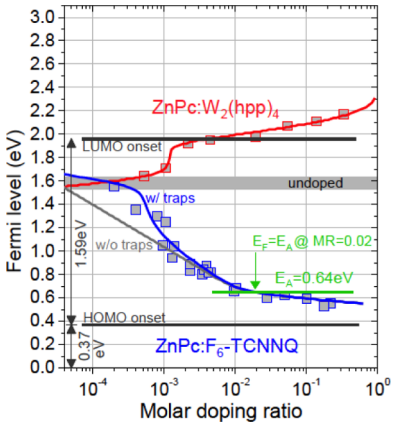

Figure 5. The p- and n-type doping of the polycrystalline material ZnPc. The model discussed in section 2.2 (solid lines) reproduces the experimental data (squares) well. Reprinted with permission from ref 47. Copyright 2015 John Wiley and Sons.

ultraviolet photoelectron spectroscopy (UPS) (symbols) agree well with the model calculation (solid lines).

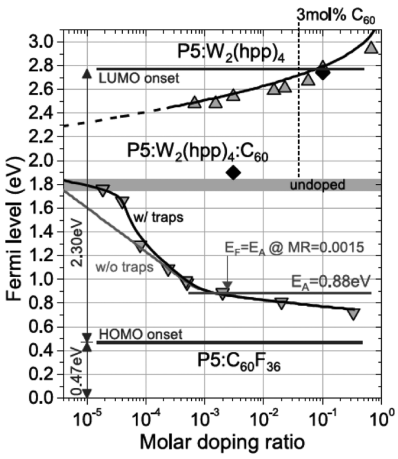

Figure 6. Shift of the Fermi level in pentacene upon p- and n-type doping. Symbols denote UPS measurements, whereas the lines are obtained by calculations. Different doping regimes are observed for p-doping: trap-limited regime at low concentrations, saturation regime at intermediate concentrations, and impurity reserve regime at large doping concentrations. The shift of the Fermi level upon n-doping is stronger and does not saturate close to the LUMO energy. Reprinted with permission from ref 47. Copyright 2015 John Wiley and Sons.

Several different doping regimes can be identified for p-doping ZnPc and pentacene. Similar to the results of the amorphous material MeO-TPD discussed above (Figures 3 and 4), doping fills almost exclusively traps at low concentrations (below 4×10^{-5} for pentacene), and the Fermi level is pinned close to the midbandgap position (trap-limited regime). At medium concentrations ($8 \times 10^{-5} < c < 10^{-3}$ for pentacene), most traps are filled, and the Fermi level shifts rapidly toward the HOMO. Still, the Fermi level is located above the activation energy of the dopant, and, as will be discussed in the next section, most dopants are activated. This regime therefore resembles the saturation regime observed in inorganic semiconductors.[47]

At a molar doping ratio of 1.5×10^{-3}, the Fermi level finally crosses the activation level of the dopant before its position finally saturates close to the HOMO. Thus, at these high doping concentrations, the Fermi level is situated between the dopant level and the HOMO. Statistically, not all dopants are activated, which is known as the impurity reserve regime in inorganic semiconductors.

2.3. Doping Efficiency

In recent publications, the doping efficiency (i.e., the ratio of the number of free charge carriers to the number of dopant molecules) was discussed controversially. Although early observations showed a nearly full transfer of charges from the dopant to the matrix molecule,[32] this does not necessarily mean that these charge carriers are free and contribute to the current flow. In later experiments, the number of free charge carriers and the actual doping efficiency were determined.[27,53−60] Surprisingly, in most reports, the doping efficiency is only on the order of 10% (16% for an n-doped system,[53] 4% for p-type doping using F_4-TCNQ,[54] and less than 2% for oxide based dopants (molybdenum trioxide (MoO_3))[58]). However, some reports show a higher doping efficiency,[56] in particular at very low doping concentrations.[61]

Several explanations for the relatively low doping efficiency have been put forward. Clustering of dopant molecules was observed for transition metal oxides,[30,55,58] and it was argued that the doping efficiency is given by a product of the dispersion efficiency and the efficiency of forming the dopant/matrix pair to form a charge transfer complex.[62,63] Furthermore, the doping efficiency can be limited by intrinsic charge carrier traps as discussed above,[46,52] or, as discussed above as well, the large dopant activation energy[63] caused by either strong Coulomb interaction[35,36] or a strong hybridization of dopant and matrix molecule.[40]

Another explanation adding to the limited doping efficiency was proposed recently.[47] It was pointed out that doped organic semiconductors usually show a significant activation energy, and furthermore relatively high doping concentrations (several wt %) are used in most organic devices. Hence, as discussed above, organic doping is used in the "freeze-out" or impurity reserve regime, where only a fraction of available dopants are thermally activated.[47] If the doping concentration is reduced, that is, if the semiconductor is studied in the saturation regime, higher doping efficiencies can be obtained. For example, Pahner et al. were able to show that the p-doping efficiency in pentacene is very high and reaches almost unity (Figure 7).[61] However, the doping efficiency drops rapidly for increasing doping concentrations, that is, if the semiconductor is operated in the impurity reserve regime.

3. CHEMISTRY OF DOPANTS

This section will briefly survey and compare the major classes of p- and n-dopants commonly used in organic semiconductors. For both the p- and the n-doping sections, the classification of dopants was driven in part by mechanistic or structural similarities, but it should also be recognized that this classification was predominantly used to simplify the discussion of an extremely diverse group of chemicals. There are many distinctions in the reaction pathways possible for each of the dopants within a class and even for the same dopant with different hosts.

3.1. p-Dopants

p-Dopants can be classified into several groups including small molecules, polyelectrolytes, covalent solids, Brønsted and Lewis acids, and elemental species. Undoubtedly, some dopants could

DOI: 10.1021/acs.chemrev.6b00329
Chem. Rev. 2016, 116, 13714−13751

Pictiva EX2009
Samsung v Pictiva
IPR2026-00129

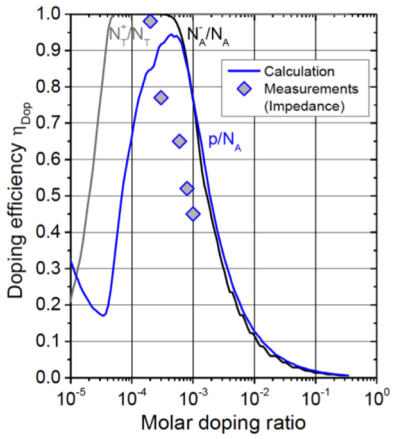

Figure 7. Efficiency of p-doping in pentacene. At low concentrations, the doping efficiency increases strongly to almost 100%. Reprinted with permission from ref 47. Copyright 2015 John Wiley and Sons.

be categorized into more than one of these groups, but for the purpose of this section these groupings will be employed.

3.1.1. Elemental Species. The following diatomics have all been recognized as p-dopants for organic semiconductors: I_2, Br_2, Cl_2, and O_2.[64] The doping of polyacetylene by chlorine, bromine, and iodine is an early example of p-doping a conjugated polymer.[65] In addition to polyacetylene doping, iodine has been used to dope pentacene, phthalocyanines, and polythiophenes, among others.[66,67] The halogens, especially iodine, can form polyanions, which further complicates their interaction with hosts.[66]

Oxygen is predominantly introduced as a contaminant upon incidental exposure to air. Exposure to oxygen is known to p-dope some organic semiconductors.[68] At least in the case of polythiophenes, it is plausible that oxygen doping occurs by a dative bond between sulfur lone pairs and the dioxygen singly occupied molecular orbital (SOMO), or by photoinduced doping from singlet oxygen.[69,70]

3.1.2. Covalent Solids. Examples of metal oxide p-dopants include MoO_3, V_2O_5, WO_3, ReO_3, and Fe_3O_4.[59,71−77]

The electron affinity of metal oxide dopants depends on the processing conditions employed, and it is well-known that their electron affinity can decrease by as much as 1 eV upon air-exposure.[78] The most commonly used metal oxide dopant is MoO_3 because it is evaporated at relatively low temperatures and can be deposited from a crucible (∼400 °C). The evaporation temperatures of V_2O_5 and WO_3 are much higher, which leads to oxygen release and substantial heating of the substrate to be coated. Sol−gel processing of metal oxides can be used to circumvent the high deposition temperatures. Depending on the processing method used, metal oxide clusters have highly heterogeneous structures and sizes, which can influence the charge generation efficiency.[55] Metal oxide dopants and their uses and processing methods in organic electronics have recently been reviewed.[78]

3.1.3. Brønsted and Lewis Acids. Practically all of the common inorganic Brønsted acids have been used as dopants for poly(anilines) (PANI) and poly(pyrroles). The doping of PANI-related polymers has been reviewed previously.[79] Recently, Brønsted acid doping has been invoked to explain the surface doping of pentacene by acidic monolayers.[80] It was proposed that pentacene near the substrate−pentacene interface is protonated to form holes resulting in a threshold voltage shift (see Figure 8). Proton transfer doping has also been used

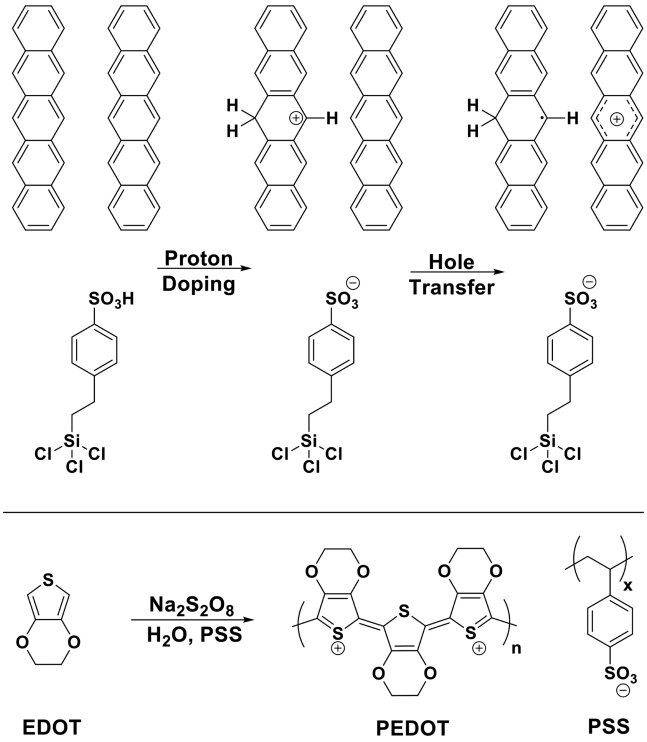

Figure 8. (Top) Brønsted acid doping of acenes by acidic monolayers.[80] (Bottom) Synthesis and structure of PEDOT:PSS.[88]

to explain the doping of polythiophenes by tridecafluoro-1,1,2,2-tetrahydrooctyl trichlorosilane (FTS).[81] Additionally, depending on the pH, proton transfer doping impacts the synthesis of poly(3,4-ethylenedioxythiophene):poly(4-styrenesulfonate) (PEDOT:PSS) and other related conducting polymers.

The most common inorganic Lewis acid dopants are $FeCl_3$ and $SbCl_5$, which have both been used to dope carbon nanotubes (CNTs), and *N*,*N*′-diphenyl-*N*,*N*′-bis(3-methylphenyl)-1,1′-biphenyl-4,4′-diamine (TPD), among other materials (Figure 9).[82,83] Lithium bis(trifluoromethylsulfonyl)imide (TFSI) has found widespread use as a p-dopant for 2,2′,7,7′-tetrakis(*N*,*N*-di-*p*-methoxyphenyl-amine)-9,9′-spiro-bifluorene (spiro-MeO-TAD), although this likely generates the actual dopant spiro-MeO-TAD-TFSI from molecular oxygen.[84,85] Bismuth carboxylates have also been used as p-dopants, and generally show a stronger doping effect with increasing fluorination of the ligand.[86] Similarly, Cu, Rh, Mo, and Cr carboxylates have been used as p-dopants with trifluoroacetate or fluorinated benzoate ligands.[86,87]

3.1.4. Small Molecules. The most common molecular p-dopant is F_4-TCNQ.[89] This material is a strong electron acceptor with a solid-state electron affinity of 5.2 eV, and the planarity of F_4-TCNQ enables efficient blending with many hosts.[90,91]

Some related TCNQ compounds form charge transfer complexes of remarkable structural order with donor molecules such as tetrathiafulvalene (TTF).[92] Derivatives of F_4-TCNQ include 2-(3-(adamantan-1-yl)propyl)-3,5,6-trifluoro-7,7,8,8-tetracyano-quinodimethane (F_3-TCNQ-Ad1), 3,6-difluoro-2,5,7,7,8,8-hexacyano-quinodimethane (F_2-HCNQ), and F_6-TCNNQ. The electron affinity of F_4-TCNQ decreases slightly upon replacement of each fluorine with a hydrogen atom from 5.2 eV for F_4-TCNQ to 4.2 eV for TCNQ (Figure 10).[35,41,93,94]

DOI: 10.1021/acs.chemrev.6b00329
Chem. Rev. 2016, 116, 13714−13751
Pictiva EX2009
Samsung v Pictiva
IPR2026-00129

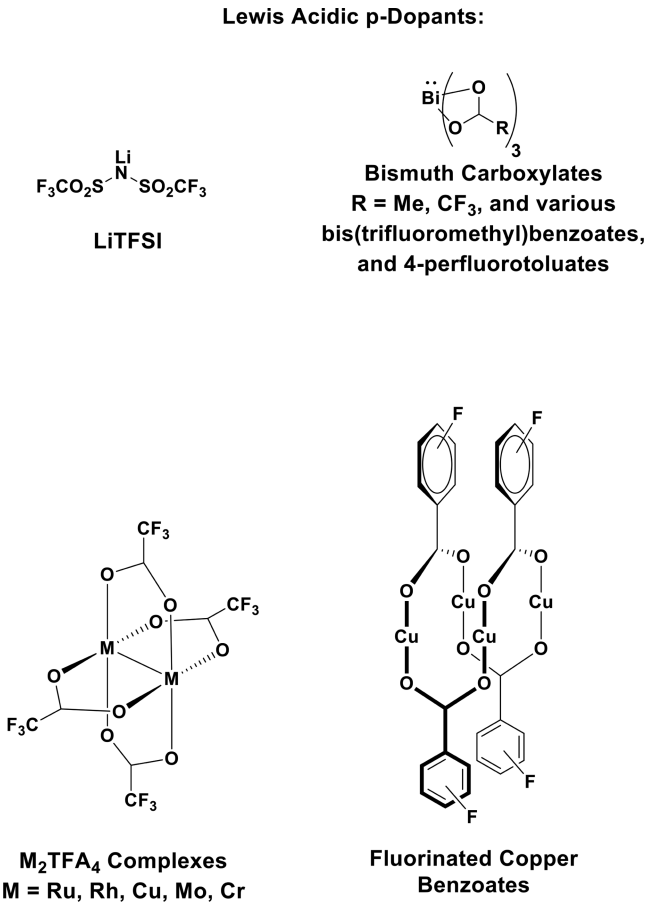

Figure 9. Lewis acidic p-dopants.[84,86,87]

F_3-TCNQ-Ad1 was developed to enable solution processing and to limit the diffusivity of this molecule in organic layers.[93]

Much larger fluorinated organic molecules based on fullerenes have also been used as organic dopants, most notably $C_{60}F_{36}$[50] and $C_{60}F_{48}$.[95] The high molecular weight of these dopants enables extremely low doping concentrations to be achieved by standard vacuum processing.[47,61] The Marder and Kahn groups have recently introduced molybdenum tris[1,2-bis(trifluoromethyl)ethane-1,2-dithiolene] ($Mo(tfd)_3$) (EA = 5.6 eV) and a more soluble analogue as very potent p-dopants.[74,96,97]

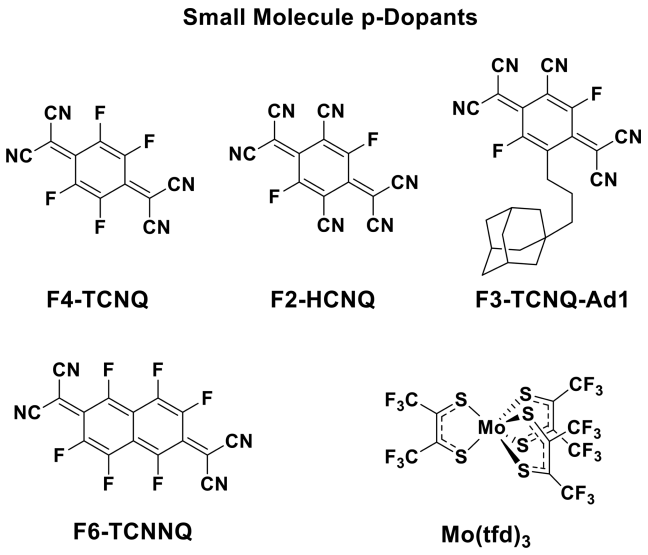

Figure 10. Examples of high electron affinity molecular p-dopants.[35,41,89,93,94,96]

3.2. n-Dopants

The low ionization energies of highly reducing n-dopants and host radical anions make air-stable n-dopants and n-doped materials the exception to the rule. Accordingly, much of the work to develop new n-dopants has focused on enhancing the air-stability of either the precursor dopant or the doped charge transfer state. From this research, several types of n-dopants have emerged, including elemental dopants, inorganic solids, low ionization potential donor molecules, organic salts, anionic dopants, hydride donor molecules, and dimers.

3.2.1. Elemental Dopants. The first and most fundamental class of n-dopants are the alkali and alkaline earth metals. Li, Na, K, and Cs are all known to reduce a wide range organic semiconductors including materials with LUMOs well above −3 eV.[98−101] As with p-type elemental dopants, alkali cations diffuse readily through organic layers leading to short operational lifetimes.[98] Moreover, the alkali metals are themselves difficult and often dangerous to handle.

3.2.2. Inorganic Salts. A much more easily handled class of dopants are the oxy metal salts of the general form X_2CO_3 where X = Li, Na, K, Rb, Cs.[102−106] Cs_3PO_4, Cs_3VO_4, CsN_3, and Li_3N have also been used as n-dopants.[86,106−108]

In all cases, these salts are processed via high temperature vacuum deposition, and at present it is not clear which products are responsible for their doping effect due to the formation of various oxides and suboxides.[109,110]

3.2.3. Low Ionization Potential Donors. n-Dopants with low ionization energies are intrinsically sensitive to oxidation, and thus care must be taken in handling these materials. Several n-dopants reported in the literature are summarized in Figure 11. TTF and the derivative bis(ethylenedithio) (BEDT)-TTF have been used as n-dopants for TCNQ, phthalocyanines, and naphthalenetetracarboxylic dianhydride (NTCDA).[92,111] Previous reviews have enumerated the various TTF derivatives and their corresponding electrochemistry.[112] The neutral tris[4-(dimethylamino)phenyl]methyl radical ($E^{0/-}$ = −1.16 V vs Fc/Fc^+) has been used as a solution processed dopant for the tris(4-nitrophenyl)methyl radical.[113] The donor TTN has been used as an n-dopant for hexadecafluorophthalocyaninatozinc (F_{16}-ZnPc).[114]

Bloom and Leo have also used bis(terpyridine)ruthenium(II) $[Ru(terpy)_2]^0$ as an n-dopant for ZnPC, which has a substantially higher LUMO than F_{16}-ZnPc, making it even more difficult to dope (dopant = −1.7 V vs Ag/Ag^+).[123] Marder and Kahn have demonstrated potent n-doping by cobaltocene and decamethylcobaltocene, which have solid-state ionization energies of 4.07 and 3.30 eV, respectively.[71,118,124,125] The donor with perhaps the lowest ionization energy for a molecular dopant is $W_2(hpp)_4$, which has a solid-state ionization energy of only 2.40 eV.[121,122,126]

3.2.4. Organic Salts. Doping by organic salts (Figure 12) was first reported by coevaporation of pyronin B chloride with NTCDA, and followed up shortly with a report of fullerene doping by crystal violet.[127,128] In the latter case, mass spectroscopic and Fourier-transform infrared (FT-IR) spectroscopy data suggest that crystal violet forms leuco-crystal violet in situ. More recently, halide salts of 1,3-dimethylbenzimidazoliums such as 2-(2-methoxyphenyl)-1,3-dimethyl-

DOI: 10.1021/acs.chemrev.6b00329
Chem. Rev. 2016, 116, 13714−13751
Pictiva EX2009
Samsung v Pictiva
IPR2026-00129

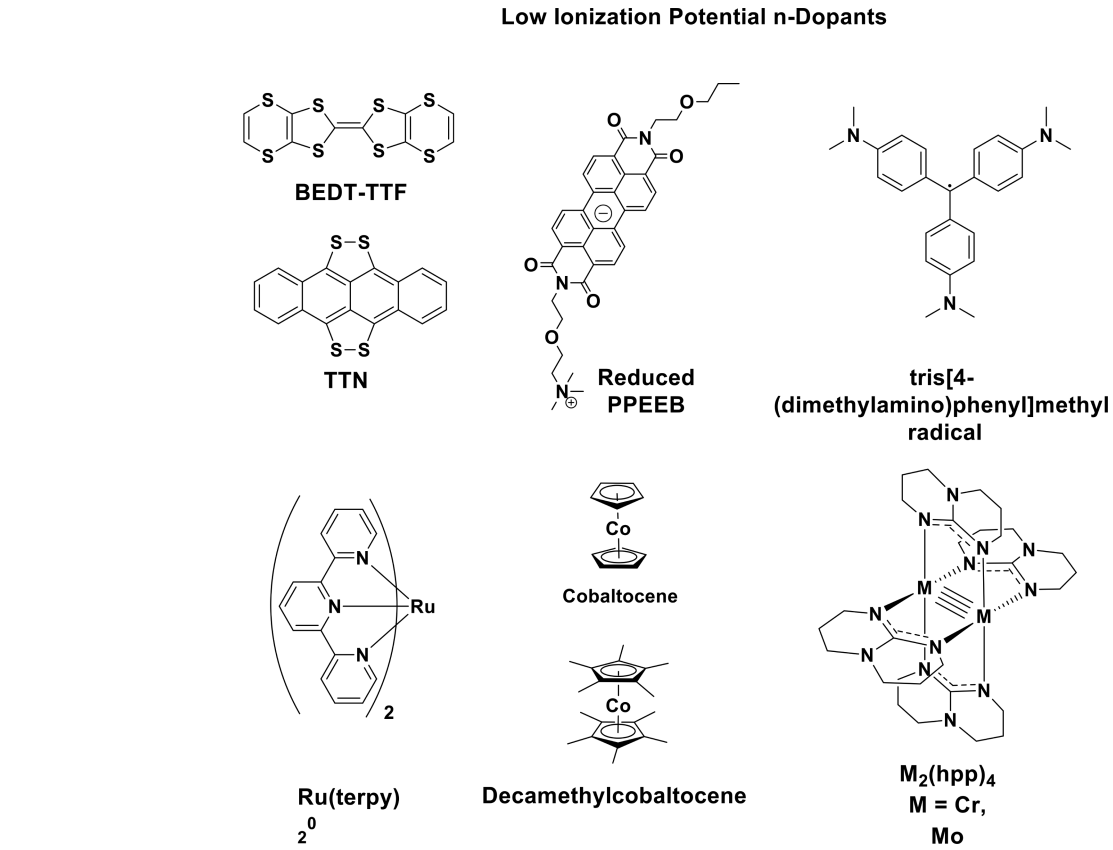

Figure 11. Examples of low ionization potential n-dopants.[111,114−122]

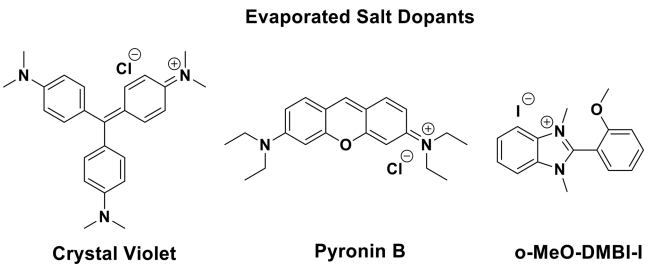

Figure 12. Examples of organic salt n-dopants.[128,129,131]

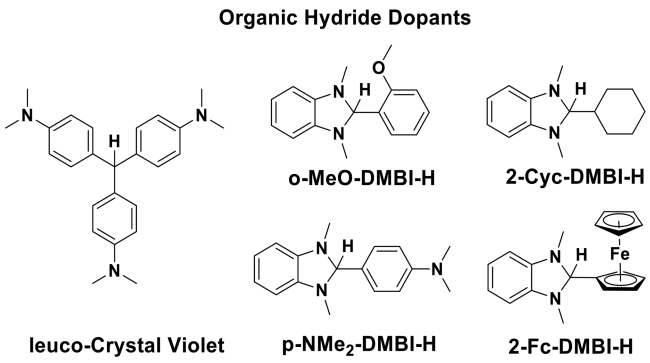

Figure 13. Examples of organic hydride donor n-dopants.[25,128,134,137]

1*H*-benzoimidazol-3-ium iodide (o-MeO-DMBI-I) have been used as potent n-dopants for C_{60}.[129,130] In o-MeO-DMBI-I doped C_{60}, no iodide was found in the film by X-ray photoelectron spectroscopy (XPS), suggesting a decomposition reaction during the doping process, but this result does not exclude the incorporation of halide impurities below the detection limit of the instrument.

3.2.5. Hydrides. The first report on possible hydride doping (Figure 13) was that of leuco-crystal violet processed in vacuum.[128] Similarly, pyronin B depositions may form the hydride donor leuco pyronin B.[127] More recently, 2,3-dihydro-1*H*-benzimidazoles (DMBI-H) compounds based on hydride-reduced benzimidazolium compounds were used as dopants for [6,6]-phenyl-C_{61}-butyric acid methyl ester (PCBM) and poly[*N*,*N*′-bis(2-octyl-dodecyl)-1,4,5,8-napthalenedicarboximide-2,6-diyl]-*alt*-5,5′-(2,2′-bithiophene) (P(NDI2OD-T2)).[132−136]

The mechanism of the doping reaction between DMBI-H dopants and PCBM was explored in solution, and it was determined that the doping process begins with a hydride transfer.[138] Subsequent electron transfer steps result in the formation of PCBM radical anions. This aspect of DMBI-H and related hydride dopants makes it difficult to predict their doping effect due to the unknown hydrogenation thermodynamics/kinetics with most acceptors. Additionally, the hydride donor dopants may introduce hydride-reduced impurities with unpredictable effects on charge transport.

3.2.6. Anion Doping. Studies on anion π-interactions between anhydrous halide ions and acceptors with strong positive quadropole moments have inspired several groups to exploit these interactions for n-doping.[139] The UV−vis spectra of fluoride doped fullerenes are consistent with the formation of fullerene radical anions.[140] It has been proposed that the fullerene radical anions form as a result of direct electron transfer between fluoride and fullerene. However, Weber et al. provided evidence in support of an alternative nucleophilic mechanism by which fluoride anions generate fullerene radical

DOI: 10.1021/acs.chemrev.6b00329
Chem. Rev. 2016, 116, 13714−13751

Pictiva EX2009
Samsung v Pictiva
IPR2026-00129

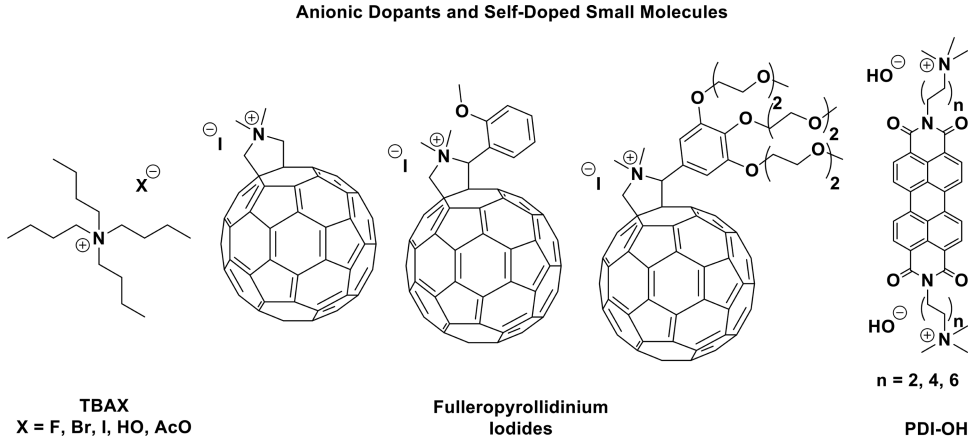

Figure 14. Examples of anionic n-dopants and self-n-doped small molecules.[140,144−146]

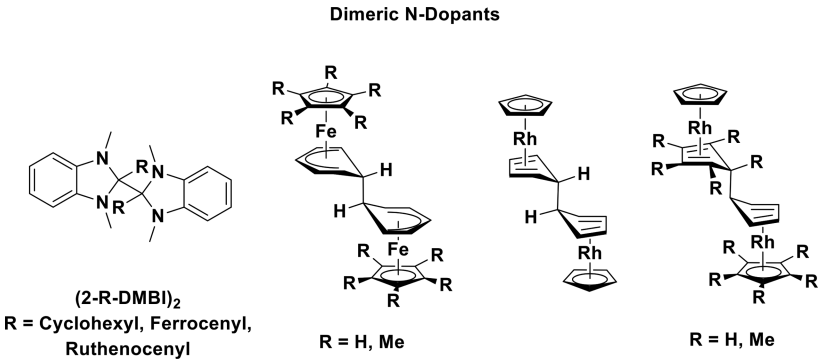

Figure 15. Examples of $(DMBI)_2$ and various metallocene dimer n-dopants.

anions,[141] although it is not clear how broadly this mechanism will apply for different anion/host systems. A detailed study on the interaction of a perylenediimide acceptor (PDI) with various anions presented data that were consistent with a net thermal electron transfer between the PDI and F^- and HO^- in several aprotic solvents, but no products of electron transfer were detected for weaker Lewis basic anions (Figure 14).[142] Similar results have been observed by Ballester et al. between fluoride and the strong electron acceptor 1,4,5,8,9,12-hexaazatriphenylene ($HAT(CN)_6$), although it was proposed that the host radical anions formed by way of a charge transfer complex followed by dissociation into a solvent caged radical pair and finally loss of the fluoride radical to sacrificial reactions that prevent back electron transfer.[143] Despite the consistency of both of these studies with a net thermal electron transfer reaction between fluoride and π-acceptors, they do not preclude the possibility that the organic radical anions form by reaction with an undetected intermediate. Nevertheless, and perhaps a more relevant detail for those interested in the electronic properties on anion-doped organic electronic devices, Li et al. observed similar conductivities for fullerene doping by TBAX salts ($X^- = F^-, Br^-, I^-, AcO^-, HO^-$) whether or not radical anions were detected in solution for a given anion.[140]

3.2.7. Dimers. Dimers of organic radicals (Figure 15) were first proposed as dopants in a patent.[147] The dimer n-dopant concept is based upon the idea that an air-sensitive dopant radical can be stabilized by dimerization through a weak C−C σ bond. Thus, radicals that are oxidized at very negative potentials can be stabilized in air at a potentially low energetic cost if the C−C bond is itself very weak.

The main advantages of this class of dopants are their air-stability and ability to dope weak electron acceptors. They are both solution and vacuum processed, and the size of the cation is tunable to enable some control over ion diffusivity, deposition rates, and morphological effects. At this time, most dimer n-dopants are synthesized by alkali metal reductions, which present a barrier to their widespread adoption.

Dimers of 19-electron metallocenes were first reported as n-dopants by the Marder and Kahn groups.[148,149] This work was extended to dimers of organic radicals of DMBI compounds by the Bao and Marder groups.[134] A comparison of the doping effect of DMBI-H and $(DMBI)_2$ analogues revealed faster formation of the host anions and a more reliable doping effect between hosts with similar electron affinities for the $(DMBI)_2$ dopants in comparison to the DMBI-H analogues.[134] Remarkably, several organometallic and $(DMBI)_2$ dimers have effective ionization potentials similar to that of decamethylcobaltocene $E^{0/-} = -1.86$ V vs Fc/Fc^+, but despite their strong reducing character, they can be handled in air as solids.[150,151] A detailed study of the metallocene dimers by Barlow et al. revealed that the metallocene dimers react in solution with hosts predominantly via either electron transfer first followed by cleavage of the dimer or cleavage of the dimer first followed by electron transfer, and in some cases both mechanisms may be operative.[148]

DOI: 10.1021/acs.chemrev.6b00329
Chem. Rev. 2016, 116, 13714−13751

Pictiva EX2009
Samsung v Pictiva
IPR2026-00129

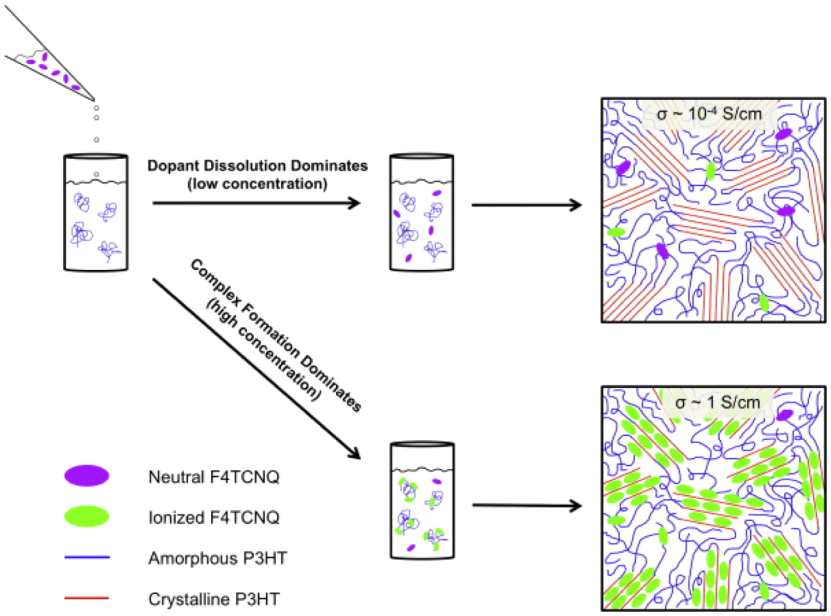

Figure 16. Weak and strong doping regime in P3HT. At low doping concentrations, F_4-TCNQ anions are mainly incorporated into amorphous regions of the film. At higher concentrations, a mixed crystalline phase consisting of P3HT and F_4-TCNQ is formed. Reprinted with permission from ref 90. Copyright 2013 Elsevier.

4. DOPING OF POLYCRYSTALLINE ORGANIC SEMICONDUCTORS

Organic doping is most commonly used in OLEDs[48] and OSCs.[152] These devices consist of amorphous layers only, and thus existing reviews almost exclusively summarize doping in amorphous materials (e.g., ref 28). In these materials, both the charge carrier concentration and the charge carrier mobility increases with increasing doping concentration, which leads to a superlinear increase in conductivity.[28]

Doping crystalline or polycrystalline materials is by far more challenging to describe. A delicate interplay between crystal structure, charge carrier concentration, and trap filling leads to a complex dependency of the conductivity on the doping concentration.

Therefore, following the discussion of the chemistry of the dopant, this section focuses on the host material. Recent results on doping (poly)crystalline materials used in OFETs are summarized, and most common dopant and matrix materials are presented.

4.1. Doping of P3HT

Doping of organic polymers stems back to the late 1970s[65,153] and is commonly seen as the starting point of organic electronics. The ability to tune the conductivity of a polymer material from highly insulating to a level close to the conductivity of metals raised significant interest and resulted in the Nobel Prize in Chemistry in 2000.[154]

Doping of the polymeric semiconductor poly(3-hexylthiophene) (P3HT) by the p-dopant F_4-TCNQ is one of the most intensively studied systems relevant for OFETs.[90,155−167] In its intrinsic form, regioregular P3HT is semicrystalline; for example, it self-organizes in a lamellar structure with two-dimensional sheets with strong $\pi-\pi$ interactions surrounded by amorphous regions of insulating side chains.[168] This semicrystalline phase leads to efficient charge transport and relatively high charge carrier mobilities of intrinisc P3HT.

Doped P3HT films are usually deposited by spin-coating from a mixture of P3HT and F_4-TCNQ. Charge transfer between P3HT and F_4-TCNQ is readily observed in solution[156,160] even before film formation. This charge transfer is visible as novel sub-bandgap gap signals in the absorption spectra, which can be assigned to F_4-TCNQ anions, P3HT bipolarons, and P3HT aggregates.[156] The charge transfer in solution is efficient. Pingel et al.[160] and Wang et al.[156] estimate that about 60% of all F_4-TCNQ molecules are ionized in solution. Furthermore, the observation of a strong F_4-TCNQ anion signal indicates that an integer type charge transfer is more likely[160] than the formation of an hybrid state involving partial charge transfer.

The interaction between F_4-TCNQ and P3HT was found to be highly localized. From absorption spectra taken at different doping concentrations, Wang et al. were able to show that one F_4-TCNQ anion interacts with approximately 4.9 P3HT monomers.[156] This is in agreement with an earlier study showing that charge transfer complexes formed in doped P3HT are localized to about four thiophene units.[159,163]

Thin doped P3HT films can be formed by spin coating. The structure of these doped P3HT films depends on the concentration of F_4-TCNQ (see Figure 16). At low doping concentrations and increased temperature during spin coating, the structure of the doped films resembles the structure of undoped P3HT.[90] Duong et al. argue that in this so-called weak doping regime, the dopant ions are incorporated into the amorphous region of the film. Charge transfer to P3HT is weak but still visible in highly sensitive photothermal deflection spectroscopy spectra.[90]

At increased concentrations, F_4-TCNQ anions are incorporated into the crystalline region of the film leading to a distinct change in film structure. In particular, the lamellar spacing increases.[90] Mixed crystals coexist with pure P3HT phases in the film and contribute to a strong increase in conductivity.[158] Hence, this phase was denoted as the strong doping phase. If the lamellar structure of P3HT is suppressed, as, for example, in regiorandom P3HT, doping was found to be much less efficient.[157]

DOI: 10.1021/acs.chemrev.6b00329
Chem. Rev. 2016, 116, 13714−13751

Pictiva EX2009
Samsung v Pictiva
IPR2026-00129

At even increased doping ratios, the crystalline phase of P3HT becomes saturated with F_4-TCNQ anions, and pure F_4-TCNQ crystals form. The onset of the saturation corresponds well with the observation that one F_4-TCNQ anion interacts with approximately four P3HT monomers.[90]

The changes in structure are reflected in the charge transport properties intensively studied by Pingel and Neher[160,161] (see Figure 17). Although charge transfer from F_4-TCNQ to P3HT monomers is highly efficient, only about 5% of all F_4-TCNQ anions contribute a free hole to P3HT.[161] This effect, commonly observed in other materials as well and discussed in section 2, is explained by a strong Coulomb interaction between the F_4-TCNQ anion and positively charged P3HT monomer, leading to a large activation energy of doping and hence a low probability of activation of dopants.

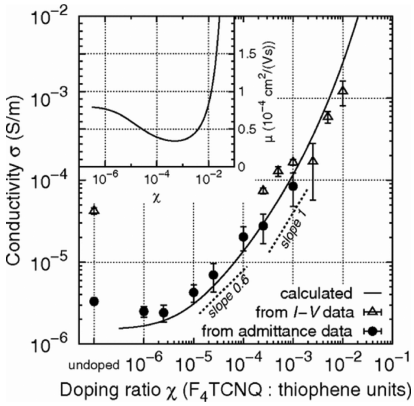

Figure 17. Conductivity and charge carrier mobility in doped P3HT films. At low doping concentrations the mobility drops, which is explained by a broadening of the density of transport states. This trend is reversed at large doping concentrations; that is, the charge carrier mobility increases. Reprinted with permission from ref 160. Copyright 2013 American Physical Society.

At intermediate doping concentrations, Pingel and Neher observe a decrease in charge carrier mobility.[161] Furthermore, by Kelvin potential measurements, they observe a broadening of the density of states in P3HT upon doping, which is explained by the analytical model of Arkhipov et al.[169] They argue that randomly distributed dopant anions Coulombically interact with free charges, which increases the energetic disorder in the film and thus broadens the density of transport states. In particular, low lying states act as trapping sites, effectively decreasing the charge mobility.

At larger doping concentrations, the trend is reversed, and an increase in mobility is observed.[160] This effect is rationalized by a coupling of the Coulomb potential of dopant ions leading to a lower effective activation energy as proposed by Mityashin et al.,[36] and a substantial filling of low lying states in the density of states by donated holes. Thus, charge is transported at an increased density of states, leading to higher hopping rates and increased mobility.

4.2. Doping of Pentacene

If P3HT is a model compound for a doped polymer, pentacene is the archetype of a high mobility small molecular organic semiconductor. For long, it set the record in charge carrier mobility for vacuum processed OFETs. It is in the range of the mobility of amorphous silicon (1 $cm^2/(V{\cdot}s)$),[170,171] which triggered strong interest in this material early on in the development of OFETs.

The high mobility of pentacene can be explained by a crystal structure favorable for charge transfer between adjacent pentacene molecules. Pentacene crystallizes in the triclinic unit cell shown in Figure 18. In thin films, the long axis of the molecule is aligned approximately perpendicular to the substrate. Within the *ab* plane, the molecules adopt a herringbone structure, which maximizes the orbital overlap along the lamella of the herringbone structure, and results in a high mobility in the plane parallel to the substrate.

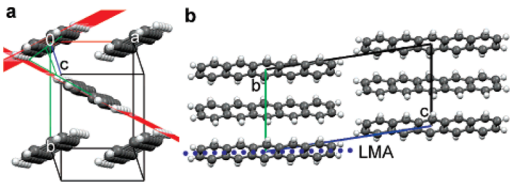

Figure 18. Structure of the thin film polyomorph of pentacene. Pentacene crystallizes in a layered structure with the long axis of the molecule perpendicular to the substrate. Large orbital overlap in the *ab* plane due to the herringbone structure leads to efficient charge transport. Reprinted with permission from ref 172. Copyright 2007 American Chemical Society.

Several different polymorphs of this thin film structure are reported, but they are assumed to share the herringbone arrangement.[173] They differ slightly in the tilt angle of the pentacene crystal and therefore in the layer periodicity *d*(001), that is, in the distance between the *ab* planes.

4.2.1. p-Doping of Pentacene by Iodine. Doping of pentacene has been studied since the early 1990s.[174−180] In these early reports, p-doping of pentacene was accomplished by exposing the pentacene films or single crystals to iodine vapor.[174] Iodine is incorporated into the pentacene crystal and electrons are transferred from pentacene to iodine, leaving behind a hole on the pentacene crystal. This charge transfer was proven, for example, by UV−vis absorption, which shows the appearance of new absorption bands in doped films assigned to the formation of ionized iodine and pentacene,[181] and Raman spectroscopy, which shows signatures of I_3^- and I_5^- species in the film.[181,182]

Iodine doping increases the hole density in the film. It has been estimated to be rather high, up to 10^{21} cm^{-3} at high doping ratios.[177] Furthermore, as the charge carrier mobility is not significantly reduced upon doping, a high conductivity of up to 150 S/cm is reached.[177] Even a transition to metallic behavior was proposed,[177] which, however, was questioned later.[180]

The high mobility and conductivity in these doped films implies that the crystal structure remains largely undisturbed even at higher doping concentrations. The details of the structure of iodine doped pentacene were studied by X-ray diffraction (XRD),[178,183] and Raman and IR spectroscopy.[182] XRD data show that the distance between the *ab* planes of pentacene molecules is increased, whereas the molecular structure in the *ab* plane remains almost unchanged. For example, Minakata found an increase from 15.3 Å of the undoped film to 19.3 Å of the doped film.[178] This "swelling" of the film has been interpreted as an intercalation of iodide ions between the layers of pentacene (see Figure 19). Considering that pentacene shows its highest mobility in the *ab* plane, which

DOI: 10.1021/acs.chemrev.6b00329
Chem. Rev. 2016, 116, 13714−13751
Pictiva EX2009
Samsung v Pictiva
IPR2026-00129

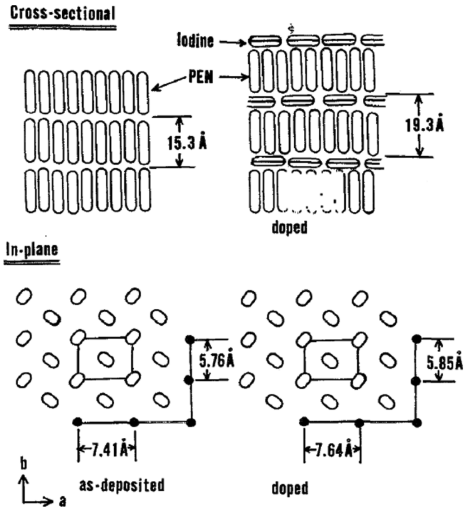

Figure 19. Doping pentacene by iodine. Iodine accumulates between the layers of pentacene to form an intercalated structure. The high in-plane mobility is preserved. Reproduced with permission from ref 178. Copyright 1992 AIP Publishing.

remains almost undisturbed, it is not surprising that the in-plane mobility remains high. However, as observed by Minakata et al. as well, doped pentacene films show a huge anisotropy between the out-of-plane and in-plane conductivity, which is as high as 8 orders of magnitude.[174]

This model of intercalation of iodine between layers of pentacene was confirmed by a more detailed study of Ito et al.[183] They found two transitions of pentacene upon doping. At intermediate doping concentrations, they observed a transition from the triclinic unit cell of undoped pentacene to an orthorhombic one. In agreement with Minakata, the lattice constants in the *ab* plane are nearly unaltered, but the lattice parameter *c* is increased from 14.5 to 19.28 Å. This phase was identified as the highly conductive phase reported by Minakata. However, they found an additional phase at higher doping concentrations, where the in-plane lattice constants are increased, which they explain by an incorporation of iodine into the pentacene layer. Raman and IR spectroscopy confirm the presence of the additional structure at high doping concentrations.[181,182] Because of the increase of the *ab* lattice constants, the in-plane mobility and conductivity of this phase decrease.[181]

Overall, iodine doping of pentacene is highly effective. As iodine is mainly intercalated between the planes of pentacene, leaving the in-plane herringbone structure intact, doping does not deteriorate charge carrier mobility, which results in high conductivities and effective charge transport. However, iodine doping comes with severe disadvantages, which render it impractical for real devices. First, exposing the pentacene film to a vapor of the dopant leads to inhomogeneous doping profiles, which are difficult to control.[181] Furthermore, the doping effect is not stable; that is, the incorporated iodine is desorbed from the layer in ambient conditions, which leads to a drop in conductivity over time.[177]

4.2.2. p-Doping of Pentacene by Molecular Dopants. Although highly efficient, iodine tends to diffuse in pentacene, rendering the doping effect unstable and precluding use of iodine in organic devices. This shortcoming has fueled research in organic dopants, which are more bulky and do not diffuse in the organic host layers.[28] However, the increased stability comes at a high price for polycrystalline materials. Because of the larger size of the dopant, it is expected that the crystal structure of the matrix material is disturbed, leading to a reduction in charge carrier mobility.

The most commonly used molecular dopant is F_4-TCNQ.[7] It is heavily used to increase the conductivity of hole transport layers of OLEDs[48] and OSCs.[28] Furthermore, it is known to dope polycrystalline pentacene as well.[34,184]

Ha and Kahn studied the microscopic structure of F_4-TCNQ doped pentacene films by STM.[38] They found that F_4-TCNQ molecules diffuse into vacancies of the pentacene lattice and were able to show that the dopant does not disturb the crystal lattice of pentacene.

However, Ha et al. studied low doping concentrations only. At higher concentrations, it was shown that the crystallinity of pentacene is indeed reduced.[185] For concentrations above 1 wt %, the average crystallite size decreases (see Figure 20), which results in a continuous decrease in charge carrier mobility. This decrease is even stronger for larger dopants such as F_6-TCNNQ.

This reduction in crystallinity leads to a drop in mobility. Consequently, the conductivity of a doped pentacene layer increases at first due to the increase in charge carrier concentration. However, it reaches a maximum of approximately 0.1 S/cm at 6 wt % (F_4-TCNQ) or 2 wt % (F_6-TCNNQ), before it drops due to the decrease in charge carrier mobility induced by doping.

This increase in disorder at higher doping concentrations was as well observed for another p-dopant, $C_{60}F_{36}$,[50] by Pahner et al.[61] They report on a broadening of the density of occupied states at higher doping concentrations, which can be understood as a direct result of increased disorder. However, in

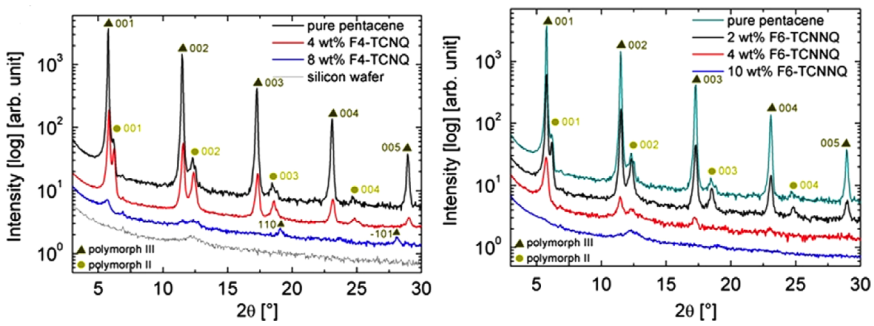

Figure 20. Doping pentacene by F_4-TCNQ and F_6-TCNNQ. XRD shows weaker reflections at higher doping concentrations, corresponding to smaller crystallite size. Reprinted with permission from ref 185. Copyright 2012 Elsevier.

DOI: 10.1021/acs.chemrev.6b00329
Chem. Rev. 2016, 116, 13714−13751

Pictiva EX2009
Samsung v Pictiva
IPR2026-00129

accordance with Ha et al.,[38] no broadening was observed at low doping concentrations.

Most interestingly, Pahner et al. were as well able to deduce the concentration of free charge carriers in the doped film from the capacitive response of a Schottky diode. They observed that the density of free charge carriers is thermally activated and found an activation energy of 54 meV for $C_{60}F_{36}$ and 19 meV for F_6-TCNNQ. This activation energy of $C_{60}F_{36}$ in pentacene was confirmed qualitatively by UPS measurements.[47] As discussed in section 2, this activation energy can be explained by Coulomb interactions between transferred charges[36] or activation from the bonding state of dopant-pentacene hybrid.[39]

4.2.3. p-Doping of Pentacene by Transition Metal Oxides. Transition metal oxides are well-known dopants used in OLEDs and OSCs.[78] These materials exhibit a very large electron affinity of around 6.7 eV (MoO_3 and V_2O_5) or 6.5 eV (WO_3), which makes them capable of doping wide gap materials.

Several authors report on doping pentacene by MoO_3.[23,186−188] Charge transfer from dopant to pentacene was proven by UPS[23] and XPS.[187]

As for F_4-TCNQ, Ha et al. studied doping pentacene by MoO_3 using STM.[186] They deposited a low amount of MoO_3 on top of a crystalline pentacene surface. In contrast to doping with F_4-TCNQ, MoO_3 does not diffuse toward vacancies in the pentacene lattice, and smaller and larger clusters of MoO_3 are formed on the pentacene surface (see Figure 21). This clustering is in accordance with the observations of Berkowitz et al., who found that MoO_3 forms clusters already in the gas phase when sublimed.[189]

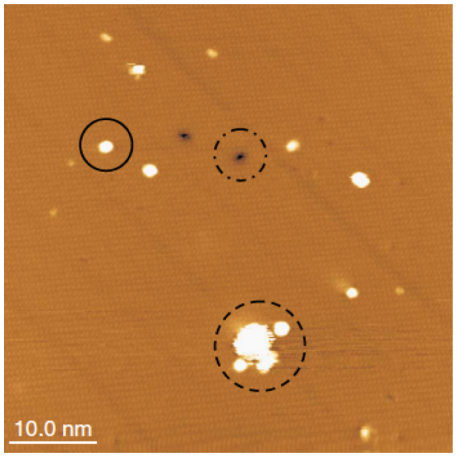

Figure 21. Doping pentacene with MoO_3. Clusters of MoO_3 are seen in STM images of a crystalline pentacene surface. Reprinted with permission from ref 186. Copyright 2010 American Physical Society.

Ha et al. observe that a layer of pentacene grown on the clusters of dopants exhibits the regular crystal structure, which indicates that doping by MoO_3 does not degrade the structural order of the film, at least not at low concentrations. For higher concentrations (above 0.5 mol %), a reduction in order[23] and crystallite size[187] is observed.

4.2.4. n-Doping of Pentacene. n-Doping of pentacene is by far more challenging than p-doping. Because of the low electron affinity of pentacene (approximately 2.72 eV[124]), the n-dopant has to show a very low ionization potential to allow for an electron transfer, which renders most potential candidates instable in air. However, as will be discussed below, air-stable and effective n-dopants for pentacene were found as well.

In first studies, n-doping of pentacene by alkali metals such as sodium, potassium, and rubidium,[179] lithium,[190] or cesium[191] was studied. All metals show a doping effect in pentacene. A conductivity of 10^{-5} S/cm is found for Na doping,[179] 6×10^{-3} S/cm for lithium,[190] 100 S/cm for potassium,[192] 47 S/cm for rubidium,[191] and 74 S/cm for cesium doping.[191] This high conductivity and the observation that the conductivity increases with decreasing temperature is sometimes even interpreted as a metallic transport in these mixed layers.[191]

For many alkali metal dopants, an intercalated structure as for iodine doping of pentacene was found as well. For example, Hansson et al. report on a molecular dynamics (MD) and density functional theory (DFT) study of the structure of potassium doped pentacene.[193] At low concentration, potassium intercalates between the pentacene layers, leaving the herringbone structure almost unchanged. At higher concentrations, however, the herringbone structure vanishes due to an incorporation of ions into the *ab* plane. This leads to a strong $\pi-\pi$-interaction along the *c*-axis, which should increase the out-of-plane mobility.

However, despite the high conductivity observed in these films, doping by alkali metals has significant drawbacks. In particular, it is challenging to control the doping ratio (the pentacene films are often exposed to a vapor of the alkali metal), and the doped films often show a low stability. Finally, the high concentrations of alkali metals sometimes used to prepare films with high conductivity (up to a 1:1 ratio) show that rather than having a doped film of pentacene, a mixed hybrid film of pentacene with alkali metal is studied, which makes the interpretation of results challenging.

These shortcomings can be avoided by molecular dopants. Chan et al. reported on the doping effect of the strong electron donor decamethylcobaltocene $CoCp_2^*$ in pentacene in 2008.[124] Although the ionization energy of $CoCp_2^*$ is larger than the electron affinity of pentacene, the generation of free electrons on the pentacene matrix was proven by UPS. By capacitance−voltage measurements, they were able to estimate the concentration of free electrons in the film and showed that the doping efficiency, that is, the ratio of free electrons to dopant molecules, is only about 1%.

Still, $CoCp_2^*$ is highly volatile, and doping is achieved by exposing the sample to a background pressure of the dopant during growth of the film. Although it was shown that the dopant is indeed incorporated into the pentacene film,[124] a dopant with a lower vapor pressure is desirable as it would allow for a better control in doping concentration.

A larger dopant, bis(4,4′,4″-tri-*tert*-butyl-2,2′:6′,2″-terpyridine)ruthenium ($[Ru(t\text{-but-terpy})_2]^0$), was proposed by Harada et al.[34] Doping was studied by UPS and thermovoltage measurements. It could be shown that n-doping shifts the Fermi level of the doped layers toward the LUMO states, as would be expected from classical semiconductor statistics. Harada et al. combined n- and p-doping by F_4-TCNQ to process a p−i−n homojunction and were able to show that the built-in voltage of the junction (1.65 V) is related to the open circuit voltage if the junction is operated as solar cell.

$[Ru(t\text{-but-terpy})_2]^0$, as most n-dopants, is air sensitive and has to be handled under protective environments. In 2012, Guo et al. proposed a novel concept for air-stable n-dopants, which are strong enough to dope pentacene.[148,149,194] On the basis of

DOI: 10.1021/acs.chemrev.6b00329
Chem. Rev. 2016, 116, 13714−13751

Pictiva EX2009
Samsung v Pictiva
IPR2026-00129

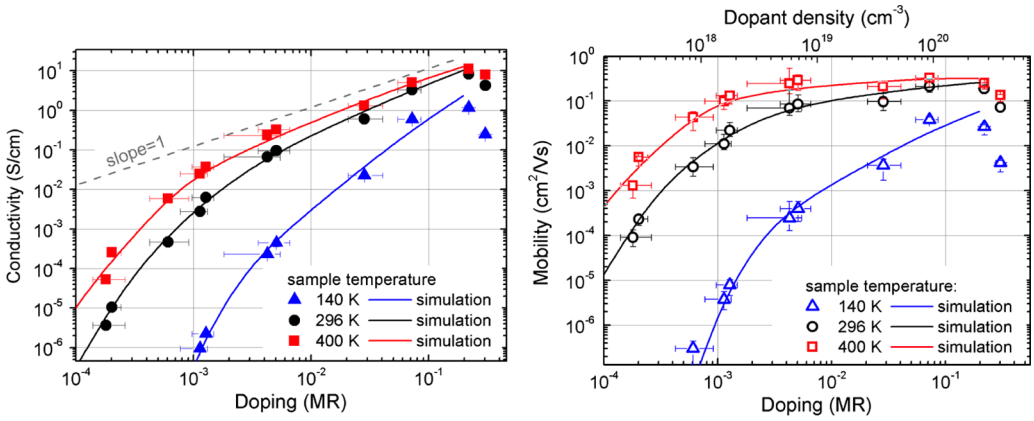

Figure 22. Conductivity and charge carrier mobility of films of C_{60} doped by the n-dopant $[RuCp^*(mes)]_2$. A superlinear increase in conductivity and increase in mobility is found for low doping concentrations, which is due to a filling of traps states by dopants. Reprinted with permission from ref 52. Copyright 2012 American Physical Society.

their results on doping pentacene by decamethylcobaltocene,[124] they synthesized organometallic dimers of rhodocene ($[RhCp_2]_2$) and similar dimers, for example, ruthenium-(pentamethylcyclopenta-dienyl)(1,3,5-triethylbenzene) $[Cp^*Ru(TEB)]_2$ (see Figure 15). In contrast to the monomers, the dimers are relatively air-stable, have a lower vapor pressure, and can be coevaporated with the matrix material, allowing for a precise control of the doping concentration.

These dopants were shown to be capable of doping a wide range of matrix materials, including pentacene and 6,13-bis(triisopropyl-silylethynyl) (TIPS)-pentacene. The current density was shown to increase greatly in doped layers, and the Fermi level shifts toward the LUMO.[149] Two mechanisms are discussed to explain doping. In the first mechanism, the dimer is cleaved first, which alone is an endergonic or unfavorable process. However, this process is followed by a rapid charge transfer to pentacene, stabilizing the result. In the second mechanism, it is assumed that the electron transfer from dopant to pentacene happens first, which is followed by a cleavage of the dimer. Depending on the choice of dopant and matrix materials, both mechanisms can be in effect.[194]

In some of these doping studies, it is shown that pentacene possesses a significant density of electron traps[34] and that filling these traps by doping can inactivate these traps electronically.[149] This effect was used to prepare films of TIPS-pentacene with a very high electron mobility. Doping these films by o-MeO-DMBI, which is not strong enough to supply free electrons to the LUMO of TIPS-pentacene, leads to a filling of electron traps located in the HOMO/LUMO gap. It was shown that filling these traps leads to highly efficient electron transport and a mobility of 3.2 $cm^2/(V\cdot s)$ on average.[133] Furthermore, the crystal structure of the doped films is not disturbed by the dopant. Most probably a phase segregation is taking place, which is in accordance to the relatively large doping concentrations needed (50 mol %).

4.3. Doping of Fullerene C_{60}

Whereas pentacene is the archetype of an organic p-type semiconductor, C_{60} and its soluble counterpart PCBM are heavily used as n-type channel material in OFETs.

n-Doping of C_{60} by alkali metals was found to be very efficient in 1991 by Haddon et al.[195] Furthermore, superconductivity was observed for potassium doped films.[196,197]

Haddon and Hebard exposed films of C_{60} to vapors of Cs, Rb, K, Na, or Li, which lead to a pronounced increase in conductivity.[195] A conductivity of 500 S/cm was reached for the most efficient dopant, potassium. The authors explain this observation by a doping effect and argue that the crystal structure of C_{60} leaves enough free space for alkali metal ions to incorporate into the structure. However, at even higher concentrations the conductivity started to decrease. In particular for the largest ion, Cs, the film darkened and became rough, which was understood as a disruption of the crystal lattice due to difficulties of incorporating too many Cs ions.

Although n-doping by alkali metals is highly efficient, the same shortcomings as for pentacene apply. In particular, the low stability of these films precludes the use of these dopants in organic devices. However, many larger molecular dopants were reported in the literature, and many compounds were proven to be effective. For n-doping, rhodamine B,[127] Ca,[198] ruthenium-(pentamethylcyclopentadienyl)(1,3,5,-trimethylbenzene) dimer ($[RuCp^*(mes)]_2$),[51,52] N-DMBI,[25] 2-(1,3-dimethyl-1*H*-benzoimidazol-3-ium-2-yl) phenolate hydrate (DMBI-POH),[130] acridine orange base (AOB),[131,199] leuco-crystal violet,[128] and $W_2(hpp)_4$[120−122] were proposed.

Although a small reduction in charge carrier mobility with increasing n-doping concentration was found,[199] in most reports doping did not degrade the charge transport properties or the crystallinity of the samples.

Instead, even an increase in mobility with the doping concentration is found, which is a remarkable difference from p-type doping of pentacene[51,52] (see Figure 22). This effect was explained by filling of trap states, which hinder electron transport in intrinsic layers. Filling these traps is assumed to electrically passivate traps, which leads to more effective charge transport[52] and even to an increase in air stability of the doped films.[132] Only at very high doping concentrations (molar ratio of 20%) is a decrease in conductivity and mobility found (see Figure 22), indicating a reduction in order in these films.

Most of the n-dopants reported in the literature degrade rapidly upon exposure to air. However, recently it was shown that doping C_{60} by the air-sensitive n-dopant $W_2(hpp)_4$ leads to a passivation of the n-dopant, which renders the film at least partially stable in air.[121] Although the conductivity of the doped film drops in air, it can be recovered by thermal annealing in vacuum. This effect was explained by electron transfer and the higher stability of the $W_2(hpp)_4$ cation.[120] It furthermore depends on the position of the LUMO of the host material. For hosts with an even larger electron affinity as compared to C_{60},

DOI: 10.1021/acs.chemrev.6b00329
Chem. Rev. 2016, 116, 13714−13751

Pictiva EX2009
Samsung v Pictiva
IPR2026-00129

for example, *N,N*-bis(fluoren-2-yl)-naphthalenetetracarboxylic diimide (bis-Hfl-NTCDI),[11,120] the effect is increased and yields organic films doped by an air-sensitive n-dopant, which are nevertheless stable in ambient conditions.[120]

p-Doping is much more challenging given the low HOMO edge of approximately 6.4 eV. So far only doping using the transition metal oxide MoO_3 has been reported.[198,200−202] Combining p- and n-type doping, Shinmura was able to prepare a C_{60}-based homojunction[202] similar to the pentacene homojunction of Harada et al.[34] As for n-doping, the crystal structure of C_{60} seems not to be heavily disturbed by the dopant. For example, it was shown that doping C_{60} by MoO_3 only slightly reduced the grain size of the polycrystalline film from 9 to 7 nm[201] and that the dopant is evenly distributed in the film.

4.4. Doping Other Organic Semiconductors with High Charge Carrier Mobility

Until 2007, pentacene was the unbeaten record holder and exhibited the highest hole mobility (in the range of 1−3 $cm^2/(V{\cdot}s)$). In the search for compounds with a higher air-stability, the molecule dinaphtho[2,3-*b*:2′,3′-f]thieno[3,2-*b*]thiophene (DNTT) was developed,[13,203] which turned out to be more stable and shows a slightly increased mobility ($\mu \approx 3$ $cm^2/(V{\cdot}s)$). It was found that the mobility can be improved further, if alkane spacer chains are attached to both sides of the DNTT core (Cn-DNTT), yielding a mobility as high as 8.5 $cm^2/(V{\cdot}s)$.[204−207] Recently, an off-center spin-coating technique has been presented that yields thin crystalline films of the compound 2,7-dioctyl[1]benzothieno[2,3-*b*][1]-benzothiophene (C8-BTBT) with a maximum mobility of 43 $cm^2/(V{\cdot}s)$, which is one of the highest values reported so far for organic semiconductors deposited on large areas.[208]

Although the use of well-known electron acceptors such as F_6-TCNNQ or F_4-TCNQ was reported for some of these materials, so far the dopant is mainly deposited as a pure layer on top of the organic semiconductor to improve injection at the source and drain contacts,[13,206,207] and doping in mixed layers is seldomly reported.

C8-BTBT or the related semiconductor 2,7-didecyl(C10)-BTBT is an exception. Mendez et al. studied the doping of C10-BTBT by F_4-TCNQ and found a unit cell consisting of dimers of the conjugated core of C10-BTBT and F_4-TCNQ (see Figure 23). An increase in conductivity was found at low doping concentrations; however, it remained unclear if F_4-TCNQ is actually providing free holes to C10-BTBT or if the increase in conductivity is due to filling of traps. Considering the results reported by Soeda et al.,[209] who studied doping of C8-BTBT by F_4-TCNQ in organic transistors, trap filling is more probable. Soeda et al. find no increase in the off-state current of OFETs upon doping, but a reduction in threshold voltage, similar to the results of Olthof et al. for n-doping C_{60}[51] discussed above (see section 5.2.2 for a more detailed discussion).

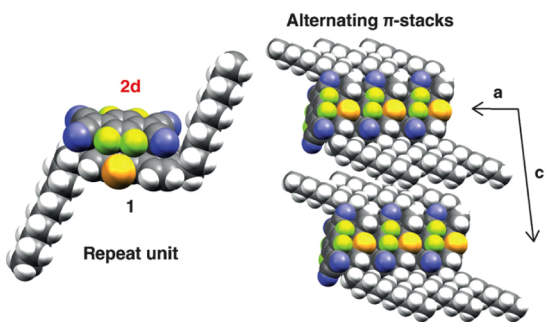

Figure 23. Doping C10-BTBT by F_4-TCNQ. Dimers of C10-BTBT and F_4-TCNQ are formed. Reprinted with permission from ref 41. Copyright 2013 John Wiley and Sons.

A similar packing motif was found by Cochran et al. for the polymer poly(2,5-bis(3-tetradecylthiophen-2-yl)thieno-[3,2-*b*]-thiophene) (PBTTT-C14) doped by F_4-TCNQ.[91] The authors found that F_4-TCNQ stacks cofacially with the conjugated backbone of the polymer forming an intercalated crystalline microphase leading to high charge transfer probabilities. Most interestingly, their data suggest that instead of a random arrangement of the dopant in the crystalline region, some polymer chains are highly decorated with F_4-TCNQ, whereas other chains are not. Thus, the distribution of dopants is not entirely random as assumed in most transport models, but correlated.

Most organic dopants disrupt the structure of the matrix material leading to a decrease in charge carrier mobility (see as well Figure 20). To minimize this disruption, Gregg et al. proposed a dopant/matrix system where the dopant is commensurate with the lattice.[37,57,115,210] They doped the liquid crystalline semiconductor PPEEB by a derivative of the same molecule with a covalently bound positive countercharge added to the end of the alkyl chain. They observed a superlinear increase in conductivity,[210] which was explained by a decrease in activation energy of the doped charge carriers.[115]

5. DOPED ORGANIC TRANSISTORS

The general setup of a p-type OFET is shown in Figure 24. From bottom to top, the transistor consists of a metallic gate

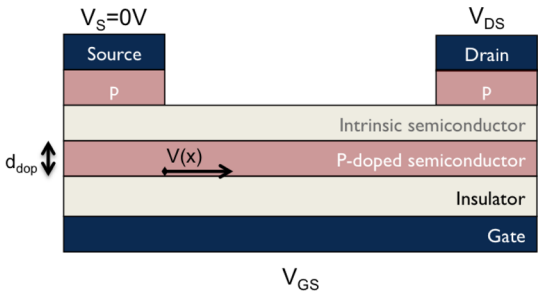

Figure 24. Setup of a p-doped organic transistor. In some reports, only a thin layer at the interface to the oxide is doped (thickness d_{dop}). To ensure efficient injection of holes, the source and drain regions can be p-doped as well.

electrode covered by an insulating layer and a thin layer of a p-type organic semiconductor. The organic semiconductor is furthermore contacted by two electrodes, the source and drain electrodes. To operate the OFET, a voltage is applied between the source and the drain electrode (V_{DS}) and the current leaving the transistor at the drain I_D is measured. The drain current is modulated by the voltage applied between the source and the gate electrode V_{GS}. If, for example, a negative voltage is applied to the gate with respect to the source electrode, holes are electrostatically accumulated at the interface between the organic semiconductor and the gate insulator. As the conductivity of the organic semiconductor increases with the

DOI: 10.1021/acs.chemrev.6b00329
Chem. Rev. 2016, 116, 13714−13751
Pictiva EX2009
Samsung v Pictiva
IPR2026-00129

charge carrier density, the drain current increases as well; that is, the transistor switches on. If, however, a positive voltage is applied to the gate, all free holes are repelled from the gate insulator. The semiconductor is fully depleted of charge carriers, the local conductivity drops to zero, and the transistor switches off.

Doping can improve OFETs in various ways. It can be used to increase the saturation current and transconductance of OFETs, to fine-control transistor behavior, and to make transistors more reliable.

Contact doping as reviewed in section 5.1 is the most common use of doping in transistors,[13−17,19,20,211] and has been recently identified to be essential for further improving the switching frequency of organic transistors.[211]

Besides contact doping, doping of the channel of the transistors[21−24,166,209] leads to a precise control of the threshold voltage and to an increase in stability.[26,132] Details and limits of channel doping will be discussed in section 5.2.

Last but not least, doping adds a further dimension in the control of the electric properties of organic semiconductors. In particular, the control of the Fermi level position (see, e.g., Figure 6) allows one to control the majority charge carrier species,[133,201] to realize inversion OFETs based on minority charge carriers,[21,212] or to control ambipolar behavior of transistors[213] (section 5.2.3).

5.1. Contact Doping

Efficient charge injection is essential for high-performance of OFETs because it is the starting point of the electrical operation. Even if organic semiconductors with extremely high charge carrier mobility are used, the performance of organic transistors will be severely limited by inefficient injection.

In most OFET architectures, metal electrodes are utilized to establish contact with the organic semiconductor layer and to inject charges into (or extract charges from) it. Therefore, charge injection is mostly dominated by the interfacial properties between the metal electrodes and organic semiconductors. It is of crucial importance to not only develop a physical model of charge injection but to understand all physical phenomena occurring at a metal/organic interface as well. Hence, enormous efforts have been devoted to describe injection into organic semiconductors and to characterize the electronic structure and the energy alignment at the interface.[12,214−222]

The energy level structure of the junction formed between metal and organic semiconductor is schematically sketched in Figure 25. When two heterogeneous materials are brought into contact, a thermodynamic equilibrium is established via charge carrier transfer across the interface. This process commonly gives rise to a space charge region at the metal/organic interface, leading to a bending of the energy levels depending on the relative energy alignment of metal work function (ϕ_m) and Fermi level (E_F) of the organic semiconductor. Interface dipoles (Δ) induced by the interaction between the organic semiconductor and the metal will modify the metal work function, which additionally alters the electronic structure of the interface.[223]

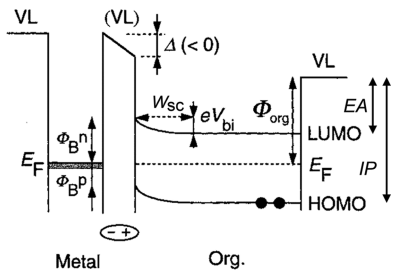

Figure 25. Interfacial energy diagram at the metal/organic junction. Adapted with permission from ref 214. Copyright 1999 John Wiley and Sons.

The contact resistance impeding efficient charge injection originates from potential barriers formed at the interface. The energy barriers at the interface for hole (ϕ_B^p) and electron (ϕ_B^n) injection shown in Figure 25 are given by

$$\phi_B^p = \mathrm{IP} - \phi_m - \Delta \tag{6}$$

$$\phi_B^n = \phi_m - \mathrm{EA} + \Delta \tag{7}$$

A straightforward strategy to improve charge injection is to eliminate the energy barrier at the metal/organic interface so that the contact resistance is minimized and a so-called Ohmic contact is formed. According to eqs 6 and 7, the charge injection barrier can be minimized by matching the metal work function to the charge transport level, that is, HOMO and LUMO of the organic semiconductors.

However, most metals that would enable efficient electron injection are usually highly reactive rendering the transistor unstable in ambient conditions. Therefore, a wide range of approaches to engineer contacts and/or tune the metal work function were introduced. For example, self-assembled monolayers (SAMs)[222,224−226] or other injection layers were used to minimize injection barriers.[227−230] Among these techniques, contact doping was studied extensively and was proven to be a promising approach to realize quasi-Ohmic contacts.

In this section, we summarize the fundamental theory of the contact resistance and contact doping, and review recent studies on contact doping used in a wide variety of transistors.

5.1.1. Contact Resistance. The total resistance R_{tot} of OFETs is usually modeled as a series connection of the contact resistance R_c and the channel resistance R_{ch} as illustrated in Figure 26 for an inverse staggered configuration:

$$R_{tot} = R_{ch} + R_c \tag{8}$$

When the channel length L of OFETs is reduced, R_{ch} decreases as well, whereas the contact resistance remains unchanged as it is inherently governed by interfacial properties. Thus, the overall electrical performance of short channel devices is limited by the contact properties.

R_c consists of two contributions, the interface resistance R_{int} determined by the energy barrier at the metal/organic interface and the bulk resistance R_{bulk}, that is, the resistance of the organic material itself.[19] In the so-called coplanar architecture, where the charge accumulation channel and source/drain electrodes lie in the same plane, that is, at the semiconductor/dielectric interface, R_{bulk} can be neglected because charges are directly injected into the channel. However, it has been shown that charge injection in coplanar devices is generally poorer than in the staggered structure. This difference was rationalized by the argument that in the staggered configuration injection can occur through the entire contact area defined by the overlap of the source/drain area with the gate electrode.[231−234]

In 1969, Murrmann and Widmann proposed an analytical model named "current crowding model" to estimate the contact resistance between metal and semiconductor.[235,236] As

DOI: 10.1021/acs.chemrev.6b00329
Chem. Rev. 2016, 116, 13714−13751
Pictiva EX2009
Samsung v Pictiva
IPR2026-00129

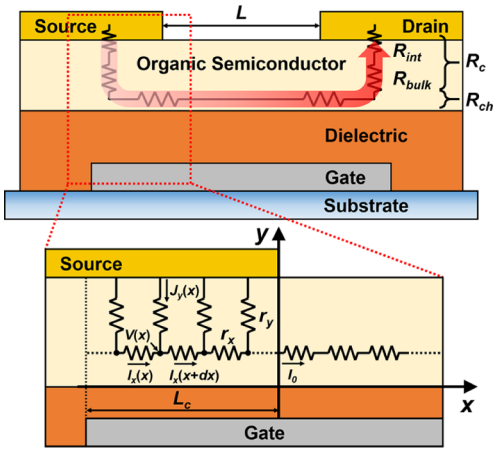

Figure 26. Simplified modeling of the total resistance in an inverse staggered OFET (top-contact bottom-gate structure) (top) and equivalent circuit of the current crowding model for extracting the contact resistance (bottom).

illustrated in Figure 26, they described charge injection by a network of infitesimal small resistors representing the vertical resistance (denoted by r_y) and lateral bulk resistance (denoted by r_x). This model has been successfully used to investigate the contact effects not only of silicon-based transistors,[237,238] but of OFETs as well, especially in the staggered structure.[211,234,239,240] The model is based on a few assumptions. It is assumed that (i) the mobility and resistivity are constant throughout the whole semiconductor film, (ii) charge carriers are vertically injected from the contact and transported horizontally in the accumulated channel, and (iii) the vertical current flows only in the contact area, that is, in the region of the device defined by the gate/source and gate/drain overlap.

For the numerical analysis, r_x and r_y are defined as

$$r_x = R_{sh}\, dx/W \tag{9}$$

$$r_y = \rho_c/W\, dx \tag{10}$$

Here, R_{sh} is a sheet resistance (units of $\Omega/\square$), and ρ_c is the specific contact resistivity ($\Omega \cdot cm^2$) equal to $R_c \times A_c$ with $A_c = WL_c$ (A_c is the contact area, W is the contact (or channel) width, and L_c is the contact length). $J_y(x)$ is the vertical current density at x. Using these definitions, one obtains from Figure 26:

$$\frac{dI_x(x)}{dx} = J_y(x)W = \frac{V_x(x)}{\rho_c}W \tag{11}$$

$$\frac{dV_x(x)}{dx} = I_x(x)\frac{R_{sh}}{W} \tag{12}$$

With the boundary conditions of $I_x(0) = I_0$ and $I_x(-L_c) = 0$, eqs 11 and 12 can be solved for $V_x(x)$:

$$V_x(x) = I_0 L_T \frac{R_{sh}}{W}\frac{\cosh[(L_c - |x|)/L_T]}{\sinh(L_c/L_T)} \tag{13}$$

where $L_T = \sqrt{\rho_c/R_{sh}}$ is the characteristic length of injection denoted as the transfer length. It can be considered as the critical distance over which most of the charges are injected from the metal contacts into the semiconductor.[241] At $x = 0$, the width-normalized source contact resistance r_S can be expressed as (R_S is source contact resistance):

$$r_S = R_S \cdot W = L_T R_{sh} \coth\left(\frac{L_c}{L_T}\right) \tag{14}$$

Under the assumption that ρ_c is identical for source and drain electrodes region, we obtain $R_c = 2R_S$.

Recently, Ante et al. reported an analysis of the influence of R_c and L_c on the effective mobility and the operating frequency in staggered OFETs based on the current crowding model.[211] They aggressively scaled the contact and channel dimension down to a few micrometers and investigated the relationship between L_T, L_c, and R_c.

In Figure 27, effective mobilities of DNTT OFETs and width-normalized R_c are plotted as a function of L_c in (a) and

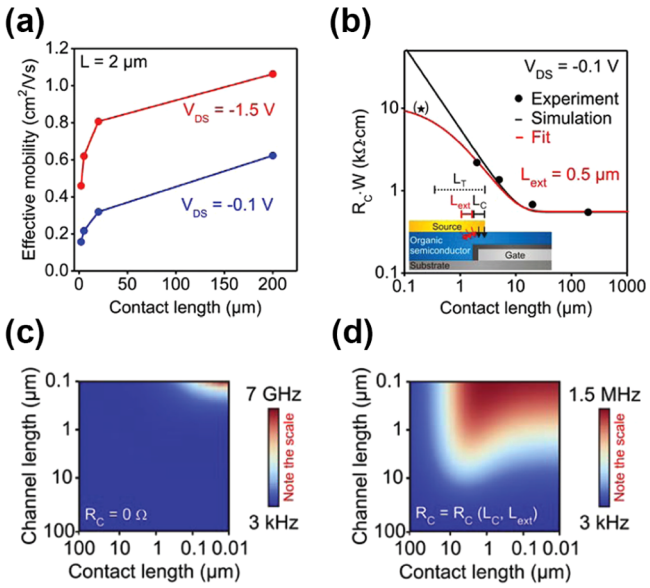

Figure 27. (a) Effective mobilities of DNTT OFETs as a function of L_c in the saturation (red curve) and the linear regimes (blue curve) (L = 2 μm). (b) Width-normalized R_c as a function of L_c. Simulation results of cutoff frequency depending on L and L_c of staggered OFETs assuming that $R_c = 0$ (c) or that R_c depends on L_c (d). Adapted with permission from ref 211. Copyright 2012 John Wiley and Sons.

(b), respectively.[211] Reducing L_c below L_T leads to a significant increase in R_c and thus to a decrease in the effective mobility. For best fitting results, an extended contact length L_{ext} was added to the contact length L_c to calculate the contact resistance from eq 14. The extended contact length L_{ext} is motivated by the fact that charge is not only injected vertically at these small dimensions. At the edges of the overlap area between source electrode and gate, charge is injected in a nonperpendicular direction as well due to the electrostatic potential distribution in the organic semiconductor, which was found in a two-dimensional numerical model simulation.[233]

Figure 27c and d shows results of a simulation examining the influence of the contact resistance on the maximum switching frequency of OFETs. The cutoff frequency of staggered OFETs is plotted for varying L and L_c assuming that $R_c = 0$ (c) or that R_c is a function of L_c described by eq 14 (d). In the ideal case of zero R_c, the cutoff frequency increases dramatically into the gigahertz range by reducing L_c and L. However, when contact effects induced by the variation of L_c and L are taken into account, the cutoff frequency is found to be strongly limited. According to the dynamic performance of the actual OFET devices, indeed, the measured switching frequency shows

DOI: 10.1021/acs.chemrev.6b00329
Chem. Rev. 2016, 116, 13714−13751

Pictiva EX2009
Samsung v Pictiva
IPR2026-00129

reasonable agreement with the simulation results in Figure 27d. This indicates that R_c of OFETs plays a significant role limiting the effective mobility as well as the operating frequency. Therefore, contact doping, which can reduce R_c efficiently, is a promising strategy to improve the operating frequency beyond the megahertz level.

To extract the contact resistance R_c experimentally, the transfer (or transmission) line method (TLM) is commonly used in the field of OFETs,[242,243] even though it was first developed for amorphous silicon thin-film transistors (TFTs).[244] The TLM method relies on the approximation that the contact resistance does not depend on the channel length L, but is mostly governed by the interfacial properties, whereas R_{ch} scales with the channel length L.

From the drain current I_D versus voltage V_{DS} relation in the linear regime, the channel resistance R_{ch} can be determined by

$$R_{ch} = \left.\frac{\partial V_{DS}}{\partial I_D}\right|_{V_{DS}\to 0} = \frac{L}{\mu C_{ins} W (V_G - V_T)} \tag{15}$$

where μ denotes the field-effect mobility, C_{ins} is the capacitance of the dielectric per unit area, V_G is the gate voltage, and V_T is the threshold voltage. Hence, if the total resistance R_{tot} is plotted versus the channel length L at a given V_G, a linear relationship is obtained. According to eqs 8 and 15, the y-axis intercept can be interpreted as the contact resistance R_c. This relation can be used as well to obtain other parameters such as the charge carrier mobility μ and the threshold voltage V_T by varying V_G.[245] In Figure 28, a representative example for the TLM technique is shown.[243] Here, the TLM can be used to determine the dependency of R_c on V_G from the y-axis intercept variation for varying V_G.

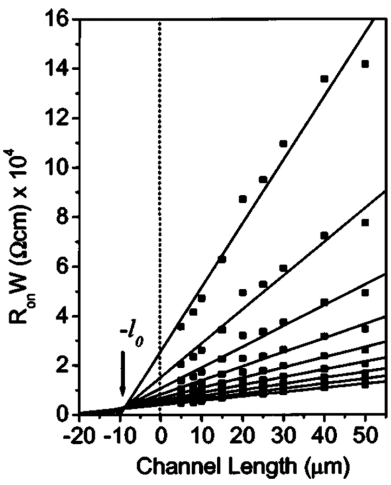

Figure 28. Normalized device resistance as a function of L for gate voltages V_G ranging from −20 to −100 V, extracted from pentacene transistors with L between 5 and 50 μm and a channel width of 400 μm. The y-intercepts of the solid lines give the contact resistance R_c at varying V_G. Reprinted with permission from ref 243. Copyright 2003 AIP Publishing.

Although the TLM technique is often used to extract the contact resistance R_c and is straightforward to interpret, it shows some major drawbacks, which are in particular caused by the implicit assumption that the device parameters are identical for different samples with varying channel length L. However, sample-to-sample variations are hard to avoid in the experiment, especially if the transistors are not based on single-crystalline materials. In these TFTs, the electrical performance is sensitive to morphological changes in the organic films as well as small changes in the fabrication conditions, making it difficult to reduce a significant spread in device parameters.[246] To overcome these problems, Xu et al. proposed to modify the conventional TLM by plotting R_{tot}/L versus $1/L$ instead of R_{tot} versus L. Thus, the slope of the fitted line becomes a function of R_c, which generally shows less variation as compared to the channel-related parameters, which leads to more reliable fitting results.[247]

The gated four-point-probe (gFPP) technique is another measurement method that is used to directly determine the contact resistance of a single OFET device. Originally, it was proposed for inorganic TFTs and was used to measure the intrinsic electrical performance,[248] but it has been extended to quantify the contact resistance R_c as well.[240,249,250] The fundamental circuit diagram and the principle of the gFPP technique are schematically illustrated in Figure 29.

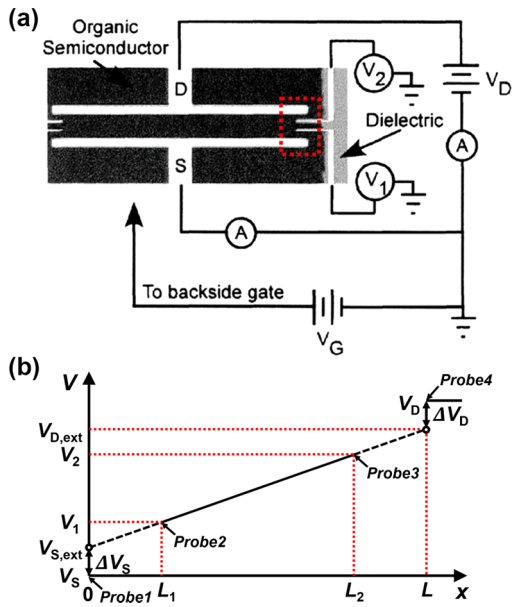

Figure 29. (a) Sketch of the gFPP measurement configuration. Reproduced with permission from ref 249. Copyright 2004 AIP Publishing. (b) Principle of gFPP. The schematic represents the area enclosed by the red dotted line in (a).

Two additional high-impedance probes are defined in the channel between the source and drain to measure the local potential inside the channel. As shown in Figure 29, the channel potential at the source and drain electrode $V_{S,ext}$ and $V_{D,ext}$, that is, at $x = 0$ and $x = L$, can be extrapolated from the two potentials V_1 and V_2 at the position of the two additional probes located at $x = L_1$ and $x = L_2$. From the difference between the externally applied potential, that is, V_S and V_D, and the extrapolated potential, the voltage drops ΔV_S and ΔV_D at both contacts are extracted, which can be converted to the contact resistance at source R_S and drain R_D electrodes by Ohm's law ($R_S = \Delta V_S/I_{DS}$).

The gFPP method is only exact if a constant mobility is assumed, which is usually not fulfilled at high drain voltages or low gate voltages, that is, when the device is in the saturation regime.[249] Furthermore, the gFPP technique requires the deposition of two additional electrodes, which adds to the

DOI: 10.1021/acs.chemrev.6b00329
Chem. Rev. 2016, 116, 13714−13751
Pictiva EX2009
Samsung v Pictiva
IPR2026-00129

device complexity. Still, due to its ability to extract R_S and R_D directly from measurements on a single device, it is highly beneficial for the study of contact effects at the metal/organic interface as recently reviewed by Natali and Caironi.[245]

5.1.2. Quasi-Ohmic Contacts Realized by Doping. Doping primarily creates free charges by a charge transfer between the host and the dopant molecules, which leads to an increase of electrical conductivity by several orders of magnitude in the bulk.[33] However, at the organic/metal interface, doping can have an even more pronounced effect on the electrical performance of organic electronic devices.

As shown in Figure 25, a space charge layer is formed at the metal/organic interface. Without doping, the width of the space charge region (W_{sc}) is relatively large (e.g., >10 nm), and charges are injected by thermionic emission across the energy barrier. Therefore, unless a metal contact is chosen, whose work function is similar to the LUMO level of organic semiconductor (for electron injection) or similar to the HOMO (for hole injection), these energy barriers greatly hinder the efficient charge injection.

Doping can help to overcome this limitation. In 2001, Blochwitz et al. investigated the level alignment at the interface between indium tin oxide (ITO) and either intrinsic ZnPc or ZnPc doped with F_4-TCNQ by UPS and XPS.[12] Figure 30

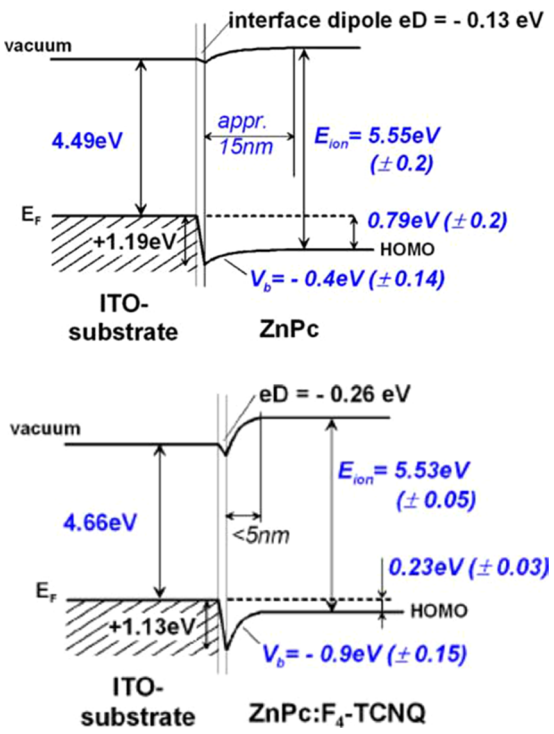

Figure 30. Energy level diagrams derived from UPS and XPS for undoped (top) and F_4-TCNQ-doped (bottom) ZnPc at the contact to ITO. Reprinted with permission from ref 33. Copyright 2003 Elsevier.

shows the energy level scheme obtained from the experiment. It can be observed that the HOMO level of doped ZnPc is shifted toward the Fermi level and the level bending becomes stronger as compared to the intrinsic layer. This observation agrees well with the Fermi level shift observed in doped pentacene shown in Figure 6 (section 2).

Although the hole injection barrier is almost identical for the doped and intrinsic case (about 1.2 eV), the thickness of the space charge region shrinks to less than 5 nm in the doped case. This very thin space charge layer allows for effective charge injection by tunneling, which was not achieved in the intrinsic layer. Hence, a quasi-Ohmic contact known from inorganic semiconductors is formed, which ensures efficient injection into the semiconductor.

This mechanism was studied for a wide range of electrode/organic semiconductor combinations as shown in Figure 31.[54]

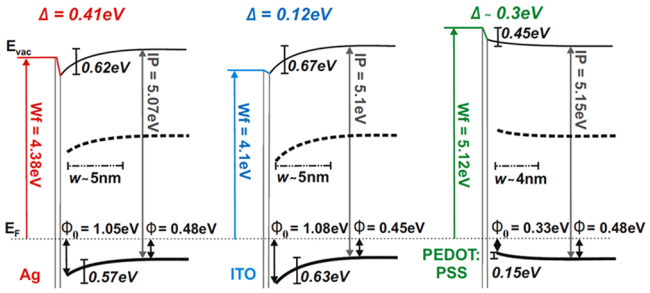

Figure 31. Energy level diagrams obtained from UPS and XPS measurements for F_4-TCNQ-doped MeO-TPD at the interfaces on the different electrodes (Ag, ITO, and PEDOT:PSS). Reprinted with permission from ref 54. Copyright 2009 AIP Publishing.

For all cases shown in Figure 31, doping leads to strong level bending at the interface between contact and organic layer. The space charge layer is approximately 5 nm thick, which can be easily tunneled through. Hence, the interfacial barrier height ϕ_0 only plays a minor role for charge injection; that is, charge injection is not limited by a mismatch between the metal work function and the organic transport level.

The influence of quasi-Ohmic contacts realized by doping is shown in Figure 32. As seen from the $J-V$ characteristics of a

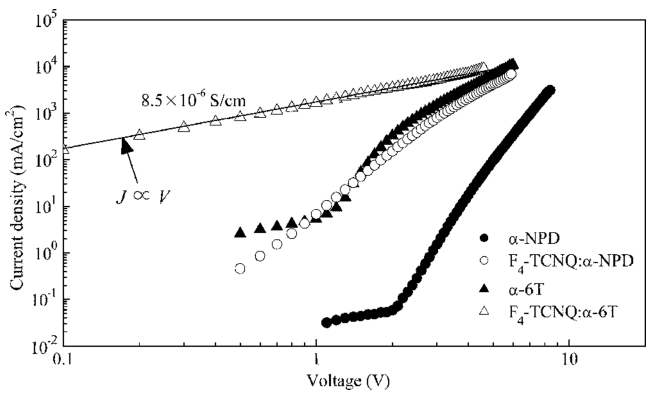

Figure 32. Current density−voltage characteristics of hole only transport devices, that is, ITO/organic layer/Ag/Al, with α-NPD, F_4-TCNQ-doped α-NPD, α-6T, and F_4-TCNQ-doped α-6T layers. Reprinted with permission from ref 251. Copyright 2006 AIP Publishing.

metal−organic semiconductor−metal structure, using doped layers (F_4-TCNQ-doped *N,N′*-diphenyl-*N,N′*-bis(1-naphthyl)-1,1′-biphenyl-4,4′-diamine (α-NPD) or α-sexithiophene (α-6T)) leads to a linear, that is, Ohmic, relationship between current and voltage.[251] Therefore, contact doping generating such quasi-Ohmic contacts can be effectively applied to minimize contact resistances and to develop high performance OFETs.

5.1.3. Contact Doping for p-Type Transistors. As discussed so far, the main goal of contact doping is to reduce

DOI: 10.1021/acs.chemrev.6b00329
Chem. Rev. 2016, 116, 13714−13751

Pictiva EX2009
Samsung v Pictiva
IPR2026-00129

the contact resistance and accordingly to enhance charge injection in OFETs. The most straightforward way to realize a doped organic contact is to insert a pure dopant layer, for example, a layer of metal oxides,[227,252−255] metal halides,[15,20,256,257] or molecular dopants,[13,207,258] between the metal and the organic semiconductor.

Ante et al. studied the effect of a pure dopant layer on the contact resistance of p-type OFETs with submicrometer channel length (see Figure 33).[13] The OFETs consist of a

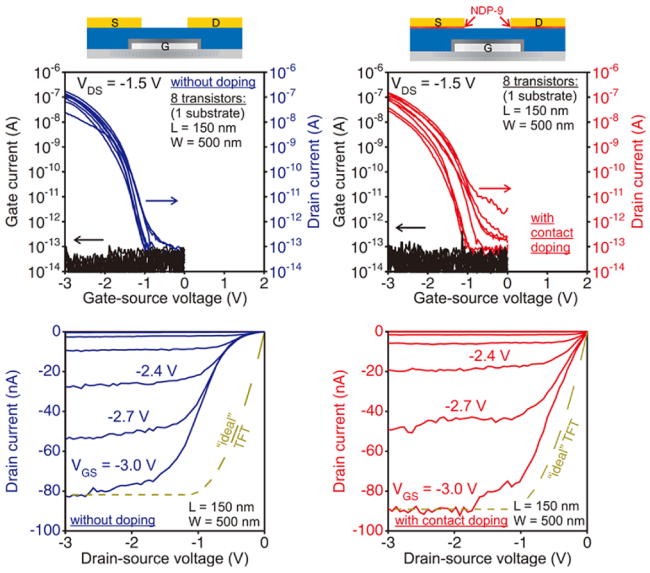

Figure 33. Device structure and transfer/output characteristics of submicrometer OFETs without (left) and with (right) contact doping. Reprinted with permission from ref 13. Copyright 2011 John Wiley and Sons.

5.7 nm-thick AlO_x gate dielectric, an organic SAM grown on top of the oxide layer, a layer of the organic semiconductor DNTT, and gold source/drain contacts. For a contact doping, a pure layer of the proprietary dopant NDP-9 (Novaled GmbH) is inserted between the metal and the organic layer. The source/drain contacts are structured by a suspended resist bridge defined by electron-beam lithography used as shadow mask, which yields nanoscale channel lengths.[14]

As clearly seen in the output curves of Figure 33, contact doping with NDP-9 not only increases the drain current but as well diminishes the nonlinearity at a low voltages as compared to the undoped case. For example, the drain current at V_{GS} = −3 V and V_{DS} = −0.5 V increases from −5 to −30 nA. This increase of the drain current is obviously attributed to a reduction in the contact resistance at the contact/semiconductor interfaces by contact doping.

Another viable strategy to realize efficient contact doping is the codeposition of host and dopant materials. This process has been extensively investigated either in solution processed films[162,166,213] or in films prepared by coevaporation.[21,188,259−261] A representative study is summarized in Figure 34.[16] Tiwari et al. used $Mo(tfd)_3$ as p-dopant for pentacene OFETs. As mentioned in section 3, the electron affinity of $Mo(tfd)_3$ was reported as 5.6 eV,[96] which is large enough to dope pentacene. For contact doping, a 10 nm thick layer of a 1:1 mixture of $Mo(tfd)_3$ and pentacene is selectively deposited in the source/drain electrodes area (see Figure 34a for a sketch of the structure). From the electrical characteristics,

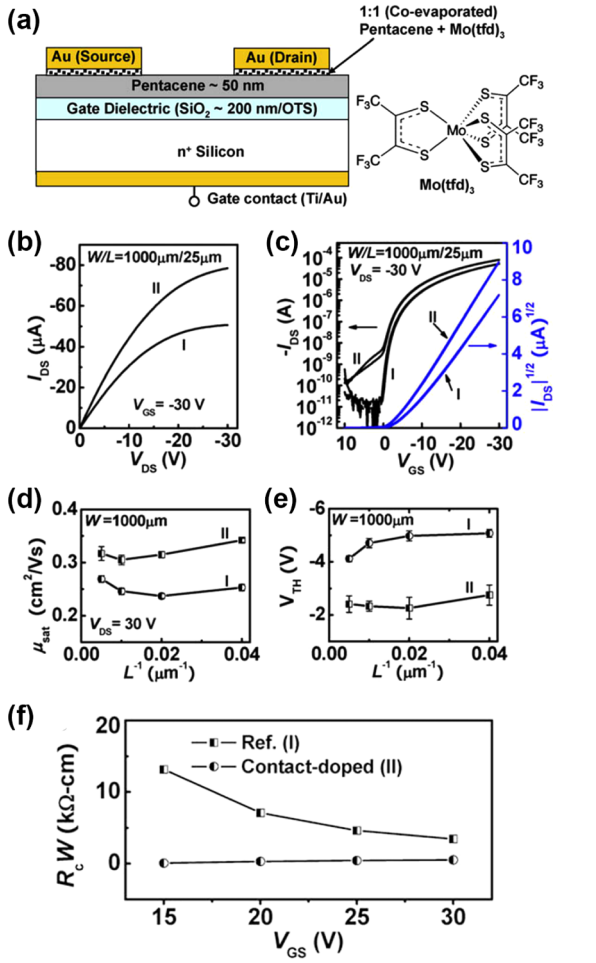

Figure 34. (a) Device structure and chemical structure of $Mo(tfd)_3$. (b) The output and (c) the transfer characteristics of OFETs without and with contact doping. Comparison of (d) the mobility, (e) the threshold voltage, and (f) the contact resistance. Adapted with permission from ref 16. Copyright 2010 Elsevier.

it is seen that I_D increases about 50% by contact doping for devices with W/L = 1000 μm/25 μm. Figure 34d and e shows the improvement of the effective mobility and the threshold voltage as compared to the undoped OFETs regardless of the channel length. To examine the effect of doping more specifically, the contact resistance for each type of devices is extracted using TLM as discussed above. The plots of width-normalized contact resistance R_cW at different V_{GS} are compared in Figure 34f, and it is found that the contact resistance is indeed decreased, for example, from 3.4 to 0.5 kΩ cm in the strong accumulation regime (V_{GS} = −30 V).

OFETs using the staggered structure usually show a lower contact resistance than coplanar OFETs, which is due to the relatively large charge injection area. From an industrial point of view, however, bottom gate and bottom contact configurations offer the possibility to employ high-resolution lithography to structure devices without damaging the organic semiconductor. To take advantage of this configuration, the doped injection layer has to be structured by lithography as well to avoid unwanted channel doping and a decrease in the ON/OFF ratio of the transistor.

Nicht et al. demonstrated a promising approach that combines the properties of SAMs, which selectively attach to gold electrodes, with molecular doping to improve charge

DOI: 10.1021/acs.chemrev.6b00329
Chem. Rev. 2016, 116, 13714−13751

Pictiva EX2009
Samsung v Pictiva
IPR2026-00129

injection into coplanar OFETs (cf. Figure 35).[262] In this study, F_4-TCNQ is functionalized with sulfur-containing triazole

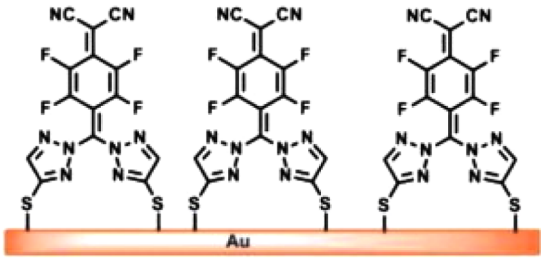

Figure 35. Functionalizing organic dopants by groups that selectively bind to metals allows for the directed assembly of self-assembled monolayers of dopants on source and drain electrodes. Nicht et al. proposed a sulfur-functionalized F_4-TCNQ derivative to increase injection into bottom contact OFETs. Reprinted with permission from ref 262. Copyright 2014 Elsevier.

anchor groups via nucleophilic substitution in a simple substitution reaction. By selective assembly of a sulfur-functionalized F_4-TCNQ derivative exclusively on the source and drain electrodes, current injection is significantly increased in pentacene-based OFETs. The effective mobility is also improved by a factor of 3 from 0.08 to 0.24 $cm^2/(V{\cdot}s)$, which indicates that a SAM of functionalized dopant is effective for the reduction of contact resistance.

The morphological stability of doped films is a major concern of doping in particular for elemental dopants (see as well section 4). If dopants are mobile in the film, there is a possibility of dopants diffusing into the channel, which would lead to unintentional doping of the channel and an increase in the off-state current. However, Figure 36 shows that molecular dopants and transistion metals show sufficient stability in the transistors. The results of bias stress measurements for NDP-9-doped submicrometer OFETs[13] and $Mo(tfd)_3$-doped pentacene OFETs[16] are summarized. In both cases, the electrical

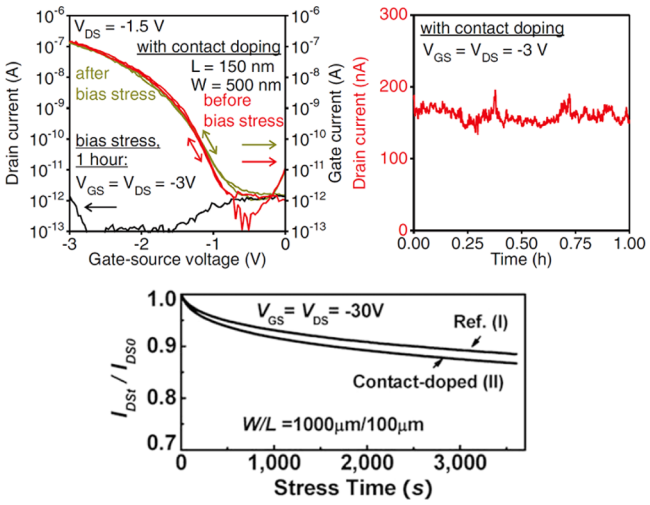

Figure 36. Bias stress measurement for contact-doped OFETs. Transfer characteristics of a submicrometer OFET with contact doping before and after bias stress, and the measured drain current during bias stressing time (top). Reprinted with permission from ref 13. Copyright 2011 John Wiley and Sons. Decay of drain current measured continuously over a period of 1 h (bottom). Reprinted with permission from ref 16. Copyright 2010 Elsevier.

properties are not significantly changed for increasing stressing times, which indicates that contact doping is effective without compromising the electrical stability.

5.1.4. Contact Doping for n-Type Transistors. As was already mentioned in section 4, n-doping is rather challenging as compared to p-doping due to the increased sensitivity of n-dopants to air exposure. However, to design complementary circuits, the development of n-channel OFETs with a performance comparable to that of p-channel OFETs is essential. Therefore, similar to p-contact doping, a wide range of approaches have been proposed to induce n-doping, leading to the improvement of charge injection of n-type transistors. For example, interlayers of Ca,[263] TiO_x,[229] conjugated polyelectrolyte,[264] or water-soluble polyfluorene derivatives[265] were introduced between organic semiconductor and electrodes and soluble mixtures such as CsF-doped PCBM,[213] P(NDI2OD-T2) mixed with $CoCp_2$ or CsF,[266] and C_{60}, C_{70}, or PCBM doped by N-DMBI were shown to improve injection as well.[267]

Recently, Singh et al. demonstrated the reduction of the contact resistance by selective contact doping in bottom-gate and top-contact C_{60} OFETs using rhodocene dimer as a dopant (Figure 37a).[17] In Figure 37b and c, the transfer and the output

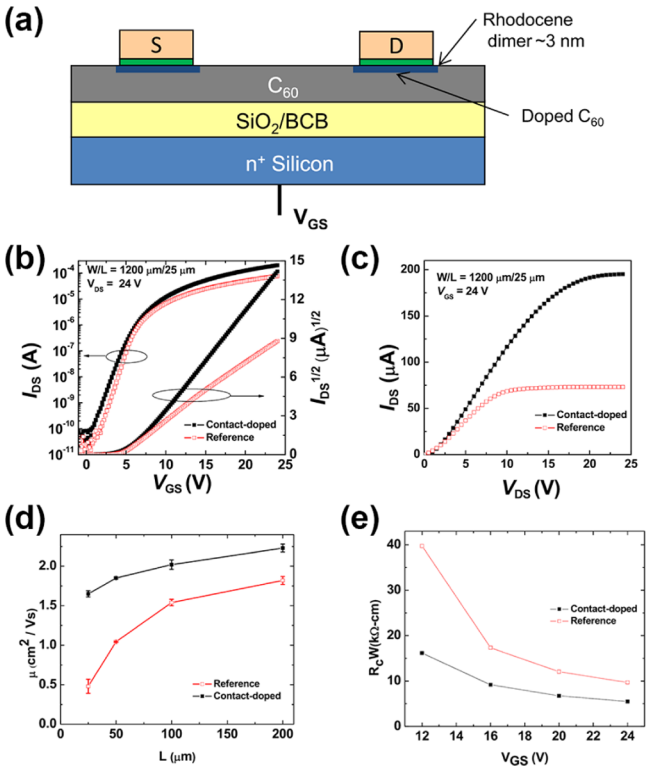

Figure 37. (a) Device structure of contact-doped C_{60} OFETs. (b) Transfer and (c) output characteristics of OFETs without and with contact doping. Comparison of (d) the mobility and (e) the contact resistance at varying channel lengths. Reproduced with permission from ref 17. Copyright 2013 AIP Publishing.

curves of contact-doped and undoped OFETs with a channel geometry of W/L = 1200 μm/25 μm are plotted, respectively. The output characteristics at V_{GS} = 24 V show that contact doping leads to a 3-fold increase in I_D as compared to the reference devices. Note that the off-current remains unchanged after doping, which is an indication that only the contact area is

DOI: 10.1021/acs.chemrev.6b00329
Chem. Rev. 2016, 116, 13714−13751

Pictiva EX2009
Samsung v Pictiva
IPR2026-00129

doped. As shown in Figure 37d, the mobility decreases for both doped and reference devices as the channel length reduces, but this decrease is more pronounced for the undoped case. The average mobility values for the undoped and the doped devices are extracted as 0.48 and 1.65 $cm^2/(V{\cdot}s)$ for $L = 25\ \mu m$; that is, the mobility is enhanced by about a factor of 3 by contact doping.

Singh et al. studied as well the effect of doping on the contact resistance using the TLM. The results indeed confirm that the contact resistance is reduced from 9.7 kΩ cm of reference OFETs to 5.5 kΩ cm of contact-doped devices at $V_{GS} = 24$ V (Figure 37e).

The influence of n-doping on the air-stability of n-channel OFETs was studied by Oh et al.[268] In this study, an active layer, *N,N′*-dibutyl-1,7-difluoroperylene-3,4:9,10-tetracarboxylic diimide (F-PTCDI-C4), is doped by pyronin B (see Figure 38a). Doping is introduced either in the contact region, in the whole bulk of the organic semiconductor, or selectively at the source/drain contacts.

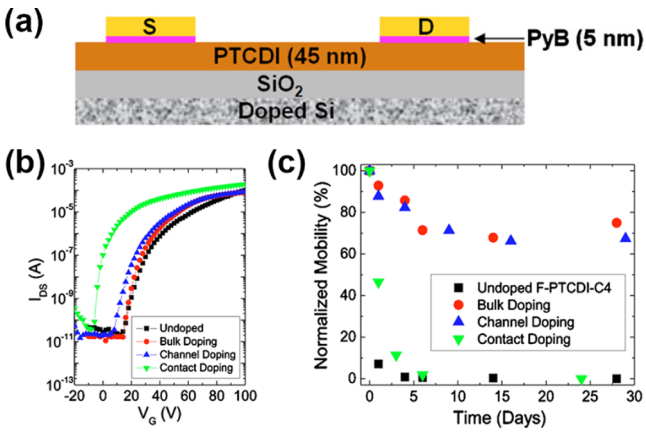

Figure 38. (a) Device structure of contact-doped F-PTCDI-C4 OFET. (b) Transfer characteristics of OFETs without and with n-doping. (c) Comparison of the normalized mobility. Reproduced with permission from ref 268. Copyright 2010 AIP Publishing.

In Figure 38b, the transfer characteristics of doped and undoped F-PTCDI-C4 OFETs measured in N_2 atmosphere are plotted. Field-effect mobilities of 0.2−0.3 $cm^2/(V{\cdot}s)$ are obtained with on/off ratios of 10^6, regardless of the position of the doped layer in the device. However, as compared to undoped, bulk doped, or channel doped devices, the threshold voltage of contact doped OFETs shifts toward more negative voltages, indicating that the devices are switched on at lower voltages. The air-stability of pyronin B-doped F-PTCDI-C4 OFETs is also investigated by periodically measuring the electrical performance while the devices are being stored in air. In Figure 38c, the extracted mobilities are normalized by those initially obtained in N_2 atmosphere for comparison. Interestingly, the performance of undoped F-PTCDI-C4 OFETs exhibits an immediate degradation by air-exposure, and the contact-doped devices gradually degrade as well. This means that contact doping leads to the enhancement of charge injection, but charge trapping in the channel region by air-exposure still remains a major issue in this particular study. In contrast, the air-stability of channel-doped F-PTCDI-C4 OFETs is improved significantly. The detailed underlying principles are discussed in section 5.2.

Contact doping was as well shown to be effective for solution-processed OFETs. A recent study argued that PCBM-based transistors can be n-doped by cesium fluoride (CsF) by either solution blending or inkjet printing. Ohmic injection independent of the gate bias is observed.[213] Particularly, in this study, the selective tuning of the operational mode from ambipolar to unipolar transport is achieved by molecular doping, which will be discussed in detail section 5.2.3. Here, PCBM and a perfluoropolymer, CYTOP, are utilized as the pristine organic semiconductor and the gate dielectric, respectively, and the top-gate/bottom-contact (TG/BC) structure is adopted to investigate the doping effect on the charge injection and transport. In this system, as the Fermi level of CsF (1.9−2.0 eV) lies above the LUMO level of PCBM (∼3.7 eV), electron transfer from CsF into PCBM is energetically favorable, leading to efficient n-doping.

Figure 39a and b shows the transfer characteristics of CsF-doped PCBM OFETs for p-channel and n-channel operation. It is clearly seen that the undoped devices originally show ambipolar charge transport; however, p-channel operation is increasingly suppressed while n-channel operation becomes dominant as the n-doping concentration increases. This conversion from the ambipolar to unipolar feature is mainly attributed to the Fermi level shift toward the transport level by doping. For 1.0 wt % CsF-doped OFETs, the electron mobility and the hole mobility are remarkably changed from 0.067 and 0.030 $cm^2/(V{\cdot}s)$ to 0.13 and 5.9×10^{-5} $cm^2/(V{\cdot}s)$, respectively, indicating negligible hole transport.

The output curves of undoped and n-doped PCBM OFETs are plotted in Figure 39c and d. The nonlinearity at low V_d originates from large charge injection barriers for undoped devices, but disappears after n-doping, which confirms that the contact resistance is reduced. The contact resistance is extracted using modified-TLM introduced above (Figure 39e). It turns out that for n-type doping the contact resistance is dramatically reduced, and becomes independent of the gate voltage, that is, exhibiting an Ohmic contact behavior. This is a strong evidence that CsF doping reduces the thickness of the depletion layer and enables tunneling injection at the interface of electrode and doped PCBM.

5.2. Channel Doping

Although contact doping is much more common, doping the channel region of the transistor receives increasing attention as well. Channel doping has a couple of advantages; most importantly it presents a way to fine-tune the transistor characteristic, to control the threshold voltage, and to increase the stability of the transistors.

5.2.1. Doped Organic MIS Junctions. A doped metal−insulator−semiconductor (MIS) junction is at the heart of every doped organic transistor. The band structure of a p-doped MIS junction is shown in Figure 40. Here, W_f denotes the work-function of the metal, IP the ionization potential of the organic semiconductor, η the difference between the ionization potential and the Fermi level in the organic semiconductor, and δ a dipole located at the interface between the insulator and the semiconductor.

Similar to metal/semiconductor junctions discussed previously (section 5.1), charge is redistributed inside the junction until the work function of the metal and the organic semiconductor align and a constant Fermi level is formed. For example, if the work function of the semiconductor exceeds the work function of the metal (i.e., $IP - \eta > W_f$), the p-doped

DOI: 10.1021/acs.chemrev.6b00329
Chem. Rev. 2016, 116, 13714−13751
Pictiva EX2009
Samsung v Pictiva
IPR2026-00129

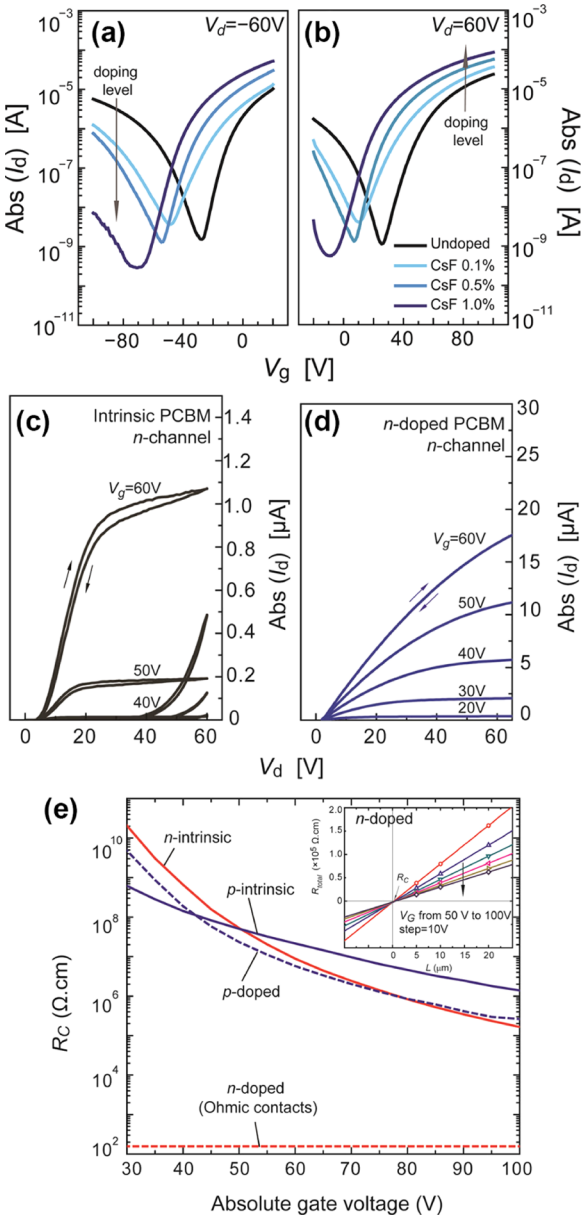

Figure 39. Transfer characteristics of CsF-doped PCBM OFETs for (a) p-channel and (b) n-channel operation. Output characteristics of (c) undoped and (d) doped PCBM OFETs for n-channel operation. (e) R_c of TG/BC PCBM OFETs with varied gate-voltage. Inset shows R_c of CsF-doped PCBM OFETs extracted by modified-TLM. Adapted with permission from ref 213. Copyright 2014 John Wiley and Sons.

layer is depleted at the interface to the insulator, which generates a negative space charge layer.[54] The thickness of this depletion layer d_{dep} can be calculated as[68,269]

$$d_{dep} = \frac{\varepsilon_0 \varepsilon_s}{C_{ins}}\left[\sqrt{1 + \frac{2C_{ins}^2(V - V_{FB})}{eN_A\varepsilon_0\varepsilon_s}} - 1\right] \quad (16)$$

with ε_0 the permittivity of vacuum, ε_s the relative permittivity of the semiconductor, C_{ins} the capacitance of the insulator per unit area, $e = +1.6 \times 10^{-19}$ C the elementary charge, V the voltage applied between metal and semiconductor (counting the potential on the metal positive), and N_A the doping concentration in the p-doped semiconductor.

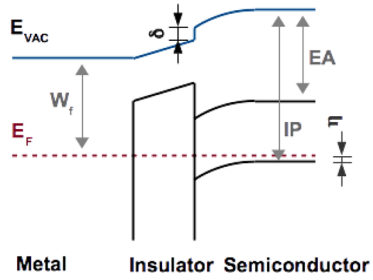

Figure 40. Alignment of energy levels in a metal−insulator-p-doped semiconductor junction. Because of the difference in chemical potential of the metal and semiconductor, a thin layer at the insulator−semiconductor interface is depleted forming a negative space charge layer. The thickness of this depletion layer can be modulated by the voltage applied between the metal and the semiconductor.

V_{FB} denotes the so-called flatband voltage, which is defined as the voltage that has to be applied between the organic semiconductor and the metal to induce flat energy levels. Including charged trap states Q_{trap} at the insulator/organic semiconductor interface, in the insulator, or in the organic semiconductor, the flatband voltage becomes:

$$eV_{FB} = W_f - (IP - \eta) - \delta - Q_{trap}/C_{ins} \quad (17)$$

The thickness of the depletion layer (eq 16) and the flatband voltage (eq 17) can be determined experimentally by UPS. Olthof et al. studied the alignment of energy levels in a MIS junction consisting of a silver electrode, 5 nm of the intrinsic organic semiconductor MeO-TPD operating as insulator, and a p-doped MeO-TPD layer of varying thickness.[54] The position of the HOMO level for different thickness of the doped layer is shown in Figure 41. As expected, the HOMO level bends

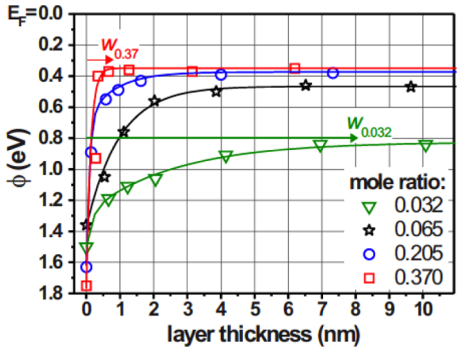

Figure 41. Evolution of the HOMO level (Φ) of an organic MIS junction consisting of a silver cathode, an intrinsic layer of MeO-TPD, and a p-doped layer of Meo-TPD of varied thickness. From the plot, the thickness of the depletion layer and the flatband voltage can be deduced, which shows the same trends as predicted by eqs 16 and 17. Reprinted with permission from ref 54. Copyright 2009 AIP Publishing.

upward at the interface between the intrinsic and the doped MeO-TPD layer, indicating the formation of a depletion layer. Level bending becomes stronger for increased doping concentrations, and, in accordance with eq 16, the depletion layer shrinks with increasing doping concentrations. Olthof et al. found a depletion layer thickness of 8 nm for a molar doping ratio of 0.032, which decreases to 0.6 nm at a molar doping ratio of 0.37. In the same way, the flatband voltage increases

DOI: 10.1021/acs.chemrev.6b00329
Chem. Rev. 2016, 116, 13714−13751

Pictiva EX2009
Samsung v Pictiva
IPR2026-00129

from 0.66 V (MR = 0.032) to 1.4 V (MR = 0.37), which can be explained by the shift of the Fermi level of the doped organic semiconductor toward the HOMO level, for example, by a decrease of η in eq 17.

5.2.2. Doped Organic Transistors. Tuning the MIS junction of an organic transistor by doping has profound influences on the transistor operation. The general setup of a p-doped transistor was already shown in Figure 24. The semiconductor layer is doped by a p-dopant, for example, by F_4-TCNQ or F_6-TCNNQ. In some cases, doping is restricted to a thin layer (thickness d_{dop}) at the interface to the insulator. Finally, the source and drain contacts can be p-doped[21] or a metal can be used that shows sufficient hole injection to ensure efficient hole injection.

A representative transfer characteristic of a p-doped transistor is shown in Figure 42. As indicated in the figure,

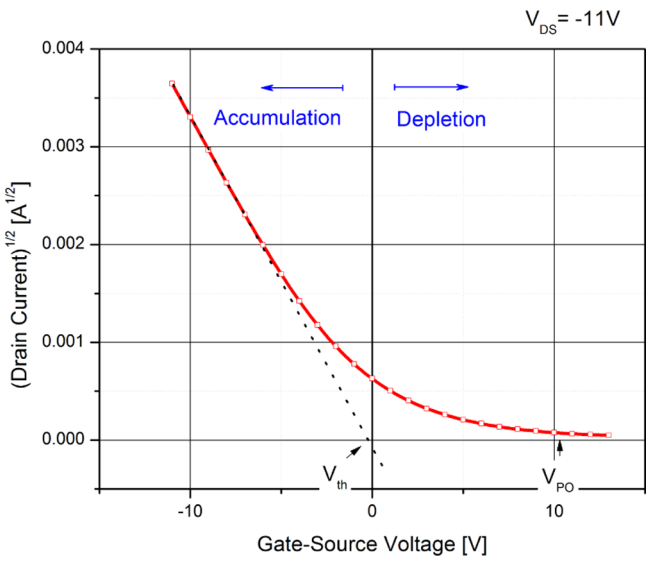

Figure 42. Transfer characteristic of a doped organic transistor as sketched in Figure 24. The transistor consists of p-doped pentacene channel (d_{dop} = 8 nm, doping concentration 2 wt %), intrinsic pentacene, and p-doped injection contacts. Details of the device structure and preparation conditions are given in ref 21.

the transistor can be operated in two regimes. At large negative voltages ($V_{GS} < V_{th}$), holes are electrostatically accumulated at the insulator/organic layer (accumulation regime), whereas at large positive voltages ($V_{GS} > V_{th}$), the doped channel is increasingly depleted (depletion regime). To fully deplete the doped channel and switch the transistor off, the so-called pinch-off voltage V_{PO} has to be applied to the gate. In the following, the accumulation and depletion regime are discussed separately.

5.2.2.1. Accumulation Regime. If large negative voltages are applied to the gate of the p-doped transistor (i.e., for $V_{GS} < V_{th}$), holes are accumulated in the channel, which increases the density of free holes beyond the doping concentration. Although the density of accumulated holes can significantly exceed the density of holes introduced by doping, doping has still a pronounced influence on the threshold voltage. This influence can be understood by considering the total density of free holes in the channel given by

$$p(x) = \frac{C_{ins}w(V(x) - (V_{GS} - V_{FB}))}{eA} + N_A \quad (18)$$

$$= \frac{C_{ins}w\left(V(x) - V_{GS} + V_{FB} + \frac{edN_A}{C_{ins}}\right)}{eA} \quad (19)$$

where w denotes the width of the channel, e is the elementary charge, $A = dw$ is the cross-section of the channel, d is the thickness of the accumulation layer, and N_A is the density of ionized dopants in the channel.

Using the relation $j = ep(x)E_x\mu_p$ (E_x is the electric field in x-direction, μ_p is the hole mobility) and integrating across the whole channel leads to the following relation for the drain current I_D:[269]

$$-I_D = \frac{\mu_p C_{ins}w}{L}\left[\left(V_{GS} - V_{FB} - \frac{edN_A}{C_{ins}}\right)V_{DS} - \frac{1}{2}V_{DS}^2\right] \quad (20)$$

$$= \frac{\mu_p C_{ins}w}{L}\left[(V_{GS} - V_{th})V_{DS} - \frac{1}{2}V_{DS}^2\right] \quad (21)$$

Equation 21 resembles the relation for the drain current of standard, that is, undoped transistors, except that the threshold voltage is altered. Under the assumption that the thickness of the doped layer d_{dop} is small, one obtains:

$$V_{th} \approx V_{FB} + \frac{eN_A d_{dop}}{C_{ox}} \quad (22)$$

Hence, the threshold voltage depends on the doping concentration and the thickness of the doped channel and can be shifted by the doping concentration and thickness of the doped layer.

Equation 22 has been confirmed by several authors in the past. A shift of the threshold voltage due to doping was observed for a wide variety of material combinations including p- and n-type transistors and polymer and small molecular semiconductors. For example, transistors based on pentacene doped by MoO_x,[23] F_4-TCNQ,[259] or F_6-TCNNQ,[21,212] TIPS-pentacene doped by tris-[1-(trifluoroethanoyl)-2-(trifluoromethyl)ethane-1,2-dithiolene] ($Mo(tfd\text{-}COCF_3)_3$),[270] P3HT doped by F_4-TCNQ,[166] perylene diimides doped by pyronin B,[268] PCBM doped by N-DMBI,[132] poly[4-(4,4-dihexadecyl-4*H*-cyclopenta[1,2-*b*:5,4-*b*′]dithiophen-2-yl)-*alt*-[1,2,5]thiadia-zolo-[3,4-*c*]pyridine] (PCDTPT) doped by I_2 vapor,[271] P3HT doped by gold nanoparticles,[272] or a mixed layer of sexithiophene and dihexylsexithiophene doped by oxygen[273] show a shift of the threshold voltage with increasing doping concentration.

One representative example reported by the Heeger group is shown in Figure 43.[271] Lee et al. prepared polymer-based transistors using the high-mobility material PCDTPT on top of a nanogrooved gate oxide to improve the alignment and order in the polymer film. The transistors are reported to show a charge carrier mobility of 18.1 $cm^2/(V\cdot s)$ in the linear region and as high as 58.6 $cm^2/(V\cdot s)$ in the saturation regime (Figure 43). Lee et al. argue that the as-prepared transistors show some unintentional doping leading to a threshold voltage of approximately V_{th} = 7 V. Exposing the devices to iodine p-dopes the film further, resulting in an increase in threshold voltage to 14 V, whereas exposing the devices to ammonia vapor compensates the p-doping effect and a shift of the threshold voltage to close to 0 V.

DOI: 10.1021/acs.chemrev.6b00329
Chem. Rev. 2016, 116, 13714−13751
Pictiva EX2009
Samsung v Pictiva
IPR2026-00129

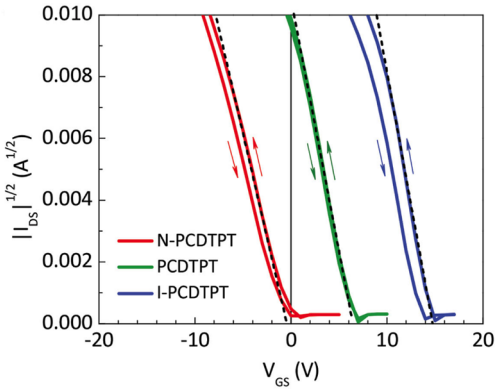

Figure 43. Doping the high mobility polymer PCDTPT leads to a strong shift in the transfer characteristic of the corresponding transistor.[271] The intrinisic transistor (green) shows a threshold voltage of around 7 V. The p-doping by exposing the device to iodine vapor results in a shift toward higher voltages (blue), whereas exposing the device to ammonia vapor deactivates doping (red). Reprinted with permission from ref 271. Copyright 2016 John Wiley and Sons.

Most reports on doped organic transistors study the influence of the doping concentration on the threshold voltages. However, according to eq 22, the thickness of the doped layer can be used as well to tune the transfer characteristic. This effect was studied by the Leo group,[21] and the results are shown in Figure 44. Indeed, an increase in doped layer thickness d_{dop} increases the threshold voltage linearly.

Doping in organic transistors often comes at the expense of a reduced charge carrier mobility due to an increase in disorder in the film (see, e.g., the discussion in section 4).[185] To overcome this limitation, some researchers propose not to dope the organic semiconductor directly, that is, not to mix a low concentration of dopants into the matrix semiconductor, but to add a dopant layer on top[22,24,274] or below an intrinsic charge transport layer instead,[80,209,275−278] which is called surface, transfer, or remote[260] doping.

For example, Hählen et al.[24] deposited a pure layer of F_4-TCNQ on top of a pentacene bottom-gate transistor and showed that the threshold voltage is increasing with increasing F_4-TCNQ coverage (Figure 45). However, this effect strongly depends on the thickness of the intrinsic pentacene layer; that is, the shift of the threshold voltage for thicker pentacene layer is significantly reduced. Still, even at a thickness of 10 monolayers of pentacene, a small shift in V_{th} is observed, which is rationalized by the grain structure of pentacene films and the ability of F_4-TCNQ to accumulate at grain boundaries.

The group of Kahn et al. proposed a similar approach to remotely dope pentacene films.[260] They add a doped layer of α-NPD on top of an intrinsic layer of pentacene. The α-NPD film is reported to transfer some of the holes generated by doping to the intrinsic pentacene. Hence, the conductivity of the pentacene film increases and the threshold voltage shifts toward positive voltages.[260]

SAMs are another example of successful surface doping. Adding a SAM on top of the gate insulator is known to have a strong influence on the threshold voltage.[279−281] Often, this effect is explained by the molecular dipole introduced at the insulator/organic interface δ, which is supposed to shift the flatband voltage according to eq 17. Indeed, it was found that the shift of the threshold voltage scales with the dipole moment

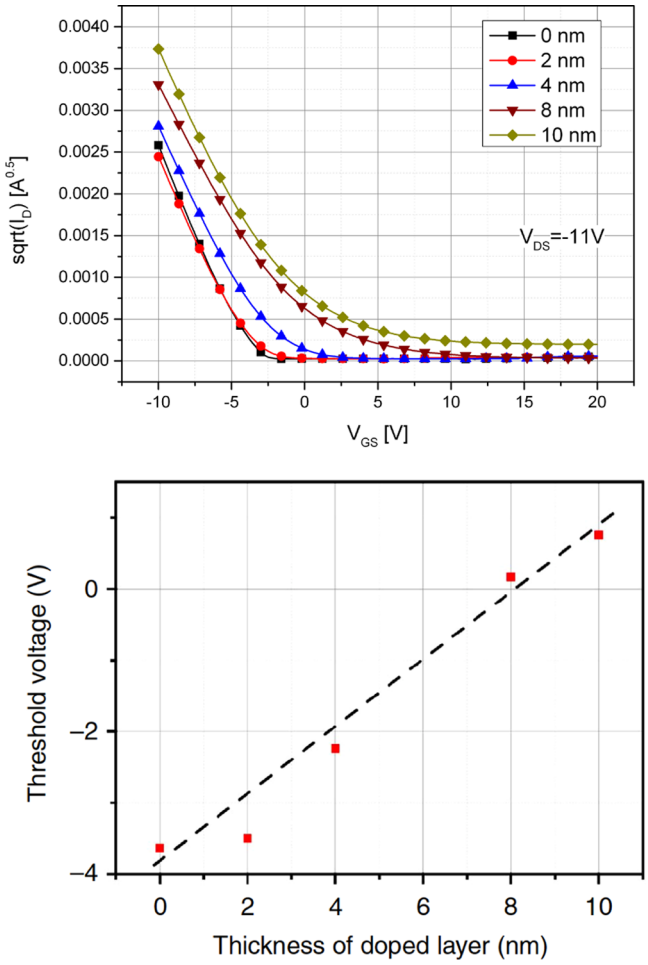

Figure 44. Influence of the thickness of the doped layer d_{dop} on the transfer characteristic of pentacene-based transistors (top). As predicted by eq 22, the threshold voltage increases for increasing d_{dop} (bottom). Reprinted with permission from 21. Copyright 2013 Nature Publishing Group.

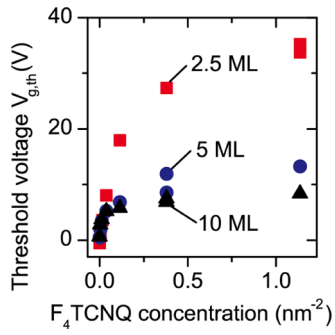

Figure 45. Transfer doping as proposed by Hählen et al.[24] Instead of doping the channel as in Figure 24, a pure F_4-TCNQ layer is deposited on top of an intrinsic pentacene layer. The strength of the shift of the threshold voltage depends on the thickness of the intrinsic pentacene layer. Reprinted with permission from ref 24. Copyright 2015 AIP Publishing.

of the SAM.[282,283] However, it has been argued that interface dipoles can only explain small shifts in threshold voltage (up to a few volts)[284] and that space charge layers induced by electronic coupling between the SAM and the organic

DOI: 10.1021/acs.chemrev.6b00329
Chem. Rev. 2016, 116, 13714−13751

Pictiva EX2009
Samsung v Pictiva
IPR2026-00129

semiconductor have to be taken into account to explain the observed threshold voltage shift.[277,285]

A very successful example of an interfacial SAM layer that introduces additional space charge at the interface and operates as a local doping layer was studied by the group of Zojer.[80,275,276] They functionalized the SAM with acidic end groups, which protonate the organic semiconductor at the interface (see as well section 3.1.3 for a detailed discussion of the doping mechanism). The SAM hence creates a local doped channel, which shifts the threshold voltage according to eq 22.

Doping can not only shift the threshold voltage by a generation of free charge carriers, but can as well be used to fill traps at the interface between gate insulator and organic semiconductor or in the organic semiconductor itself.[89] Figure 46 shows a recent example of this effect reported by Olthof et al.[51] Small amounts of the n-dopant $[RuCp^*(mes)]_2$ (see section 3.2.7) were added to either highly purified or as-received C_{60}. The corresponding shift of the threshold voltage is shown in Figure 46. The threshold voltage shift is much stronger for the unpurified material as compared to the purified C_{60}, which was interpreted as indication that doping mainly fills trap states in the device.[51]

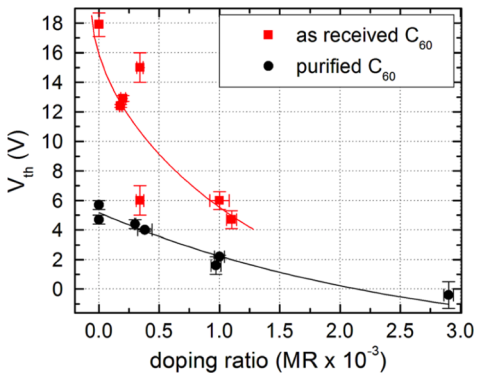

Figure 46. Filling traps in unpurified C_{60} by the n-dopant $[RuCp^*(mes)]_2$ leads to a strong shift of the threshold voltage. Reprinted with permission from ref 51. Copyright 2012 AIP Publishing.

Filling of matrix trap states by doping has the advantage that free charge carriers are not necessarily generated and that the ON/OFF ratio is not compromised by doping. This effect was used by Soeda et al.,[209] who used F_4-TCNQ to p-dope the organic semiconductor C8-BTBT. Although the EA of F_4-TCNQ is too small to generate free holes on the C8-BTBT matrix, the threshold voltage of doped transistors is reduced to almost zero volts and the hysteresis of doped transistors is significantly reduced.[209]

Passivation of traps in doped organic layers was furthermore used by Wei et al.[25] to improve the stability of n-type transistors. Doping the organic semiconductor PCBM with DMBI-derivatives[129] (see section 3.2.5) leads to a strong increase in air stability, which was rationalized in terms of a compensation of O_2 induced traps in PCBM. p-Doping has a positive influence on stability as well. As observed by Hein et al., p-doping the channel region can lead to a reduction in gate bias stress effects in pentacene-based transistors.[26] Similarly, Noh et al. found an improved air stability and smaller gate bias stress in doped ambipolar transistors.[213]

5.2.2.2. Depletion Regime. Doped organic transistors can as well be operated in the depletion region, for example, at $V_{GS} > V_{th}$ (see Figure 42). No charges are accumulated in this regime, but the doped organic layer is successively depleted. The thickness of the depletion layer varies with the distance from the source electrode; it is largest at the drain electrode, where the potential difference between the channel and the gate electrode is largest, and smallest at the source, where this potential difference is smallest. Between these two extrema, the depletion layer varies. If $V(x)$ denotes the potential in the channel at a distance x from the source (see Figure 24), the thickness of the depletion layer $d_{dep}(x)$ follows from eq 16 by replacing $V-V_{FB}$ by $V_{GS}-V(x)-V_{FB}$:

$$d_{dep} = \frac{\varepsilon_0\varepsilon_s}{C_{ins}}\left[\sqrt{1 + \frac{2C_{ins}^2(V_{GS} - V(x) - V_{FB})}{eN_A\varepsilon_0\varepsilon_s}} - 1\right] \quad (23)$$

The output characteristic of a doped pentacene transistor (d_{dop} = 8 nm) operated in the depletion region is shown in Figure 47. At low drain-source voltages and constant gate voltages the transistor shows a drain current I_D, which is proportional to the drain source voltage V_{DS} (linear regime). Thus, similar to undoped organic transistors, the transistors behave like a resistor, whose resistance is controlled by the gate voltage.

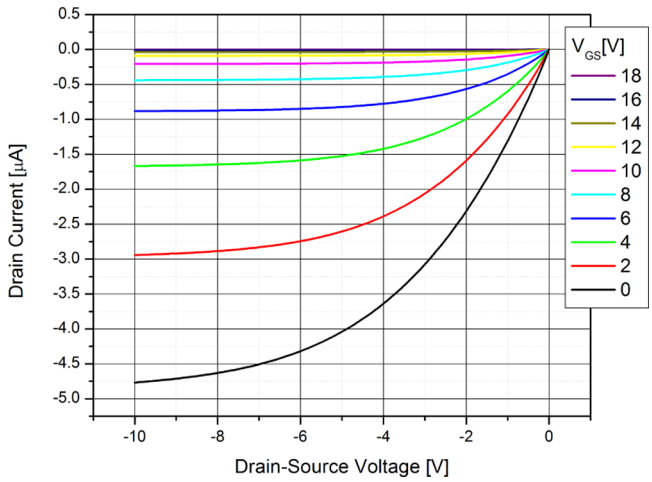

Figure 47. Output characteristic of the p-doped transistor sketched in Figure 24 operated in the depletion regime. The p-doped channel is 8 nm thick. Details of the device structure and preparation conditions are given in ref 21.

At a larger drain potential V_{DS}, the current saturates. This behavior can be understood by a full depletion of the doped layer at the drain contact; that is, the channel is pinched off at the drain. Setting the depletion layer thickness d_{dep} to the thickness of the doped layer d_{dop} and replacing the potential $V-V_{FB}$ by $V_{GS}-V_{FB}-V_{DS}^{sat}$ (the potential difference between gate and channel at the drain) in eq 16, one finds the following condition for saturation:[269]

$$V_{DS}^{sat} = V_{GS} - V_{PO} \quad (24)$$

Here, V_{PO} is the so-called pinch-off voltage, defined as[269]

$$V_{PO} = V_{FB} + \frac{eN_A d_{org}^2}{2\varepsilon_0\varepsilon_s}\left(1 + 2\frac{d_i}{d_{org}}\frac{\varepsilon_s}{\varepsilon_i}\right) \quad (25)$$

with ε_i as the relative permittivity of the insulator and d_i as the thickness of the insulator.

DOI: 10.1021/acs.chemrev.6b00329
Chem. Rev. 2016, 116, 13714−13751

Pictiva EX2009
Samsung v Pictiva
IPR2026-00129

For drain-source voltages larger than the saturation voltage, the pinch-off point moves slightly toward the source.[286] However, the potential at the pinch-off point remains at V_{DS}^{sat}. Furthermore, assuming that the channel length of the OFET is large (i.e., much larger than the movement of the pinch-off point), the electric field in the channel remains constant and hence the drain current saturates.

To completely turn the transistor off, the whole transistor channel has to be depleted. To reach a full depletion, the gate potential has to be large enough to deplete the channel at the source as well. Replacing $V-V_{FB}$ with $V_{GS}-V_{FB}$ in eq 16 leads to

$$V_{GS} = V_{PO} \tag{26}$$

That is, the pinch-off voltage has to be applied to fully switch the transistor off.

The increase in the pinch-off voltage by doping was studied systematically by Meijer et al.,[68] who exposed a circular polymer-based OFET to ambient air for a well-defined time. The result is shown in Figure 48. For longer exposure times, a higher voltage has to be applied to the gate to switch the channel off. Meijer et al. argue that this increase in the pinch-off voltage stems from p-doping due to oxygen. Indeed, using eq 25, they were able to deduce the doping concentration, which ranges from 10^{-16} to 10^{-17} cm^{-3}.

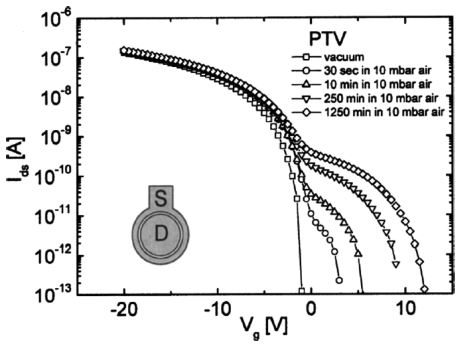

Figure 48. Increase in pinch-off voltage of polymer-based transistors due to doping. The transistors consisting of poly(2,5-thienylene vinylene), PTV, were exposed to ambient air for increasing times, which led to an increase in p-doping due to oxygen. Reprinted with permission from ref 68. Copyright 2003 AIP Publishing.

The increase of the pinch-off voltage V_{PO} with doping concentration (eq 25) often results in a decrease in the ON/OFF ratio of transistors.[23,25,166,287−289] To solve this problem, either the doping concentration has to be very small,[51] or the thickness of the doped layer d_{dop} has to be decreased to a couple of nanometers. The dependency of the pinch-off voltage on the thickness of the doped channel is shown in Figure 49. As seen in this figure, not only does the threshold voltage V_{th} shift according to eq 22 (Figure 44), but the pinch-off voltage increases as well from around −4 V for the intrinsic transistor to more than 10 V for the transistor with the 8 nm thick doped channel.

Instead of decreasing the doping concentration or the thickness of the doped layer, Lu et al. doped an organic transistor consisting of a mixture of insulating polystyrene and P3HT as active layer.[289] Indeed, they found that doping does not significantly increase the off current, but increases the on current. This phenomenon was explained by the three-dimensional network of P3HT formed inside the polystyrene bulk. The network is sparse at the gate insulator/semiconductor interface; that is, it is possible to deplete parts of the P3HT network at the insulator interface, leading to a complete off switching of the transistor.

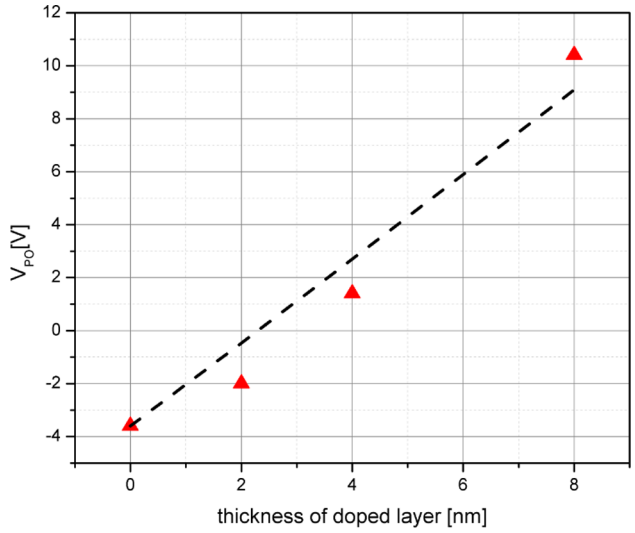

Figure 49. To avoid a decrease in ON/OFF ratio of doped organic transistors, the thickness of the doped layer d_{dop} can be limited to several nanometers. The influence of the thickness of the doped layer on the pinch-off voltage of p-doped pentacene transistors is shown above. Increasing the thickness to 8 nm leads to an increase in pinch-off voltage to more than 10 V.

A variant of the organic depletion transistors was reported in 2014, the organic junction field-effect transistor (organic JFET).[290] In the JFET, the gate insulator is replaced by an organic p−i−n junction. Applying a reverse voltage to the junction leads to an increased depletion, for example, in the p-doped layer.[56] This increase in depletion layer thickness leads to a modulation of the conductance of the layer, which can be sensed by the source and drain contact.[290]

Organic electrochemical transistors (OETs) are another popular example of an organic transistor, which is commonly operated in depletion mode.[291] OETs consist of source and drain contact and a highly doped organic semiconductor bridging the gap between the two electrodes. PEDOT:PSS (section 3.1.3) is one of the most common choices as it combines a high electrical conductivity with a significant ionic mobility.

OETs are operated in ionic solutions, for example, in salt water. If a positive voltage is applied between an electrode immersed into the solution and the transistor channel, mobile cations move into the organic semiconductor and dedope the film. The conductivity of the film decreases, which is seen by a decrease in drain current.

It was shown by Bernards et al. that the density of cations entering and dedoping the organic semiconductor can be modeled by a capacitor, resulting in a straightforward electrical model of the transistor resembling the structure of standard depletion OFETs discussed above.[292] Indeed, the electrical behavior of OETs is very similar to that of doped OFETs. A representative output characteristic of an OET as reported by the Malliaras group is shown in Figure 50.[293]

OETs have the advantage that they convert ionic currents into electric signals, they operate in liquid environments, and some of the materials used, in particular PEDOT:PSS, are biocompatible. Therefore, these transistors are often used in the

DOI: 10.1021/acs.chemrev.6b00329
Chem. Rev. 2016, 116, 13714−13751
Pictiva EX2009
Samsung v Pictiva
IPR2026-00129

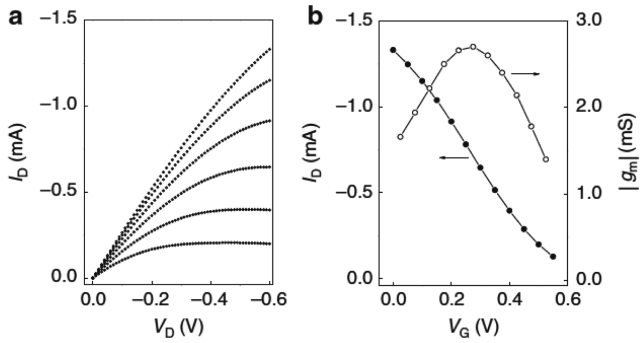

Figure 50. Output and transfer characteristic of an organic electrochemical transistor with a very large transconductance. Reprinted with permission from ref 293. Copyright 2013 Nature Publishing Group.

field of organic bioelectronics.[294,295] The field of OETs has been reviewed recently, for example, by Owens et al.,[296] Kergoat et al.,[297] and Ates,[298] and the reader is referred to these reviews for a more detailed summary of the advances in the field of OETs.

5.2.3. Majority and Minority Charge Carriers in Doped Transistors. Doping adds a further dimension in the control of the electronic properties of organic semiconductors. Doping defines the majority charge carrier type; if the Fermi level is close to the HOMO state, holes are dominating, whereas electrons are dominating if the Fermi Level is close to the LUMO. This effect is seen, for example, in Figure 5 for the polycrystalline material ZnPc and Figure 6 for pentacene; adding more electrons to the material by doping leads to a shift of the Fermi level toward the LUMO, whereas p-doping shifts the Fermi level toward the HOMO.

This control on the majority charge carrier type can be used to influence charge transport in organic semiconductors, which for long have been thought of as unipolar conductors. For example, Lee et al. showed that C_{60}-based transistors can be operated as p-type transistors as well, if they are heavily doped by the p-dopant MoO_3[201] (see section 4.3 for a discussion of p-type doping of C_{60}).

Similarly, Naab et al. showed that TIPS-pentacene can form n-type transistors if doped by DMBI-derivatives (see section 3.2.5) acting as n-type dopants.[133] Relying on their solution sheering method,[208] very large n-type mobilities of up to 6.8 $cm^2/(V{\cdot}s)$ were observed.

Doping can as well be used to control the balance in electron and hole currents in ambipolar organic transistors.[213,299] In particular, as ambipolar transistors are often unwanted for complementary logic circuits, doping can be used to define the majority charge carrier type and to turn the ambipolar behavior on or off. The group of Noh et al. reported on selectively doping PCBM-type transistors.[213] The results are shown in Figure 39. Without doping, the transistors show a strong ambipolarity. Adding the n-dopant CsF to the layer of PCBM leads to a reduction in hole transport and increase in electron transport, whereas adding F_4-TCNQ leads to a suppression of electron transport and increase in hole transport.

In all transistors discussed above, majority charge carriers are accumulated at the insulator/organic semiconductor interface. This type of operation is in marked contrast to the dominating inorganic transistor technology, inversion-based MOSFETs. Here, a thin layer of minority charge carriers is accumulated at the insulator/semiconductor interface; for example, holes are accumulated in an n-doped layer or electrons in a p-doped layer. The organic semiconductor is said to be inverted, that is, transformed from a p-doped layer into an n-doped layer (or vice versa).

Very low off-currents and large ON/OFF ratios are a major advantage of inversion-based FETs. For organic semiconductors, this suppression of off-state currents might prove to be beneficial in transistors with very short channel lengths, for example, realized by vertically structuring the transistors.[300] Indeed, it was shown recently that organic inversion FETs can be realized.[21,212] The transistors consist of p-doped injection contacts to ensure an efficient hole injection into the organic semiconductor pentacene. The channel region is doped by the n-dopant $W_2(hpp)_4$. Thus, to switch the transistor on, the n-doped channel has to be depleted first, before an inversion layer of holes can be formed at the insulator/organic interface. This effect was seen to result in a shift of the threshold voltage toward more negative voltages (see Figure 51).[21,212]

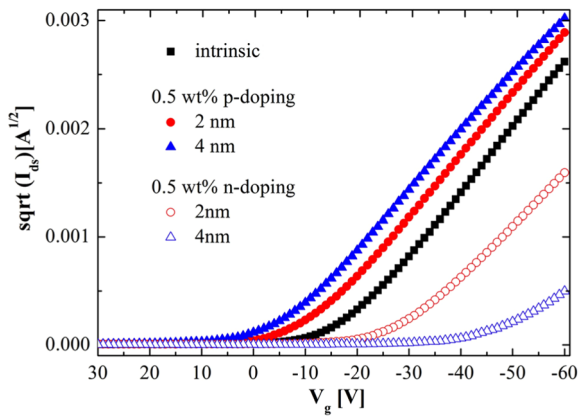

Figure 51. Doped top-gate organic transistors. Both p- and n-doping lead to a shift in the threshold voltage. For n-doped channels, a p-minority channel has to be formed in the doped layer; that is, the transistor is operated in inversion. Reprinted with permission from ref 212. Copyright 2015 AIP Publishing.

6. OUTLOOK AND CONCLUSIONS

Organic doping has become a key in the development of highly efficient optoelectronic devices[301] such as OLEDs[48] or OSCs.[10,152] As compared to OLEDs and OSCs, doping of organic transistors is lagging behind, and the vast majority of OFET publications is relying on intrinsic materials. However, in recent years, the benefits of doping for OFETs have increasingly been accepted, and a concise understanding of the influence of doping on the OFET performance has been developed.

This progress was made possible by a broad library of dopants developed in the past, which spans n- and p-type dopants and with various doping strength, sizes, and stability in air. Doping has a strong influence on the structure of most polycrystalline materials as commonly used in thin film transistors. A wealth of studies have been reported that clarify the structure of doped organic high-mobility layers, and several structural models were proposed. However, in most cases, a reduction in crystallinity is still observed at high doping concentrations, leading to a reduction in charge carrier mobility, and more efforts to design dopants that incorporate

DOI: 10.1021/acs.chemrev.6b00329
Chem. Rev. 2016, 116, 13714−13751

Pictiva EX2009
Samsung v Pictiva
IPR2026-00129

into the crystal lattice rather than disrupt the order in the matrix are needed.

Doping can be used at different positions in the device. The most common use of doping is to improve charge carrier injection and extraction at the source and drain contact. In fact, suppression of injection at the source electrode was identified as a major factor limiting the switching speed of the best OFETs, and realizing quasi-Ohmic contacts by doping is a promising route to increase the transconductance and cutoff frequency of OFETs significantly.

Channel doping is another use of doping in OFETs. In the channel, doping will influence the flatband and threshold voltage, and it will determine the pinch-off behavior of the channel. Thus, doping provides an important design parameter to control device performance. Furthermore, doping was reported to fill unwanted trap states in the device, which results in more stable devices and even increases the stability of n-type OFETs in air.

In summary, doping adds a new dimension to the design of highly efficient OFETs. Considering the importance of doping in inorganic FETs, doping will in the future not only be used to improve conventional transistors, but it will enable new device concepts that are based on tuning and controlling the Fermi level position in the organic semiconductor.

AUTHOR INFORMATION

Corresponding Authors

*E-mail: blussem@kent.edu.
*E-mail: leo@iapp.de.

Present Address

‖B.N.: Dow Electronic Materials, The Dow Chemical Company, 455 Forest Street, Marlborough, Massachusetts 01752, United States.

Notes

The authors declare no competing financial interest.

Biographies

Björn Lüssem is an Assistant Professor of Physics at Kent State University. Before joining Kent State in 2014, he was a project leader at Materials Science Laboratory of Sony in Stuttgart (2006−2008) and group leader at the Institut für Angewandte Photophysik (IAPP), TU Dresden (2008−2013). Lüssem authored more than 100 publications in international journals (h-index > 25). His research interests range from new design principles of organic devices, to charge transport in organic semiconductors and novel organic semiconductors with improved performance. His work has been awarded the VDE-Promotionspreis and the Günther-Leibfried-Preis.

Chang-Min Keum received his Ph.D. degree in electrical engineering from Seoul National University (South Korea) in 2014 under the guidance of Prof. Sin-Doo Lee. During doctoral studies, his research topics were mainly on interface phenomena, device physics, and architecture of organic electronic devices such as organic field-effect transistors and vertical-structured organic light-emitting transistors. Since he joined the group of Prof. Lüssem at Kent State University as a postdoctoral research associate in 2015, he has been working on the enhancement of the light outcoupling efficiency in organic light-emitting diodes and the development of vertical organic light-emitting transistors.

Daniel Kasemann, Doctor of Science (Dr. rer. nat., Physics), received his Ph.D. in 2011 for research on singlet−triplet-annihilation in OLEDs under extremely high current densities at the IAPP (Institut für Angewandte Photophysik), Technische Universität Dresden, Chair of Prof. Karl Leo. After a postdoc, on novel vertical organic transistors, he took over the group leadership of the "New Devices" group at the same institute. Since mid 2015, he is project manager at CreaPhys, a company supplying universities with the tools for research in organic electronics.

Benjamin Naab received a Ph.D. in chemistry in 2015 from Stanford University in California for his thesis on molecular n-dopants for organic electronics. He is currently a chemist in Dow Electronic Materials of The Dow Chemical Co. His main research interests are in the field of molecular dopants for organic electronics and interconnect technologies for printed circuit boards. He is also interested in metallization chemistry for emerging dielectric materials.

Zhenan Bao is a Professor of Chemical Engineering at Stanford University. Prior to joining Stanford in 2004, she was a Distinguished Member of Technical Staff in Bell Laboratories, Lucent Technologies, from 1995−2004. She has over 400 refereed publications and over 60 U.S. patents with a Google Scholar h-index > 120. She pioneered a number of design concepts for organic electronic materials. Her work has enabled flexible electronic circuits and displays. In her recent work, she has developed skin-inspired organic electronic materials, which resulted in unprecedented performance or functions in medical devices, energy storage, and environmental applications. Bao is an academic member of the National Academy of Engineering. She is a Fellow of MRS, ACS, AAAS, SPIE, ACS PMSE, and ACS POLY. She served on the Board of Directors for MRS in 2003−2005 and as an Executive Committee Member for the Polymer Materials Science and Engineering division of the American Chemical Society. She is an Associate Editor for *Chemical Sciences*. Bao was selected as Nature's Ten people who mattered in 2015 for her work on artificial electronic skin. She was awarded the AICHE Andreas Acrivos Award for Professional Progress in Chemical Engineering in 2014, ACS Carl Marvel Creative Polymer Chemistry Award in 2013, ACS Cope Scholar Award in 2011, she was the recipient of the Royal Society of Chemistry Beilby Medal and Prize in 2009, the IUPAC Creativity in Applied Polymer Science Prize in 2008, American Chemical Society Team Innovation Award 2001, R&D 100 Award, and R&D Magazine's Editors Choice of the "Best of the Best" new technology for 2001. She was selected in 2002 by the American Chemical Society Women Chemists Committee as one of the 12 "Outstanding Young Woman Scientist who is expected to make a substantial impact in chemistry during this century". She was also selected by MIT Technology Review magazine in 2003 as one of the top 100 young innovators for this century. Bao is a cofounder and on the Board of Directors for C3 Nano, a silicon-valley venture funded start-up commercializing flexible transparent electrodes.

Karl Leo obtained the Diplomphysiker degree from the University of Freiburg in 1985, working with Adolf Goetzberger at the Fraunhofer-Institut für Solare Energiesysteme. In 1988, he obtained the Ph.D. degree from the University of Stuttgart for a Ph.D. thesis performed at the Max-Planck-Institut für Festkörperforschung in Stuttgart under the supervision of Hans Queisser. From 1989 to 1991, he was postdoc at AT&T Bell Laboratories in Holmdel, NJ. From 1991 to 1993, he was with the Rheinisch-Westfälische Technische Hochschule (RWTH) in Aachen, Germany. Since 1993, he is full professor of optoelectronics at the Technische Universität Dresden. His main interests are novel semiconductor systems like semiconducting organic thin films, with special emphasis to understand basic device principles and the optical response. His work was recognized by a number of awards, including Otto-Hahn-Medaille (1989), Bennigsen-Förder-Preis (1991), Leibniz-Award (2002), award of the Berlin-Brandenburg Academy (2002), Manfred-von-Ardenne-Preis (2006), Zukunftspreis of the German

DOI: 10.1021/acs.chemrev.6b00329
Chem. Rev. 2016, 116, 13714−13751

Pictiva EX2009
Samsung v Pictiva
IPR2026-00129

president (2011), Rudolf-Jäckel-Prize (2012), and a Dr. techn. h.c. of the University of Southern Denmark (2013). He is the cofounder of several companies, including Novaled GmbH and Heliatek GmbH.

ACKNOWLEDGMENTS

We thank M. L. Tietze, H. Kleemann, P. Pahner, and A. Günther for their input to this manuscript. B.L. acknowledges financial support from the Binational Science Foundation (grant no. 2014396), and the National Science Foundation (grant no. 1639073). Part of the work leading to these results has received funding from the European Community's Seventh Framework Programme under Grant Agreement no. FP7-267995 (NUDEV). K.L. and D.K. gratefully acknowledge support from the excellence cluster cfaed. B.N. and Z.B. acknowledge support from the Air Force Office of Scientific Research (grant no. FA9550-12-1-0190) and NSF Materials Network (grant no. DMR-1209468). Furthermore, support from J. Blochwitz-Nimoth and Novaled GmbH is gratefully acknowledged by B.L., D.K., and K.L.

REFERENCES

(1) Yamamoto, Y.; Yoshino, K.; Inuishi, Y. Electrical-Properties of Phthalocyanine Halogen Complexes. *J. Phys. Soc. Jpn.* **1979**, *47*, 1887−1891.

(2) Kearns, D. R.; Tollin, G.; Calvin, M. Electrical Properties of Organic Solids. II. Effects of Added Electron Acceptor on Metal-Free Phthalocyanine. *J. Chem. Phys.* **1960**, *32*, 1020−1025.

(3) Maitrot, M.; Guillaud, G.; Boudjema, B.; Andre, J.; Simon, J. Molecular Material Based Junctions: Formation of a Schottky Contact with Metallophatlocyanine Thin Films Doped by the Cosublimation Method. *J. Appl. Phys.* **1986**, *60*, 2396−2400.

(4) Andre, J.; Simon, J.; Even, R.; Boudjema, B.; Guillaud, G.; Maitrot, M. Molecular Semiconductors and Junction Formation: Phthalocyanine Derivatives. *Synth. Met.* **1987**, *18*, 683−688.

(5) Marks, T. Electrically Conductive Metallomacrocyclic Assemblies. *Science* **1985**, *227*, 881−889.

(6) Lous, E.; Blom, P.; Molenkamp, L.; De Leeuw, D. Schottky Contacts on a Highly Doped Organic Semiconductor. *Phys. Rev. B: Condens. Matter Mater. Phys.* **1995**, *51*, 17251−17254.

(7) Pfeiffer, M.; Beyer, A.; Fritz, T.; Leo, K. Controlled Doping of Phthalocyanine Layers by Cosublimation with Acceptor Molecules: A Systematic Seebeck and Conductivity Study. *Appl. Phys. Lett.* **1998**, *73*, 3202−3204.

(8) Blochwitz, J.; Pfeiffer, M.; Fritz, T.; Leo, K. Low Voltage Organic Light Emitting Diodes Featuring Doped Phthalocyanine as Hole Transport Material. *Appl. Phys. Lett.* **1998**, *73*, 729−731.

(9) Reineke, S.; Lindner, F.; Schwartz, G.; Seidler, N.; Walzer, K.; Lüssem, B.; Leo, K. White Organic Light-emitting Diodes with Fluorescent Tube Efficiency. *Nature* **2009**, *459*, 234−238.

(10) Heliatek consolidates its technology leadership by establishing a new world record for organic solar technology with a cell efficiency of 12%. Press Release, 2013; http://www.heliatek.com/wp-content/uploads/2013/01/130116_PR_Heliatek_achieves_record_cell_effiency_for_OPV.pdf.

(11) Meerheim, R.; Körner, C.; Leo, K. Highly Efficient Organic Multi-junction Solar Cells with a Thiophene Based Donor Material. *Appl. Phys. Lett.* **2014**, *105*, 063306.

(12) Blochwitz, J.; Fritz, T.; Pfeiffer, M.; Leo, K.; Alloway, D. M.; Lee, P. A.; Armstrong, N. R. Interface Electronic Structure of Organic Semiconductors with Controlled Doping Levels. *Org. Electron.* **2001**, *2*, 97−104.

(13) Ante, F.; Kaelblein, D.; Zschieschang, U.; Canzler, T. W.; Werner, A.; Takimiya, K.; Ikeda, M.; Sekitani, T.; Someya, T.; Klauk, H. Contact Doping and Ultrathin Gate Dielectrics for Nanoscale Organic Thin-Film Transistors. *Small* **2011**, *7*, 1186−1191.

(14) Tsukagoshi, K.; Shigeto, K.; Yagi, I.; Aoyagi, Y. Interface Modification of a Pentacene Field-effect Transistor with A Submicron Channel. *Appl. Phys. Lett.* **2006**, *89*, 113507.

(15) Fujimori, F.; Shigeto, K.; Hamano, T.; Minari, T.; Miyadera, T.; Tsukagoshi, K.; Aoyagi, Y. Current Transport in Short Channel Top-Contact Pentacene Field-effect Transistors Investigated with the Selective Molecular Doping Technique. *Appl. Phys. Lett.* **2007**, *90*, 193507.

(16) Tiwari, S. P.; Potscavage, W. J.; Sajoto, T.; Barlow, S.; Marder, S. R.; Kippelen, B. Pentacene Organic Field-effect Transistors with Doped Electrode-Semiconductor Contacts. *Org. Electron.* **2010**, *11*, 860−863.

(17) Singh, S.; Mohapatra, S. K.; Sharma, A.; Fuentes-Hernandez, C.; Barlow, S.; Marder, S. R.; Kippelen, B. Reduction of Contact Resistance by Selective Contact Doping in Fullerene N-channel Organic Field-Effect Transistors. *Appl. Phys. Lett.* **2013**, *102*, 153303.

(18) Tukagoshi, K.; Fujimori, F.; Minari, T.; Miyadera, T.; Hamano, T.; Aoyagi, Y. Suppression of Short Channel Effect in Organic Thin Film Transistors. *Appl. Phys. Lett.* **2007**, *91*, 113508.

(19) Minari, T.; Miyadera, T.; Tsukagoshi, K.; Aoyagi, Y.; Ito, H. Charge Injection Process in Organic Field-Effect Transistors. *Appl. Phys. Lett.* **2007**, *91*, 053508.

(20) Minari, T.; Darmawan, P.; Liu, C.; Li, Y.; Xu, Y.; Tsukagoshi, K. Highly Enhanced Charge Injection in Thienoacene-based Organic Field-Effect Transistors with Chemically Doped Contact. *Appl. Phys. Lett.* **2012**, *100*, 093303.

(21) Lüssem, B.; Tietze, M. L.; Kleemann, H.; Hoßbach, C.; Bartha, J. W.; Zakhidov, A.; Leo, K. Doped Organic Transistors Operating in the Inversion and Depletion Regime. *Nat. Commun.* **2013**, *4*, 2775.

(22) Abe, Y.; Hasegawa, T.; Takahashi, Y.; Yamada, T.; Tokura, Y. Control of Threshold Voltage in Pentacene Thin-film Transistors Using Carrier Doping at The Charge-transfer Interface with Organic Acceptors. *Appl. Phys. Lett.* **2005**, *87*, 153506.

(23) Lee, C.-T.; Chen, H.-C. Performance Improvement Mechanisms of Organic Thin-Film Transistors Using MoOx-Doped Pentacene as Channel Layer. *Org. Electron.* **2011**, *12*, 1852−1857.

(24) Hählen, T.; Vanoni, C.; Wäckerlin, C.; Jung, T. A.; Tsujino, S. Surface Doping in Pentacene Thin-film Transistors with Few Monolayer Thick Channels. *Appl. Phys. Lett.* **2012**, *101*, 033305.

(25) Wei, P.; Oh, J. H.; Dong, G.; Bao, Z. Use of a 1 H-benzoimidazole Derivative as an N-type Dopant And to Enable Air-stable Solution-Processed N-Channel Organic Thin-film Transistors. *J. Am. Chem. Soc.* **2010**, *132*, 8852−8853.

(26) Hein, M. P.; Zakhidov, A. A.; Lüssem, B.; Jankowski, J.; Tietze, M. L.; Riede, M. K.; Leo, K. Molecular Doping for Control of Gate Bias Stress in Organic Thin Film Transistors. *Appl. Phys. Lett.* **2014**, *104*, 013507.

(27) Zhang, Y.; de Boer, B.; Blom, P. W. Controllable Molecular Doping and Charge Transport in Solution-Processed Polymer Semiconducting Layers. *Adv. Funct. Mater.* **2009**, *19*, 1901−1905.

(28) Walzer, K.; Maennig, B.; Pfeiffer, M.; Leo, K. Highly Efficient Organic Devices Based on Electrically Doped Transport Layers. *Chem. Rev.* **2007**, *107*, 1233−1271.

(29) Lee, J.-H.; Leem, D.-S.; Kim, H.-J.; Kim, J.-J. *Appl. Phys. Lett.* **2009**, *94*, 123306.

(30) Glaser, T.; Beck, S.; Lunkenheimer, B.; Donhauser, D.; Köhn, A.; Kröger, M.; Pucci, A. Infrared Study of the MoO3 Doping Efficiency in 4, 4 -bis (n-carbazolyl)-1, 1 -biphenyl (CBP). *Org. Electron.* **2013**, *14*, 575−583.

(31) Männig, B.; Pfeiffer, M.; Nollau, A.; Zhou, X.; Leo, K. Controlled p-type Doping of Polycrystalline and Amorphous Organic Layers: Self-consistent Description of Conductivity and Field-Effect Mobility by a Microscopic Percolation Model. *Phys. Rev. B: Condens. Matter Mater. Phys.* **2001**, *64*, 195208.

(32) Pfeiffer, M. Controlled Doping of Organic Vacuum Deposited Dye Layers: Basics and Applications. Ph.D. thesis, TU Dresden, 1999.

(33) Pfeiffer, M.; Leo, K.; Zhou, X.; Huang, J.; Hofmann, M.; Werner, A.; Blochwitz-Nimoth, J. Doped Organic Semiconductors:

DOI: 10.1021/acs.chemrev.6b00329
Chem. Rev. 2016, 116, 13714−13751

Pictiva EX2009
Samsung v Pictiva
IPR2026-00129

Physics and Application in Light Emitting Diodes. *Org. Electron.* **2003**, *4*, 89.
(34) Harada, K.; Riede, M.; Leo, K.; Hild, O. R.; Elliott, C. M. Pentacene Homojunctions: Electron and Hole Transport Properties and Related Photovoltaic Responses. *Phys. Rev. B: Condens. Matter Mater. Phys.* **2008**, *77*, 195212.
(35) Tietze, M. L.; Burtone, L.; Riede, M.; Lüssem, B.; Leo, K. Fermi Level Shift and Doping Efficiency in p-doped Small Molecule Organic Semiconductors: A Photoelectron Spectroscopy and Theoretical Study. *Phys. Rev. B: Condens. Matter Mater. Phys.* **2012**, *86*, 035320.
(36) Mityashin, A.; Olivier, Y.; Van Regemorter, T.; Rolin, C.; Verlaak, S.; Martinelli, N. G.; Beljonne, D.; Cornil, J.; Genoe, J.; Heremans, P. Unraveling the Mechanism of Molecular Doping in Organic Semiconductors. *Adv. Mater.* **2012**, *24*, 1535−1539.
(37) Gregg, B. A.; Chen, S.-G.; Cormier, R. A. Coulomb Forces and Doping in Organic Semiconductors. *Chem. Mater.* **2004**, *16*, 4586−4599.
(38) Ha, S. D.; Kahn, A. Isolated Molecular Dopants in Pentacene Observed by Scanning Tunneling Microscopy. *Phys. Rev. B: Condens. Matter Mater. Phys.* **2009**, *80*, 195410.
(39) Salzmann, I.; Heimel, G.; Duhm, S.; Oehzelt, M.; Pingel, P.; George, B. M.; Schnegg, A.; Lips, K.; Blum, R.-P.; Vollmer, A.; Koch, N. Intermolecular Hybridization Governs Molecular Electrical Doping. *Phys. Rev. Lett.* **2012**, *108*, 035502.
(40) Salzmann, I.; Heimel, G. Toward a Comprehensive Understanding of Molecular Doping Organic Semiconductors (Review). *J. Electron Spectrosc. Relat. Phenom.* **2015**, *204*, 208−222.
(41) Mendez, H.; Heimel, G.; Opitz, A.; Sauer, K.; Barkowski, P.; Oehzelt, M.; Soeda, J.; Okamoto, T.; Takeya, J.; Arlin, J.-B.; Balandier, J.-Y.; Geerts, Y.; Koch, N.; Salzmann, I. Doping of Organic Semiconductors: Impact of Dopant Strength and Electronic Coupling. *Angew. Chem., Int. Ed.* **2013**, *52*, 7751−7755.
(42) Klopman, G. Chemical Reactivity and the Concept of Charge- and Frontier-Controlled Reactions. *J. Am. Chem. Soc.* **1968**, *90*, 223−234.
(43) Pitarch-Ruiz, J.; Evangelisti, S.; Maynau, D. Does a Sodium Atom Bind to C60? *J. Chem. Theory Comput.* **2005**, *1*, 1079−1082.
(44) Roques, J.; Calvo, F.; Spiegelman, F.; Mijoule, C. Wetting-to-Nonwetting Transition In Metal-Coated C60. *Phys. Rev. Lett.* **2003**, *90*, 075505.
(45) Méndez, H.; Heimel, G.; Winkler, S.; Frisch, J.; Opitz, A.; Sauer, K.; Wegner, B.; Oehzelt, M.; Röthel, C.; Duhm, S.; Többens, D.; Koch, N.; Salzmann, I. Charge-Transfer Crystallites as Molecular Electrical Dopants. *Nat. Commun.* **2015**, *6*, 8560.
(46) Tietze, M. L.; Leo, K.; Lüssem, B. Quantification of Deep Hole-Trap Filling by Molecular P-doping: Dependence on the Host Material Purity. *Org. Electron.* **2013**, *14*, 2348−2352.
(47) Tietze, M. L.; Pahner, P.; Schmidt, K.; Leo, K.; Lüssem, B. Doped Organic Semiconductors: Trap-Filling, Impurity Saturation, and Reserve Regimes. *Adv. Funct. Mater.* **2015**, *25*, 2701−2707.
(48) Meerheim, R.; Lüssem, B.; Leo, K. Efficiency and Stability of p-i-n Type Organic Light Emitting Diodes for Display and Lighting Applications. *Proc. IEEE* **2009**, *97*, 1606−1626.
(49) Solomeshch, O.; Yu, Y. J.; Goryunkov, A. A.; Sidorov, L. N.; Tuktarov, R. F.; Choi, D. H.; Jin, J.-I.; Tessler, N. Ground-State Interaction and Electrical Doping of Fluorinated C60 in Conjugated Polymers. *Adv. Mater.* **2009**, *21*, 4456−4460.
(50) Meerheim, R.; Olthof, S.; Hermenau, M.; Scholz, S.; Petrich, A.; Tessler, N.; Solomeshch, O.; Lussem, B.; Riede, M.; Leo, K. Investigation of C60F36 as Low-Volatility p-dopant in Organic Optoelectronic Devices. *J. Appl. Phys.* **2011**, *109*, 103102.
(51) Olthof, S.; Singh, S.; Mohapatra, S. K.; Barlow, S.; Marder, S. R.; Kippelen, B.; Kahn, A. Passivation of Trap States in Unpurified and Purified C60 and the Influence on Organic Field-Effect Transistor Performance. *Appl. Phys. Lett.* **2012**, *101*, 253303.
(52) Olthof, S.; Mehraeen, S.; Mohapatra, S. K.; Barlow, S.; Coropceanu, V.; Bredas, J.-L.; Marder, S. R.; Kahn, A. Ultralow Doping in Organic Semiconductors: Evidence of Trap Filling. *Phys. Rev. Lett.* **2012**, *109*, 176601.
(53) Chan, C. K.; Kim, E.-G.; Brédas, J.-L.; Kahn, A. Molecular n-Type Doping of 1, 4, 5, 8-Naphthalene Tetracarboxylic Dianhydride by Pyronin B Studied Using Direct and Inverse Photoelectron Spectroscopies. *Adv. Funct. Mater.* **2006**, *16*, 831−837.
(54) Olthof, S.; Tress, W.; Meerheim, R.; Lüssem, B.; Leo, K. Photoelectron Spectroscopy Study of Systematically Varied Doping Concentrations in an Organic Semiconductor Layer using a Molecular p-dopant. *J. Appl. Phys.* **2009**, *106*, 103711.
(55) Lee, J.-H.; Kim, H.-M.; Kim, K.-B.; Kim, J.-J. Origin of Charge Generation Efficiency of Metal Oxide p-dopants in Organic Semiconductors. *Org. Electron.* **2011**, *12*, 950−954.
(56) Kleemann, H.; Lüssem, B.; Leo, K. Controlled Formation of Charge Depletion Zones by Molecular Doping in Organic pin-Diodes and its Description by the Mott-schottky Relation. *J. Appl. Phys.* **2012**, *111*, 123722.
(57) Chen, S.-G.; Stradins, P.; Gregg, B. A. Doping Highly Ordered Organic Semiconductors: Experimental Results and Fits to a Self-Consistent Model of Excitonic Processes, Doping, and Transport. *J. Phys. Chem. B* **2005**, *109*, 13451−13460.
(58) Hamwi, S.; Meyer, J.; Winkler, T.; Riedl, T.; Kowalsky, W. P-type Doping Efficiency of MoO3 in Organic Hole Transport Materials. *Appl. Phys. Lett.* **2009**, *94*, 253307.
(59) Lee, J.-H.; Leem, D.-S.; Kim, J.-J. Effect of Host Organic Semiconductors on Electrical Doping. *Org. Electron.* **2010**, *11*, 486−489.
(60) Lee, J.-H.; Kim, H.-M.; Kim, K.-B.; Kabe, R.; Anzenbacher, P.; Kim, J.-J. Homogeneous Dispersion of Organic p-dopants in an Organic Semiconductor as an Origin of High Charge Generation Efficiency. *Appl. Phys. Lett.* **2011**, *98*, 3303.
(61) Pahner, P.; Kleemann, H.; Burtone, L.; Tietze, M. L.; Fischer, J.; Leo, K.; Lüssem, B. Pentacene Schottky Diodes Studied by Impedance Spectroscopy: Doping Properties and Trap Response. *Phys. Rev. B: Condens. Matter Mater. Phys.* **2013**, *88*, 195205.
(62) Lee, J.-H.; Kim, J.-J. Interfacial Doping for Efficient Charge Injection in Organic Semiconductors. *Phys. Status Solidi A* **2012**, *209*, 1399−1413.
(63) Yoo, S.-J.; Kim, J.-J. Charge Transport in Electrically Doped Amorphous Organic Semiconductors. *Macromol. Rapid Commun.* **2015**, *36*, 984−1000.
(64) Rienstra-Kiracofe, J. C.; Tschumper, G. S.; Schaefer, H. F.; Nandi, S.; Ellison, G. B. Atomic and Molecular Electron Affinities: Photoelectron Experiments and Theoretical Computations. *Chem. Rev.* **2002**, *102*, 231−282.
(65) Chiang, C. K.; Fincher, C., Jr; Park, Y. W.; Heeger, A. J.; Shirakawa, H.; Louis, E. J.; Gau, S. C.; MacDiarmid, A. G. Electrical Conductivity in Doped Polyacetylene. *Phys. Rev. Lett.* **1977**, *39*, 1098−1101.
(66) Jakabovič, J.; Vincze, A.; Kováč, J.; Srnánek, R.; Dobročka, E.; Donoval, D.; Heinemeyer, U.; Schreiber, F.; Machovič, V.; Uherek, F. Surface and Interface Analysis of Iodine-doped Pentacene Structures for OTFTs. *Surf. Interface Anal.* **2011**, *43*, 518−521.
(67) Sharma, G.; Sangodkar, S.; Roy, M. Influence of Iodine on the Electrical and Photoelectrical Properties of Zinc Phthalocyanine Thin Film Devices. *Mater. Sci. Eng., B* **1996**, *41*, 222−227.
(68) Meijer, E.; Detcheverry, C.; Baesjou, P.; van Veenendaal, E.; de Leeuw, D.; Klapwijk, T. Dopant Density Determination in Disordered Organic Field-Effect Transistors. *J. Appl. Phys.* **2003**, *93*, 4831−4835.
(69) Abdou, M. S.; Orfino, F. P.; Son, Y.; Holdcroft, S. Interaction of Oxygen with Conjugated Polymers-Charge-Transfer Complex-Formation with Poly (3-Alkylthiophenes). *J. Am. Chem. Soc.* **1997**, *119*, 4518−4524.
(70) Lu, C.-K.; Meng, H.-F. Hole Doping by Molecular Oxygen in Organic Semiconductors: Band-Structure Calculations. *Phys. Rev. B: Condens. Matter Mater. Phys.* **2007**, *75*, 235206.
(71) Chan, C. Y.; Chow, C.; So, S. K. Using Transistor Technique to Study the Effects of Transition Metal Oxide Dopants on Organic Charge Transporters. *Org. Electron.* **2011**, *12*, 1454−1458.
(72) Kröger, M.; Hamwi, S.; Meyer, J.; Riedl, T.; Kowalsky, W.; Kahn, A. P-type Doping of Organic Wide Band Gap Materials by

DOI: 10.1021/acs.chemrev.6b00329
Chem. Rev. 2016, 116, 13714−13751

Pictiva EX2009
Samsung v Pictiva
IPR2026-00129

Transition Metal Oxides: A Case-Study on Molybdenum Trioxide. *Org. Electron.* **2009**, *10*, 932−938.
(73) Lehnhardt, M.; Hamwi, S.; Hoping, M.; Reinker, J.; Riedl, T.; Kowalsky, W. Charge Carrier Densities in Chemically Doped Organic Semiconductors Verified by Two Independent Techniques. *Appl. Phys. Lett.* **2010**, *96*, 193301.
(74) Qi, Y.; Sajoto, T.; Kroger, M.; Kandabarow, A. M.; Park, W.; Barlow, S.; Kim, E.-G.; Wielunski, L.; Feldman, L.; Bartynski, R. A.; Bredas, J.; Marder, S. R.; Kahn, A. A Molybdenum Dithiolene Complex as p-dopant for Hole-transport Materials: A Multitechnique Experimental and Theoretical Investigation. *Chem. Mater.* **2010**, *22*, 524−531.
(75) Kroger, M.; Hamwi, S.; Meyer, J.; Riedl, T.; Kowalsky, W.; Kahn, A. Role of the Deep-lying Electronic States of MoO3 in the Enhancement of Hole-injection in Organic Thin Films. *Appl. Phys. Lett.* **2009**, *95*, 123301.
(76) Meyer, J.; Hamwi, S.; Schmale, S.; Winkler, T.; Johannes, H.-H.; Riedl, T.; Kowalsky, W. A Strategy Towards p-type Doping of Organic Materials with HOMO Levels Beyond 6 eV using Tungsten Oxide. *J. Mater. Chem.* **2009**, *19*, 702−705.
(77) Zhang, D.-D.; Feng, J.; Chen, L.; Wang, H.; Liu, Y.-F.; Jin, Y.; Bai, Y.; Zhong, Y.-Q.; Sun, H.-B. Role of Fe3O4 as p-Dopant in Improving the Hole Injection and Transport of Organic Light-Emitting Devices. *IEEE J. Quantum Electron.* **2011**, *47*, 591−596.
(78) Meyer, J.; Hamwi, S.; Kroeger, M.; Kowalsky, W.; Riedl, T.; Kahn, A. Transition Metal Oxides for Organic Electronics: Energetics, Device Physics and Applications. *Adv. Mater.* **2012**, *24*, 5408−5427.
(79) Ćirić-Marjanović, G. Recent Advances in Polyaniline Research: Polymerization Mechanisms, Structural Aspects. *Synth. Met.* **2013**, *177*, 1−47.
(80) Ausserlechner, S. J.; Gruber, M.; Hetzel, R.; Flesch, H.-G.; Ladinig, L.; Hauser, L.; Haase, A.; Buchner, M.; Resel, R.; Schürrer, F.; Stadlober, B.; Trimmel, G.; Zojer, K.; Zojer, E. Mechanism of Surface Proton Transfer Doping in Pentacene Based Organic Thin-Film Transistors. *Phys. Status Solidi A* **2012**, *209*, 181−192.
(81) Kao, C. Y.; Lee, B.; Wielunski, L. S.; Heeney, M.; McCulloch, I.; Garfunkel, E.; Feldman, L. C.; Podzorov, V. Doping of Conjugated Polythiophenes with Alkyl Silanes. *Adv. Funct. Mater.* **2009**, *19*, 1906−1911.
(82) Duclaux, L. Review of the Doping of Carbon Nanotubes (Multiwalled and Single-walled). *Carbon* **2002**, *40*, 1751−1764.
(83) Ganzorig, C.; Fujihira, M. Improved Drive Voltages of Organic Electroluminescent Devices with an Efficient p-type Aromatic Diamine Hole-injection Layer. *Appl. Phys. Lett.* **2000**, *77*, 4211−4213.
(84) Cappel, U. B.; Daeneke, T.; Bach, U. Oxygen-induced Doping of Spiro-MeOTAD in Solid-state Dye-Sensitized Solar Cells and its Impact on Device Performance. *Nano Lett.* **2012**, *12*, 4925−4931.
(85) Nguyen, W. H.; Bailie, C. D.; Unger, E. L.; McGehee, M. D. Enhancing the Hole-Conductivity of Spiro-OMeTAD without Oxygen or Lithium Salts by Using Spiro(TFSI)2 in Perovskite and Dye-sensitized Solar Cells. *J. Am. Chem. Soc.* **2014**, *136*, 10996−11001.
(86) Pecqueur, S. Lewis Acid-Base Theory Applied on Evaluation of New Dopants for Organic Light-Emitting Diodes. Ph.D. thesis, Friedrich-Alexander-Universität Erlangen-Nürnberg (FAU), 2014.
(87) Schmid, G.; Wemken, J. H.; Maltenberger, A.; Diez, C.; Jaeger, A.; Dobbertin, T.; Hietsoi, O.; Dubceac, C.; Petrukhina, M. A. Fluorinated Copper (I) Carboxylates as Advanced Tunable p-Dopants for Organic Light-Emitting Diodes. *Adv. Mater.* **2014**, *26*, 878−885.
(88) Sun, K.; Zhang, S.; Li, P.; Xia, Y.; Zhang, X.; Du, D.; Isikgor, F. H.; Ouyang, J. Review on Application of PEDOTs and PEDOT: PSS in Energy Conversion and Storage Devices. *J. Mater. Sci.: Mater. Electron.* **2015**, *26*, 4438−4462.
(89) Maennig, B.; Pfeiffer, M.; Nollau, A.; Zhou, X.; Leo, K.; Simon, P. Controlled p-type Doping of Polycrystalline and Amorphous Organic Layers: Self-consistent Description of Conductivity and Field-Effect Mobility by a Microscopic Percolation Model. *Phys. Rev. B: Condens. Matter Mater. Phys.* **2001**, *64*, 195208.
(90) Duong, D. T.; Wang, C.; Antono, E.; Toney, M. F.; Salleo, A. The Chemical and Structural Origin of Efficient p-type Doping in P3HT. *Org. Electron.* **2013**, *14*, 1330−1336.
(91) Cochran, J. E.; Junk, M. J.; Glaudell, A.; Miller, P. L.; Cowart, J. S.; Toney, M. F.; Hawker, C. J.; Chmelka, B. F.; Chabinyc, M. L. Molecular Interactions and Ordering in Electrically Doped Polymers: Blends of PBTTT and F4TCNQ. *Macromolecules* **2014**, *47*, 6836−6846.
(92) Goetz, K. P.; Vermeulen, D.; Payne, M. E.; Kloc, C.; McNeil, L. E.; Jurchescu, O. D. Charge-transfer Complexes: New Perspectives on an Old Class of Compounds. *J. Mater. Chem. C* **2014**, *2*, 3065−3076.
(93) Rainbolt, J. E.; Koech, P. K.; Polikarpov, E.; Swensen, J. S.; Cosimbescu, L.; Von Ruden, A.; Wang, L.; Sapochak, L. S.; Padmaperuma, A. B.; Gaspar, D. J. Synthesis and Characterization of p-type Conductivity Dopant 2-(3-(adamantan-1-yl) propyl)-3, 5, 6-trifluoro-7, 7, 8, 8-tetracyanoquinodimethane. *J. Mater. Chem. C* **2013**, *1*, 1876−1884.
(94) Rangger, G. M.; Hofmann, O. T.; Bröker, B.; Zojer, E. A Particularly Strong Organic Acceptor for Tuning the Hole-injection Barriers in Modern Organic Devices. *Synth. Met.* **2010**, *160*, 1456−1462.
(95) Smets, Y.; Stark, C. B.; Schmitt, F.; Edmonds, M. T.; Lach, S.; Wright, C. A.; Langley, D. P.; Rietwyk, K. J.; Schenk, A.; Tadich, A.; Wanke, M.; Ziegler, C.; Ley, L.; Pakes, C. I. Doping Efficiency and Energy-Level Scheme in C60F48-doped Zinc-Tetraphenylporphyrin Films. *Org. Electron.* **2013**, *14*, 169−174.
(96) Qi, Y.; Sajoto, T.; Barlow, S.; Kim, E.-G.; Marder, S. R.; Kahn, A. Use of a High Electron-affinity Molybdenum Dithiolene Complex to p-dope Hole-Transport Layers. *J. Am. Chem. Soc.* **2009**, *131*, 12530−12531.
(97) Paniagua, S. A.; Baltazar, J.; Sojoudi, H.; Mohapatra, S. K.; Zhang, S.; Henderson, C. L.; Graham, S.; Barlow, S.; Marder, S. R. Production of Heavily n-and p-doped CVD Graphene with Solution-Processed Redox-Active Metal-Organic Species. *Mater. Horiz.* **2014**, *1*, 111−115.
(98) Parthasarathy, G.; Shen, C.; Kahn, A.; Forrest, S. Lithium Doping of Semiconducting Organic Charge Transport Materials. *J. Appl. Phys.* **2001**, *89*, 4986−4992.
(99) Benamara, A. A.; Galtier, M.; Montaner, A. N-doping of Polyacetylene. *Synth. Met.* **1991**, *41*, 45−48.
(100) Reed, C. A.; Bolskar, R. D. Discrete Fulleride Anions and Fullerenium Cations. *Chem. Rev.* **2000**, *100*, 1075−1120.
(101) Fröbel, M.; Schwab, T.; Kliem, M.; Hofmann, S.; Leo, K.; Gather, M. C. Get It White: Color-Tunable AC/DC OLEDs. *Light: Sci. Appl.* **2015**, *4*, e247.
(102) Kao, P.-C.; Lin, J.-H.; Wang, J.-Y.; Yang, C.-H.; Chen, S.-H. Li2CO3 as an N-type Dopant on Alq3-Based Organic Light Emitting Devices. *J. Appl. Phys.* **2011**, *109*, 094505.
(103) Kao, P.-C.; Wang, J.-Y.; Lin, J.-H.; Yang, C.-H. Effects of the Na2CO3 Dopant on Electron Injection and Transport in Organic Light Emitting Devices. *Thin Solid Films* **2013**, *527*, 338−343.
(104) Kao, P.-C.; Chang, C.-C.; Lin, S.-Y. Role Of K2CO3 as an n-type Dopant in Enhancing the Electron Injection and Transport of Organic Light-emitting Devices. *Surf. Coat. Technol.* **2013**, *231*, 135−139.
(105) Leem, D.-S.; Kim, S.-Y.; Kim, J.-J.; Chen, M.-H.; Wu, C.-I. Rubidium-carbonate-doped 4, 7-diphenyl-1, 10-phenanthroline Electron Transporting Layer for High-Efficiency pin Organic Light Emitting Diodes. *Electrochem. Solid-State Lett.* **2009**, *12*, J8−J10.
(106) Wemken, J. H.; Krause, R.; Mikolajick, T.; Schmid, G. Low-cost Caesium Phosphate as n-dopant for Organic Light-Emitting Diodes. *J. Appl. Phys.* **2012**, *111*, 074502.
(107) Lee, J.; Lee, H.; Jeon, P.; Jeong, K.; Kim, T. G.; Kim, J. W.; Yi, Y. Direct Evidence of n-type Doping in Organic Light-Emitting Devices: N Free Cs Doping From CsN3. *Appl. Phys. Lett.* **2012**, *100*, 203301.
(108) Yook, K. S.; Jeon, S. O.; Joo, C. W.; Lee, J. Y.; Lee, T.-W.; Noh, T.; Yang, H.-J.; Kang, S.-K. Air Stable and Low Temperature

DOI: 10.1021/acs.chemrev.6b00329
Chem. Rev. 2016, 116, 13714−13751
Pictiva EX2009
Samsung v Pictiva
IPR2026-00129

Evaporable Li3N as n Type Dopant in Organic Light-Emitting Diodes. *Synth. Met.* **2009**, *159*, 1664−1666.
(109) Chen, S.-Y.; Chu, T.-Y.; Chen, J.-F.; Su, C.-Y.; Chen, C. H. Stable Inverted Bottom-Emitting Organic Electroluminescent Devices with Molecular Doping and Morphology Improvement. *Appl. Phys. Lett.* **2006**, *89*, 053518.
(110) Cai, Y.; Wei, H.; Li, J.; Bao, Q.; Zhao, X.; Lee, S.; Li, Y.; Tang, J. Mechanism of Cs2CO3 as an n-type Dopant in Organic Electron-Transport Film. *Appl. Phys. Lett.* **2011**, *98*, 113304.
(111) Nollau, A.; Pfeiffer, M.; Fritz, T.; Leo, K. Controlled n-type Doping of a Molecular Organic Semiconductor: Naphthalenetetracarboxylic dianhydride (NTCDA) Doped with bis(ethylenedithio)-tetrahiafulvalene (BEDT-TTF). *J. Appl. Phys.* **2000**, *87*, 4340.
(112) Bendikov, M.; Wudl, F.; Perepichka, D. F. Tetrathiafulvalenes, Oligoacenenes, and their Buckminsterfullerene Derivatives: The Brick and Mortar of Organic Electronics. *Chem. Rev.* **2004**, *104*, 4891−4946.
(113) Vaid, T. P.; Lytton-Jean, A. K.; Barnes, B. C. Investigations of the 9, 10-diphenylacridyl Radical as an Isostructural Dopant for the Molecular Semiconductor 9, 10-diphenylanthracene. *Chem. Mater.* **2003**, *15*, 4292−4299.
(114) Tanaka, S.; Kanai, K.; Kawabe, E.; Iwahashi, T.; Nishi, T.; Ouchi, Y.; Seki, K. Doping Effect of Tetrathianaphthacene Molecule in Organic Semiconductors on their Interfacial Electronic Structures Studied by UV Photoemission Spectroscopy. *Jpn. J. Appl. Phys.* **2005**, *44*, 3760−3763.
(115) Gregg, B. A.; Chen, S.-G.; Branz, H. M. On the Superlinear Increase in Conductivity with Dopant Concentration in Excitonic Semiconductors. *Appl. Phys. Lett.* **2004**, *84*, 1707−1709.
(116) Porter, W. W.; Vaid, T. P. Doping of an Organic Molecular Semiconductor by Substitutional Cocrystallization with a Molecular n-dopant. *J. Mater. Chem.* **2007**, *17*, 469−475.
(117) Bloom, C. J.; Elliott, C. M.; Schroeder, P. G.; France, C. B.; Parkinson, B. Low Work Function Reduced Metal Complexes as Cathodes in Organic Electroluminescent Devices. *J. Phys. Chem. B* **2003**, *107*, 2933−2938.
(118) Chan, C. K.; Amy, F.; Zhang, Q.; Barlow, S.; Marder, S.; Kahn, A. N-type Doping of an Electron-Transport Material by Controlled Gas-Phase Incorporation Of Cobaltocene. *Chem. Phys. Lett.* **2006**, *431*, 67−71.
(119) Chan, C. K.; Zhao, W.; Barlow, S.; Marder, S.; Kahn, A. Decamethylcobaltocene as an Efficient n-dopant in Organic Electronic Materials and Devices. *Org. Electron.* **2008**, *9*, 575−581.
(120) Tietze, M. L.; Rose, B. D.; Schwarze, M.; Fischer, A.; Runge, S.; Blochwitz-Nimoth, J.; Lüssem, B.; Leo, K.; Brédas, J.-L. Passivation of Molecular n-Doping: Exploring the Limits of Air Stability. *Adv. Funct. Mater.* **2016**, *26*, 3730−3737.
(121) Tietze, M. L.; Wölzl, F.; Menke, T.; Fischer, A.; Riede, M.; Leo, K.; Lüssem, B. Self-Passivation of Molecular n-type Doping During Air Exposure Using a Highly Efficient Air-Instable Dopant. *Phys. Status Solidi A* **2013**, *210*, 2188−2198.
(122) Menke, T.; Ray, D.; Meiss, J.; Leo, K.; Riede, M. In-situ Conductivity and Seebeck Measurements of Highly Efficient n-dopants in Fullerene C60. *Appl. Phys. Lett.* **2012**, *100*, 093304.
(123) Harada, K.; Werner, A. G.; Pfeiffer, M.; Bloom, C. J.; Elliott, C. M.; Leo, K. Organic Homojunction Diodes with a High Built-in Potential: Interpretation of the Current-Voltage Characteristics by a Generalized Einstein Relation. *Phys. Rev. Lett.* **2005**, *94*, 036601.
(124) Chan, C. K.; Kahn, A. N-doping of pentacene by decamethylcobaltocene. *Appl. Phys. A: Mater. Sci. Process.* **2009**, *95*, 7−13.
(125) Chan, C. K.; Kahn, A.; Zhang, Q.; Barlow, S.; Marder, S. R. Incorporation of Cobaltocene as an n-dopant in Organic Molecular Films. *J. Appl. Phys.* **2007**, *102*, 014906.
(126) Cotton, F. A.; Gruhn, N. E.; Gu, J.; Huang, P.; Lichtenberger, D. L.; Murillo, C. A.; Van Dorn, L. O.; Wilkinson, C. C. Closed-Shell Molecules that Ionize More Readily than Cesium. *Science* **2002**, *298*, 1971−1974.
(127) Werner, A.; Li, F.; Harada, K.; Pfeiffer, M.; Fritz, T.; Leo, K. Pyronin B as a Donor for n-type Doping of Organic Thin Films. *Appl. Phys. Lett.* **2003**, *82*, 4495−4497.
(128) Li, F.; Werner, A.; Pfeiffer, M.; Leo, K.; Liu, X. Leuco Crystal Violet as a Dopant for n-doping of Organic Thin Films of Fullerene C60. *J. Phys. Chem. B* **2004**, *108*, 17076−17082.
(129) Wei, P.; Menke, T.; Naab, B. D.; Leo, K.; Riede, M.; Bao, Z. 2-(2-Methoxyphenyl)-1, 3-dimethyl-1 H-benzoimidazol-3-ium Iodide as a New Air-Stable n-Type Dopant for Vacuum-Processed Organic Semiconductor Thin Films. *J. Am. Chem. Soc.* **2012**, *134*, 3999−4002.
(130) Menke, T.; Wei, P.; Ray, D.; Kleemann, H.; Naab, B. D.; Bao, Z.; Leo, K.; Riede, M. A Comparison of Two Air-Stable Molecular n-dopants for C60. *Org. Electron.* **2012**, *13*, 3319−3325.
(131) Li, F.; Pfeiffer, M.; Werner, A.; Harada, K.; Leo, K.; Hayashi, N.; Seki, K.; Liu, X.; Dang, X.-D. Acridine Orange Base as a Dopant for n-doping of C60 Thin Films. *J. Appl. Phys.* **2006**, *100*, 023716.
(132) Wei, P.; Oh, J. H.; Dong, G.; Bao, Z. Use of a 1H-Benzoimidazole Derivative as an n-Type Dopant and To Enable Air-Stable Solution-Processed n-Channel Organic Thin-Film Transistors. *J. Am. Chem. Soc.* **2010**, *132*, 8852−8853.
(133) Naab, B. D.; Himmelberger, S.; Diao, Y.; Vandewal, K.; Wei, P.; Lussem, B.; Salleo, A.; Bao, Z. High Mobility N-Type Transistors Based on Solution-Sheared Doped 6,13-Bis(triisopropylsilylethynyl)-pentacene Thin Films. *Adv. Mater.* **2013**, *25*, 4663−4667.
(134) Naab, B. D.; Zhang, S.; Vandewal, K.; Salleo, A.; Barlow, S.; Marder, S. R.; Bao, Z. Effective Solution-and Vacuum-Processed n-Doping by Dimers of Benzimidazoline Radicals. *Adv. Mater.* **2014**, *26*, 4268−4272.
(135) Cho, N.; Yip, H.-L.; Davies, J. A.; Kazarinoff, P. D.; Zeigler, D. F.; Durban, M. M.; Segawa, Y.; O'Malley, K. M.; Luscombe, C. K.; Jen, A. K.-Y. In-situ Crosslinking and n-Doping of Semiconducting Polymers and Their Application as Efficient Electron-Transporting Materials in Inverted Polymer Solar Cells. *Adv. Energy Mater.* **2011**, *1*, 1148−1153.
(136) Schlitz, R. A.; Brunetti, F. G.; Glaudell, A. M.; Miller, P. L.; Brady, M. A.; Takacs, C. J.; Hawker, C. J.; Chabinyc, M. L. Solubility-Limited Extrinsic n-Type Doping of a High Electron Mobility Polymer for Thermoelectric Applications. *Adv. Mater.* **2014**, *26*, 2825−2830.
(137) Tarasov, A.; Zhang, S.; Tsai, M.-Y.; Campbell, P. M.; Graham, S.; Barlow, S.; Marder, S. R.; Vogel, E. M. Controlled Doping of Large-Area Trilayer MoS2 with Molecular Reductants and Oxidants. *Adv. Mater.* **2015**, *27*, 1175−1181.
(138) Naab, B. D.; Guo, S.; Olthof, S.; Evans, E. G.; Wei, P.; Millhauser, G. L.; Kahn, A.; Barlow, S.; Marder, S. R.; Bao, Z. Mechanistic Study on the Solution-Phase n-Doping of 1, 3-Dimethyl-2-aryl-2, 3-dihydro-1 H-benzoimidazole Derivatives. *J. Am. Chem. Soc.* **2013**, *135*, 15018−15025.
(139) Schottel, B. L.; Chifotides, H. T.; Dunbar, K. R. Anion-π Interactions. *Chem. Soc. Rev.* **2008**, *37*, 68−83.
(140) Li, C.-Z.; Chueh, C.-C.; Ding, F.; Yip, H.-L.; Liang, P.-W.; Li, X.; Jen, A. K.-Y. Doping of Fullerenes via Anion-Induced Electron Transfer and Its Implication for Surfactant Facilitated High Performance Polymer Solar Cells. *Adv. Mater.* **2013**, *25*, 4425−4430.
(141) Weber, C.; Bradley, C.; Lonergan, M. Solution Phase n-doping of C60 and PCBM Using Tetrabutylammonium Fluoride. *J. Mater. Chem. A* **2014**, *2*, 303−307.
(142) Goodson, F. S.; Panda, D. K.; Ray, S.; Mitra, A.; Guha, S.; Saha, S. Tunable Electronic Interactions Between Anions and Perylenediimide. *Org. Biomol. Chem.* **2013**, *11*, 4797−4803.
(143) Aragay, G.; Frontera, A.; Lloveras, V.; Vidal-Gancedo, J.; Ballester, P. Different Nature of the Interactions between Anions and HAT(CN)(6): From Reversible Anion-pi Complexes to Irreversible Electron-Transfer Processes (HAT(CN)(6) = 1,45,819,12-Hexaazatriphenylene). *J. Am. Chem. Soc.* **2013**, *135*, 2620−2627.
(144) Zhang, J.; Li, C.-Z.; Williams, S. T.; Liu, S.; Zhao, T.; Jen, A. K.-Y. Crystalline Co-Assemblies of Functional Fullerenes in Methanol with Enhanced Charge Transport. *J. Am. Chem. Soc.* **2015**, *137*, 2167−2170.

DOI: 10.1021/acs.chemrev.6b00329
Chem. Rev. 2016, 116, 13714−13751
Pictiva EX2009
Samsung v Pictiva
IPR2026-00129

(145) Reilly, T. H.; Hains, A. W.; Chen, H.-Y.; Gregg, B. A. A Self-Doping, O2-Stable, n-Type Interfacial Layer for Organic Electronics. *Adv. Energy Mater.* **2012**, *2*, 455−460.
(146) Russ, B.; Robb, M. J.; Brunetti, F. G.; Miller, P. L.; Perry, E. E.; Patel, S. N.; Ho, V.; Chang, W. B.; Urban, J. J.; Chabinyc, M. L.; Hawker, C.; RA, S. Power Factor Enhancement in Solution-Processed Organic n-Type Thermoelectrics Through Molecular Design. *Adv. Mater.* **2014**, *26*, 3473−3477.
(147) Limmert, M.; Hartmann, H.; Zeika, O.; Werner, A.; Ammann, M. Heterocyclisches Radikal oder Diradikal, deren Dimere, Oligomere, Polymere, Dispiroverbindungen und Polycyclen, deren Verwendung, organisches halbleitendes Material sowie elektronisches Bauelement, 2007.
(148) Guo, S.; Kim, S. B.; Mohapatra, S. K.; Qi, Y.; Sajoto, T.; Kahn, A.; Marder, S. R.; Barlow, S. n-Doping of Organic Electronic Materials using Air-Stable Organometallics. *Adv. Mater.* **2012**, *24*, 699−703.
(149) Qi, Y.; Mohapatra, S. K.; Kim, S. B.; Barlow, S.; Marder, S. R.; Kahn, A. Solution doping of organic semiconductors using air-stable n-dopants. *Appl. Phys. Lett.* **2012**, *100*, 083305.
(150) Mohapatra, S. K.; Fonari, A.; Risko, C.; Yesudas, K.; Moudgil, K.; Delcamp, J. H.; Timofeeva, T. V.; Brédas, J.-L.; Marder, S. R.; Barlow, S. Dimers of Nineteen-Electron Sandwich Compounds: Crystal and Electronic Structures, and Comparison of Reducing Strengths. *Chem. - Eur. J.* **2014**, *20*, 15385−15394.
(151) Zhang, S.; Naab, B. D.; Jucov, E. V.; Parkin, S.; Evans, E. G.; Millhauser, G. L.; Timofeeva, T. V.; Risko, C.; Brédas, J.-L.; Bao, Z.; Barlow, S.; Marder, S. n-Dopants Based on Dimers of Benzimidazoline Radicals: Structures and Mechanism of Redox Reactions. *Chem. - Eur. J.* **2015**, *21*, 10878−10885.
(152) Riede, M.; Mueller, T.; Tress, W.; Schueppel, R.; Leo, K. Small-Molecule Solar Cells - Status and Perspectives. *Nanotechnology* **2008**, *19*, 424001.
(153) Shirakawa, H.; Louis, E. J.; MacDiarmid, A. G.; Chiang, C. K.; Heeger, A. J. Synthesis of Electrically Conducting Organic Polymers: Halogen Derivatives of Polyacetylene, $(CH)_x$. *J. Chem. Soc., Chem. Commun.* **1977**, 578−580.
(154) Heeger, A. J. Semiconducting and Metallic Polymers: The Fourth Generation of Polymeric Materials. *J. Phys. Chem. B* **2001**, *105*, 8475−8491.
(155) Yim, K.-H.; Whiting, G. L.; Murphy, C. E.; Halls, J. J.; Burroughes, J. H.; Friend, R. H.; Kim, J.-S. Controlling Electrical Properties of Conjugated Polymers via a Solution-Based p-Type Doping. *Adv. Mater.* **2008**, *20*, 3319−3324.
(156) Wang, C.; Duong, D. T.; Vandewal, K.; Rivnay, J.; Salleo, A. Optical Measurement of Doping Efficiency in Poly (3-hexylthiophene) Solutions and Thin Films. *Phys. Rev. B: Condens. Matter Mater. Phys.* **2015**, *91*, 085205.
(157) Gao, J.; Niles, E. T.; Grey, J. K. Aggregates Promote Efficient Charge Transfer Doping of Poly (3-hexylthiophene). *J. Phys. Chem. Lett.* **2013**, *4*, 2953−2957.
(158) Duong, D. T.; Phan, H.; Hanifi, D.; Jo, P. S.; Nguyen, T.-Q.; Salleo, A. Direct Observation of Doping Sites in Temperature-Controlled, p-Doped P3HT Thin Films by Conducting Atomic Force Microscopy. *Adv. Mater.* **2014**, *26*, 6069−6073.
(159) Pingel, P.; Zhu, L.; Park, K. S.; Vogel, J. r.-O.; Janietz, S.; Kim, E.-G.; Rabe, J. r. P.; Brédas, J.-L.; Koch, N. Charge-Transfer Localization in Molecularly Doped Thiophene-based Donor Polymers. *J. Phys. Chem. Lett.* **2010**, *1*, 2037−2041.
(160) Pingel, P.; Neher, D. Comprehensive Picture of p-type Doping of P3HT with the Molecular Acceptor F_4TCNQ. *Phys. Rev. B: Condens. Matter Mater. Phys.* **2013**, *87*, 115209.
(161) Pingel, P.; Schwarzl, R.; Neher, D. Effect of Molecular p-doping on Hole Density and Mobility in Poly(3-hexylthiophene). *Appl. Phys. Lett.* **2012**, *100*, 143303.
(162) Zhang, Y.; Blom, P. W. Enhancement of the Hole Injection into Regioregular Poly (3-hexylthiophene) by Molecular Doping. *Appl. Phys. Lett.* **2010**, *97*, 083303−3.
(163) Aziz, E. F.; Vollmer, A.; Eisebitt, S.; Eberhardt, W.; Pingel, P.; Neher, D.; Koch, N. Localized Charge Transfer in a Molecularly Doped Conducting Polymer. *Adv. Mater.* **2007**, *19*, 3257−3260.
(164) Zhu, L.; Kim, E.-G.; Yi, Y.; Brédas, J.-L. Charge Transfer in Molecular Complexes with 2, 3, 5, 6-Tetrafluoro-7, 7, 8, 8-tetracyanoquinodimethane (F4-TCNQ): A Density Functional Theory Study. *Chem. Mater.* **2011**, *23*, 5149−5159.
(165) Unuma, T.; Fujii, K.; Kishida, H.; Nakamura, A. Terahertz Complex Conductivities of Carriers with Partial Localization in Doped Polythiophenes. *Appl. Phys. Lett.* **2010**, *97*, 3308.
(166) Ma, L.; Lee, W. H.; Park, Y. D.; Kim, J. S.; Lee, H. S.; Choa, K. High Performance Polythiophene Thin-film Transistors Doped with Very Small Amounts of an Electron Acceptor. *Appl. Phys. Lett.* **2008**, *92*, 063310.
(167) Gao, J.; Roehling, J. D.; Li, Y.; Guo, H.; Moulé, A. J.; Grey, J. K. The Effect of 2, 3, 5, 6-tetrafluoro-7, 7, 8, 8-tetracyanoquinodimethane Charge Transfer Dopants on the Conformation and Aggregation of Poly (3-hexylthiophene). *J. Mater. Chem. C* **2013**, *1*, 5638−5646.
(168) Sirringhaus, H.; Brown, P.; Friend, R.; Nielsen, M.; Bechgaard, K.; Langeveld-Voss, B.; Spiering, A.; Janssen, R.; Meijer, E.; Herwig, P.; de Leeuw, D. Two-Dimensional Charge Transport In Self-organized, High-Mobility Conjugated Polymers. *Nature* **1999**, *401*, 685−688.
(169) Arkhipov, V.; Heremans, P.; Emelianova, E.; Baessler, H. Effect of Doping on the Density-of-states Distribution and Carrier Hopping in Disordered Organic Semiconductors. *Phys. Rev. B: Condens. Matter Mater. Phys.* **2005**, *71*, 045214.
(170) Kelley, T.; Muyres, D.; Baude, P.; Smith, T.; Jones, T. High performance organic thin film transistors. *MRS Online Proc. Libr.* **2003**, *771*, 169−179. Symposium on Organic and Polymeric Materials and Devices held at the 2003 MRS Spring Meeting, San Francisco, CA, Apr 22−25, 2003.
(171) Klauk, H.; Halik, M.; Zschieschang, U.; Schmid, G.; Radlik, W.; Weber, W. High-Mobility Polymer Gate Dielectric Pentacene Thin Film Transistors. *J. Appl. Phys.* **2002**, *92*, 5259−5263.
(172) Schiefer, S.; Huth, M.; Dobrinevski, A.; Nickel, B. Determination of the Crystal Structure of Substrate-induced Pentacene Polymorphs in Fiber Structured Thin Films. *J. Am. Chem. Soc.* **2007**, *129*, 10316−10317.
(173) Siegrist, T.; Besnard, C.; Haas, S.; Schiltz, M.; Pattison, P.; Chernyshov, D.; Batlogg, B.; Kloc, C. A Polymorph Lost and Found: The High-Temperature Crystal Structure of Pentacene. *Adv. Mater.* **2007**, *19*, 2079−2082.
(174) Minakata, T.; Nagoya, I.; Ozaki, M. Highly Ordered And Conducting Thin-film Of Pentacene Doped With Iodine Vapor. *J. Appl. Phys.* **1991**, *69*, 7354−7356.
(175) Matsuo, Y.; Sasaki, A.; Yoshida, Y.; Ikehata, S. New Stage Structure of Iodine Doped Pentacene Film. *Mater. Sci. Eng., B* **1999**, *60*, 133−136.
(176) Matsuo, Y.; Sasaki, S.; Ikehata, S. Electric Properties on Iodine Doped Pentacene. *Synth. Met.* **2001**, *121*, 1383−1384.
(177) Minakata, T.; Imai, H.; Ozaki, M. Electrical-Properties of Highly Ordered and Amorphous Thin-films of Pentacene Doped with Iodine. *J. Appl. Phys.* **1992**, *72*, 4178−4182.
(178) Minakata, T.; Imai, H.; Ozaki, M.; Saco, K. Structural Studies on Highly Ordered and Highly Conductive Thin-films of Pentacene. *J. Appl. Phys.* **1992**, *72*, 5220−5225.
(179) Minakata, T.; Ozaki, M.; Imai, H. Conducting Thin-films of Pentacene Doped with Alkaline-metals. *J. Appl. Phys.* **1993**, *74*, 1079−1082.
(180) Mori, T.; Ikehata, S. Study of Magnetic and Electrical Properties of Iodine Doped Pentacene. *Mater. Sci. Eng., B* **1997**, *49*, 251−257.
(181) Brinkmann, M.; Videva, V.; Bieber, A.; Andre, J.; Turek, P.; Zuppiroli, L.; Bugnon, P.; Schaer, M.; Nuesch, F.; Humphry-Baker, R. Electronic and Structural Evidences for Charge Transfer and Localization in Iodine-doped Pentacene. *J. Phys. Chem. A* **2004**, *108*, 8170−8179.
(182) Cazayous, M.; Sacuto, A.; Horowitz, G.; Lang, P.; Zimmers, A.; Lobo, R. Iodine Insertion in Pentacene Thin Films Investigated by

DOI: 10.1021/acs.chemrev.6b00329
Chem. Rev. 2016, 116, 13714−13751
Pictiva EX2009
Samsung v Pictiva
IPR2026-00129

Infrared and Raman Spectroscopy. *Phys. Rev. B: Condens. Matter Mater. Phys.* **2004**, *70*, 081309.
(183) Ito, T.; Mitani, T.; Takenobu, T.; Iwasa, Y. Structural Analysis of Intercalation Compounds of Pentacene. *J. Phys. Chem. Solids* **2004**, *65*, 609−613.
(184) Harada, K.; Sumino, M.; Adachi, C.; Tanaka, S.; Miyazaki, K. Improved Thermoelectric Performance of Organic Thin-Film Elements Utilizing a Bilayer Structure of Pentacene and 2,3,5,6-tetrafluoro-7,7,8,8-tetracyanoquinodimethane (F4-TCNQ). *Appl. Phys. Lett.* **2010**, *96*, 253304.
(185) Kleemann, H.; Schuenemann, C.; Zakhidov, A. A.; Riede, M.; Luessem, B.; Leo, K. Structural Phase Transition in Pentacene Caused by Molecular Doping and its Effect on Charge Carrier Mobility. *Org. Electron.* **2012**, *13*, 58−65.
(186) Ha, S. D.; Meyer, J.; Kahn, A. Molecular-Scale Properties of MoO3-doped Pentacene. *Phys. Rev. B: Condens. Matter Mater. Phys.* **2010**, *82*, 155434.
(187) Lou, Y.-H.; Xu, M.-F.; Zhang, L.; Wang, Z.-K.; Naka, S.; Okada, H.; Liao, L.-S. Origin of Enhanced Electrical and Conducting Properties in Pentacene Films Doped by Molybdenum Trioxide. *Org. Electron.* **2013**, *14*, 2698−2704.
(188) Wang, Z.; Alam, M. W.; Lou, Y.; Naka, S.; Okada, H. Enhanced Carrier Injection in Pentacene Thin-Film Transistors by Inserting a MoO3-doped Pentacene Layer. *Appl. Phys. Lett.* **2012**, *100*, 043302.
(189) Berkowitz, J.; Inghram, M. G.; W.A, C. Polymeric Gaseous Species in the Sublimation of Molybdenium Trioxide. *J. Chem. Phys.* **1957**, *26*, 842−846.
(190) Fang, B.; Zhou, H.; Honma, I. Electrochemical Lithium Doping of a Pentacene Molecule Semiconductor. *Appl. Phys. Lett.* **2005**, *86*, 261909.
(191) Kaneko, Y.; Suzuki, T.; Matsuo, Y.; Ikehata, S. Metallic Electrical Conduction in Alkaline Metal-Doped Pentacene. *Synth. Met.* **2005**, *154*, 177−180.
(192) Craciun, M. F.; Giovannetti, G.; Rogge, S.; Brocks, G.; Morpurgo, A. F.; van den Brink, J. Evidence for the Formation of a Mott State in Potassium-Intercalated Pentacene. *Phys. Rev. B: Condens. Matter Mater. Phys.* **2009**, *79*, 125116.
(193) Hansson, A.; Bohlin, J.; Stafstrom, S. Structural and Electronic Transitions in Potassium-Doped Pentacene. *Phys. Rev. B: Condens. Matter Mater. Phys.* **2006**, *73*, 184114.
(194) Guo, S.; Mohapatra, S. K.; Romanov, A.; Timofeeva, T. V.; Hardcastle, K. I.; Yesudas, K.; Risko, C.; Bredas, J.-L.; Marder, S. R.; Barlow, S. n-Doping of Organic Electronic Materials Using Air-Stable Organometallics: A Mechanistic Study of Reduction by Dimeric Sandwich Compounds. *Chem. - Eur. J.* **2012**, *18*, 14760−14772.
(195) Haddon, R.; et al. Conducting Films of C60 and C70 by Alkali-Metal Doping. *Nature* **1991**, *350*, 320−322.
(196) Hebard, A.; Rosseinsky, M.; Haddon, R.; Murphy, D.; Glarum, S.; Palstra, T.; Ramirez, A.; Kortan, A. Superconductivity At 18-K in Potassium-doped C-60. *Nature* **1991**, *350*, 600−601.
(197) Palstra, T.; Haddon, R.; Hebard, A.; Zaanen, J. Electronic Transport-Properties of K3C60 Films. *Phys. Rev. Lett.* **1992**, *68*, 1054−1057.
(198) Kubo, M.; Kaji, T.; Hiramoto, M. pn-Homojunction Formation in Single Fullerene Films. *AIP Adv.* **2011**, *1*, 032177.
(199) Harada, K.; Li, F.; Maennig, B.; Pfeiffer, M.; Leo, K. Ionized Impurity Scattering in n-doped C-60 Thin Films. *Appl. Phys. Lett.* **2007**, *91*, 092118.
(200) Kubo, M.; Iketaki, K.; Kaji, T.; Hiramoto, M. Conduction-Type Control of Fullerene Films from N- to P-type by Molybdenum Oxide Doping. *Appl. Phys. Lett.* **2011**, *98*, 073311.
(201) Lee, T. H.; Luessem, B.; Kim, K.; Giri, G.; Nishi, Y.; Bao, Z. P-Channel Field-Effect Transistors Based on C-60 Doped with Molybdenum Trioxide. *ACS Appl. Mater. Interfaces* **2013**, *5*, 2337−2341.
(202) Shinmura, Y.; Yoshioka, T.; Kaji, T.; Hiramoto, M. Mapping of Band-Bending for Doped C-60 Films. *Appl. Phys. Express* **2014**, *7*, 071601.
(203) Yamamoto, T.; Takimiya, K. Facile Synthesis of Highly π-extended Heteroarenes, Dinaphtho [2, 3-b: 2′, 3′-f] Chalcogenopheno [3, 2-b] Chalcogenophenes, and their Application to Field-Effect Transistors. *J. Am. Chem. Soc.* **2007**, *129*, 2224−2225.
(204) Hofmockel, R.; Zschieschang, U.; Kraft, U.; Roedel, R.; Hansen, N. H.; Stolte, M.; Wuerthner, F.; Takimiya, K.; Kern, K.; Pflaum, J.; Klauk, H. High-Mobility Organic Thin-film Transistors Based on a Small-Molecule Semiconductor Deposited in Vacuum and by Solution Shearing. *Org. Electron.* **2013**, *14*, 3213−3221.
(205) Kang, M. J.; Doi, I.; Mori, H.; Miyazaki, E.; Takimiya, K.; Ikeda, M.; Kuwabara, H. Alkylated Dinaphtho[2,3-b:2 ′,3 ′-f]Thieno-[3,2-b] Thiophenes (C-n-DNTTs): Organic Semiconductors for High-Performance Thin-Film Transistors. *Adv. Mater.* **2011**, *23*, 1222−1225.
(206) Matsumoto, T.; Ou-Yang, W.; Miyake, K.; Uemura, T.; Takeya, J. Study of Contact Resistance of High-Mobility Organic Transistors through Comparisons. *Org. Electron.* **2013**, *14*, 2590−2595.
(207) Zschieschang, U.; Kang, M. J.; Takimiya, K.; Sekitani, T.; Someya, T.; Canzler, T. W.; Werner, A.; Blochwitz-Nimoth, J.; Klauk, H. Flexible Low-Voltage Organic Thin-film Transistors and Circuits Based on C10-DNTT. *J. Mater. Chem.* **2012**, *22*, 4273−4277.
(208) Yuan, Y.; Giri, G.; Ayzner, A. L.; Zoombelt, A. P.; Mannsfeld, S. C. B.; Chen, J.; Nordlund, D.; Toney, M. F.; Huang, J.; Bao, Z. Ultra-High Mobility Transparent Organic Thin Film Transistors Grown by an Off-Centre Spin-Coating Method. *Nat. Commun.* **2014**, *5*, 3005.
(209) Soeda, J.; Hirose, Y.; Yamagishi, M.; Nakao, A.; Uemura, T.; Nakayama, K.; Uno, M.; Nakazawa, Y.; Takimiya, K.; Takeya, J. Solution-Crystallized Organic Field-Effect Transistors with Charge-Acceptor Layers: High-Mobility and Low-Threshold-Voltage Operation in Air. *Adv. Mater.* **2011**, *23*, 3309−3314.
(210) Gregg, B. A.; Cormier, R. A. Doping Molecular Semiconductors: N-type Doping of a Liquid Crystal Perylene Diimide. *J. Am. Chem. Soc.* **2001**, *123*, 7959−7960.
(211) Ante, F.; Kaelblein, D.; Zaki, T.; Zschieschang, U.; Takimiya, K.; Ikeda, M.; Sekitani, T.; Someya, T.; Burghartz, J. N.; Kern, K.; Klauk, H. Contact Resistance and Megahertz Operation of Aggressively Scaled Organic Transistors. *Small* **2012**, *8*, 73−79.
(212) Liu, X.; Kasemann, D.; Leo, K. Top-Gate Organic Depletion and Inversion Transistors with Doped Channel and Injection Contact. *Appl. Phys. Lett.* **2015**, *106*, 103301.
(213) Khim, D.; Baeg, K.-J.; Caironi, M.; Liu, C.; Xu, Y.; Kim, D.-Y.; Noh, Y.-Y. Control of Ambipolar and Unipolar Transport in Organic Transistors by Selective Inkjet-Printed Chemical Doping for High Performance Complementary Circuits. *Adv. Funct. Mater.* **2014**, *24*, 6252−6261.
(214) Ishii, H.; Sugiyama, K.; Ito, E.; Seki, K. Energy Level Alignment and Interfacial Electronic Structures at Organic/Metal and Organic/Organic Interfaces. *Adv. Mater.* **1999**, *11*, 972−972.
(215) Hill, I.; Milliron, D.; Schwartz, J.; Kahn, A. Organic Semiconductor Interfaces: Electronic Structure and Transport Properties. *Appl. Surf. Sci.* **2000**, *166*, 354−362.
(216) Salaneck, W. R.; Lögdlund, M.; Fahlman, M.; Greczynski, G.; Kugler, T. The Electronic Structure of Polymer-Metal Interfaces Studied by Ultraviolet Photoelectron Spectroscopy. *Mater. Sci. Eng., R* **2001**, *34*, 121−146.
(217) Scott, J. Metal-Organic Interface and Charge Injection in Organic Electronic Devices. *J. Vac. Sci. Technol., A* **2003**, *21*, 521−531.
(218) Rhee, S.-W.; Yun, D.-J. Metal-Semiconductor Contact in Organic Thin Film Transistors. *J. Mater. Chem.* **2008**, *18*, 5437−5444.
(219) Braun, S.; Salaneck, W. R.; Fahlman, M. Energy-Level Alignment at Organic/Metal and Organic/Organic Interfaces. *Adv. Mater.* **2009**, *21*, 1450−1472.
(220) Coropceanu, V.; Li, H.; Winget, P.; Zhu, L.; Brédas, J.-L. Electronic-Structure Theory of Organic Semiconductors: Charge-Transport Parameters and Metal/Organic Interfaces. *Annu. Rev. Mater. Res.* **2013**, *43*, 63−87.

DOI: 10.1021/acs.chemrev.6b00329
Chem. Rev. 2016, 116, 13714−13751
Pictiva EX2009
Samsung v Pictiva
IPR2026-00129

(221) Lindell, L.; Çakır, D.; Brocks, G.; Fahlman, M.; Braun, S. Role of Intrinsic Molecular Dipole in Energy Level Alignment at Organic Interfaces. *Appl. Phys. Lett.* **2013**, *102*, 223301.
(222) Heimel, G.; Romaner, L.; Zojer, E.; Bredas, J.-L. The Interface Energetics of Self-Assembled Monolayers on Metals. *Acc. Chem. Res.* **2008**, *41*, 721−729.
(223) Osikowicz, W.; de Jong, M. P.; Braun, S.; Tengstedt, C.; Fahlman, M.; Salaneck, W. R. Energetics at Au Top and Bottom Contacts on Conjugated Polymers. *Appl. Phys. Lett.* **2006**, *88*, 193504.
(224) de Boer, B.; Hadipour, A.; Mandoc, M. M.; van Woudenbergh, T.; Blom, P. W. Tuning of Metal Work Functions with Self-Assembled Monolayers. *Adv. Mater.* **2005**, *17*, 621−625.
(225) Park, J.; Lee, W. H.; Huh, S.; Sim, S. H.; Kim, S. B.; Cho, K.; Hong, B. H.; Kim, K. S. Work-Function Engineering of Graphene Electrodes by Self-assembled Monolayers for High-Performance Organic Field-Effect Transistors. *J. Phys. Chem. Lett.* **2011**, *2*, 841−845.
(226) Fenwick, O.; Van Dyck, C.; Murugavel, K.; Cornil, D.; Reinders, F.; Haar, S.; Mayor, M.; Cornil, J.; Samorì, P. Modulating the Charge Injection in Organic Field-effect Transistors: Fluorinated Oligophenyl Self-Assembled Monolayers for High Work Function Electrodes. *J. Mater. Chem. C* **2015**, *3*, 3007−3015.
(227) Kano, M.; Minari, T.; Tsukagoshi, K. Improvement of Subthreshold Current Transport by Contact Interface Modification in p-type Organic Field-Effect Transistors. *Appl. Phys. Lett.* **2009**, *94*, 143304.
(228) Khim, D.; Baeg, K.-J.; Kim, J.; Yeo, J.-S.; Kang, M.; Amegadzea, P. S.; Kim, M.-G.; Cho, J.; Lee, J. H.; Kim, D.-Y.; Noh, Y.-Y. Electron Injection Enhancement by a Cs-salt Interlayer in Ambipolar Organic Field-effect Transistors and Complementary Circuits. *J. Mater. Chem.* **2012**, *22*, 16979−16985.
(229) Cho, S.; Seo, J. H.; Lee, K.; Heeger, A. J. Enhanced Performance of Fullerene n-Channel Field-Effect Transistors with Titanium Sub-Oxide Injection Layer. *Adv. Funct. Mater.* **2009**, *19*, 1459−1464.
(230) Bory, B. F.; Rocha, P. R.; Janssen, R. A.; Gomes, H. L.; De Leeuw, D. M.; Meskers, S. C. Lithium Fluoride Injection Layers Can Form Quasi-Ohmic Contacts for Both Holes and Electrons. *Appl. Phys. Lett.* **2014**, *105*, 123302.
(231) Gundlach, D. J.; Zhou, L.; Nichols, J. A.; Jackson, T. N.; Necliudov, P. V.; Shur, M. S. An Experimental Study of Contact Effects in Organic Thin Film Transistors. *J. Appl. Phys.* **2006**, *100*, 024509.
(232) Hill, I. Numerical Simulations of Contact Resistance in Organic Thin-Film Transistors. *Appl. Phys. Lett.* **2005**, *87*, 163505.
(233) Scheinert, S.; Paasch, G. Interdependence of Contact Properties and Field-and Density-Dependent Mobility in Organic Field-Effect Transistors. *J. Appl. Phys.* **2009**, *105*, 014509.
(234) Marinkovic, M.; Belaineh, D.; Wagner, V.; Knipp, D. On the Origin of Contact Resistances of Organic Thin Film Transistors. *Adv. Mater.* **2012**, *24*, 4005−4009.
(235) Murrmann, H.; Widmann, D. Messung des Übergangswiderstandes zwischen Metall und Diffusionsschicht in Si-Planarelementen. *Solid-State Electron.* **1969**, *12*, 879−886.
(236) Murrmann, H.; Widmann, D. Current Crowding on Metal Contacts to Planar Devices. *IEEE Trans. Electron Devices* **1969**, *16*, 1022−1024.
(237) Chiang, C.-S.; Martin, S.; Kanicki, J.; Ugai, Y.; Yukawa, T.; Takeuchi, S. Top-Gate Staggered Amorphous Silicon Thin-film Transistors: Series Resistance and Nitride Thickness Effects. *Jpn. J. Appl. Phys.* **1998**, *37*, 5914−5920.
(238) Marinkovic, M.; Hashem, E.; Chan, K.-Y.; Gordijn, A.; Stiebig, H.; Knipp, D. Microcrystalline Silicon Thin-film Transistors Operating at Very High Frequencies. *Appl. Phys. Lett.* **2010**, *97*, 073502.
(239) Jung, K.-D.; Kim, Y. C.; Kim, B.-J.; Park, B.-G.; Shin, H.; Lee, J. D. An Analytic Current-Voltage Equation for Top-Contact Organic Thin Film Transistors Including the Effects of Variable Series Resistance. *Jpn. J. Appl. Phys.* **2008**, *47*, 3174.
(240) Richards, T.; Sirringhaus, H. Analysis of the Contact Resistance in Staggered, Top-Gate Organic Field-effect Transistors. *J. Appl. Phys.* **2007**, *102*, 094510.
(241) Schroder, D. K. *Semiconductor Material and Device Characterization*; John Wiley & Sons: New York, 2006.
(242) Horowitz, G. Organic Thin Film Transistors: From Theory to Real Devices. *J. Mater. Res.* **2004**, *19*, 1946−1962.
(243) Zaumseil, J.; Baldwin, K. W.; Rogers, J. A. Contact Resistance in Organic Transistors that Use Source and Drain Electrodes Formed by Soft Contact Lamination. *J. Appl. Phys.* **2003**, *93*, 6117−6124.
(244) Luan, S.; Neudeck, G. W. An Experimental Study of the Source/Drain Parasitic Resistance Effects in Amorphous Silicon Thin Film Transistors. *J. Appl. Phys.* **1992**, *72*, 766−772.
(245) Natali, D.; Caironi, M. Charge Injection in Solution-Processed Organic Field-Effect Transistors: Physics, Models and Characterization Methods. *Adv. Mater.* **2012**, *24*, 1357−1387.
(246) Reese, C.; Bao, Z. Detailed Characterization of Contact Resistance, Gate-Bias-Dependent Field-Effect Mobility, and Short-Channel Effects with Microscale Elastomeric Single-Crystal Field-Effect Transistors. *Adv. Funct. Mater.* **2009**, *19*, 763−771.
(247) Xu, Y.; Gwoziecki, R.; Chartier, I.; Coppard, R.; Balestra, F.; Ghibaudo, G. Modified Transmission-Line Method for Contact Resistance Extraction in Organic Field-Effect Transistors. *Appl. Phys. Lett.* **2010**, *97*, 063302.
(248) Chen, C.-Y.; Kanicki, J. Gated-Four-Probe a-Si:H TFT Structure: A New Technique to Measure the Intrinsic Performance of a-Si:H TFT. *IEEE Electron Device Lett.* **1997**, *18*, 340−342.
(249) Pesavento, P. V.; Chesterfield, R. J.; Newman, C. R.; Frisbie, C. D. Gated Four-Probe Measurements on Pentacene Thin-Film Transistors: Contact Resistance as a Function of Gate Voltage and Temperature. *J. Appl. Phys.* **2004**, *96*, 7312−7324.
(250) Uemura, T.; Rolin, C.; Ke, T.-H.; Fesenko, P.; Genoe, J.; Heremans, P.; Takeya, J. On the Extraction of Charge Carrier Mobility in High-Mobility Organic Transistors. *Adv. Mater.* **2016**, *28*, 151−155.
(251) Matsushima, T.; Adachi, C. Extremely Low Voltage Organic Light-Emitting Diodes with p-doped Alpha-Sexithiophene Hole Transport and n-doped Phenyldipyrenylphosphine Oxide Electron Transport Layers. *Appl. Phys. Lett.* **2006**, *89*, 253506.
(252) Chu, C.-W.; Li, S.-H.; Chen, C.-W.; Shrotriya, V.; Yang, Y. High-Performance Organic Thin-film Transistors with Metal Oxide/Metal Bilayer Electrode. *Appl. Phys. Lett.* **2005**, *87*, 193508−193508.
(253) Kumaki, D.; Umeda, T.; Tokito, S. Reducing the Contact Resistance of Bottom-Contact Pentacene Thin-film Transistors by Employing a MoOx Carrier Injection Layer. *Appl. Phys. Lett.* **2008**, *92*, 013301.
(254) Darmawan, P.; Minari, T.; Kumatani, A.; Li, Y.; Liu, C.; Tsukagoshi, K. Reduction of Charge Injection Barrier by 1-nm Contact Oxide Interlayer in Organic Field Effect Transistors. *Appl. Phys. Lett.* **2012**, *100*, 013303.
(255) Greiner, M. T.; Lu, Z.-H. Thin-film Metal Oxides in Organic Semiconductor Devices: Their Electronic Structures, Work Functions and Interfaces. *NPG Asia Mater.* **2013**, *5*, e55.
(256) Schroeder, R.; Majewski, L. A.; Grell, M. Improving Organic Transistor Performance with Schottky Contacts. *Appl. Phys. Lett.* **2004**, *84*, 1004−1006.
(257) Gu, W.; Jin, W.; Wei, B.; Zhang, J.; Wang, J. High-Performance Organic Field-Effect Transistors Based on Copper/Copper Sulphide Bilayer Source-Drain Electrodes. *Appl. Phys. Lett.* **2010**, *97*, 243303.
(258) Günther, A. A.; Sawatzki, M.; Formánek, P.; Kasemann, D.; Leo, K. Contact Doping for Vertical Organic Field-Effect Transistors. *Adv. Funct. Mater.* **2016**, *26*, 768−775.
(259) Vanoni, C.; Tsujino, S.; Jung, T. A. Reduction of the Contact Resistance by Doping in Pentacene Few Monolayers Thin Film Transistors and Self-Assembled Nanocrystals. *Appl. Phys. Lett.* **2007**, *90*, 193119.
(260) Zhao, W.; Qi, Y.; Sajoto, T.; Barlow, S.; Marder, S. R.; Kahn, A. Remote Doping of a Pentacene Transistor: Control of Charge Transfer By Molecular-level Engineering. *Appl. Phys. Lett.* **2010**, *97*, 123305.

DOI: 10.1021/acs.chemrev.6b00329
Chem. Rev. 2016, 116, 13714−13751
Pictiva EX2009
Samsung v Pictiva
IPR2026-00129

(261) Kaschura, F.; Fischer, A.; Kasemann, D.; Leo, K.; Lüssem, B. Controlling Morphology: A Vertical Organic Transistor with a Self-Structured Permeable Base Using the Bottom Electrode as Seed Layer. *Appl. Phys. Lett.* **2015**, *107*, 033301.
(262) Nicht, S.; Kleemann, H.; Fischer, A.; Leo, K.; Lüssem, B. Functionalized p-dopants as Self-Assembled Monolayers for Enhanced Charge Carrier Injection in Organic Electronic Devices. *Org. Electron.* **2014**, *15*, 654−660.
(263) Ahles, M.; Schmechel, R.; von Seggern, H. N-type Organic Field-Effect Transistor Based on Interface-Doped Pentacene. *Appl. Phys. Lett.* **2004**, *85*, 4499−4501.
(264) Seo, J. H.; Gutacker, A.; Walker, B.; Cho, S.; Garcia, A.; Yang, R.; Nguyen, T.-Q.; Heeger, A. J.; Bazan, G. C. Improved Injection in N-type Organic Transistors with Conjugated Polyelectrolytes. *J. Am. Chem. Soc.* **2009**, *131*, 18220−18221.
(265) Kim, J.; Khim, D.; Kang, R.; Lee, S.-H.; Baeg, K.-J.; Kang, M.; Noh, Y.-Y.; Kim, D.-Y. Simultaneous Enhancement of Electron Injection and Air Stability in N-type Organic Field-Effect Transistors by Water-Soluble Polyfluorene Interlayers. *ACS Appl. Mater. Interfaces* **2014**, *6*, 8108−8114.
(266) Liu, C.; Jang, J.; Xu, Y.; Kim, H.-J.; Khim, D.; Park, W.-T.; Noh, Y.-Y.; Kim, J.-J. Effect of Doping Concentration on Microstructure of Conjugated Polymers and Characteristics in N-Type Polymer Field-Effect Transistors. *Adv. Funct. Mater.* **2015**, *25*, 758−767.
(267) Rossbauer, S.; Müller, C.; Anthopoulos, T. D. Comparative Study of the N-Type Doping Efficiency in Solution-processed Fullerenes and Fullerene Derivatives. *Adv. Funct. Mater.* **2014**, *24*, 7116−7124.
(268) Oh, J. H.; Wei, P.; Bao, Z. Molecular n-type Doping for Air-Stable Electron Transport in Vacuum-Processed n-channel Organic Transistors. *Appl. Phys. Lett.* **2010**, *97*, 243305.
(269) Horowitz, G.; Hajlaoui, R.; Bouchriha, H.; Bourguiga, R.; Hajlaoui, M. The Concept of "Threshold Voltage" in Organic Field-Effect Transistors. *Adv. Mater.* **1998**, *10*, 923−927.
(270) Belasco, J.; Mohapatra, S. K.; Zhang, Y.; Barlow, S.; Marder, S. R.; Kahn, A. Molecular Doping and Tuning Threshold Voltage in 6, 13-bis (triisopropylsilylethynyl) Pentacene/Polymer Blend Transistors. *Appl. Phys. Lett.* **2014**, *105*, 063301.
(271) Lee, B. H.; Bazan, G. C.; Heeger, A. J. Doping-Induced Carrier Density Modulation in Polymer Field-Effect Transistors. *Adv. Mater.* **2016**, *28*, 57−62.
(272) Han, S.-T.; Zhou, Y.; Xu, Z.-X.; Roy, V. Controllable Threshold Voltage Shifts of Polymer Transistors and Inverters by Utilizing Gold Nanoparticles. *Appl. Phys. Lett.* **2012**, *101*, 033306.
(273) Cosseddu, P.; Vogel, J.-O.; Fraboni, B.; Rabe, J. P.; Koch, N.; Bonfiglio, A. Continuous Tuning of Organic Transistor Operation from Enhancement to Depletion Mode. *Adv. Mater.* **2009**, *21*, 344−348.
(274) Kim, J. H.; Yun, S. W.; An, B.-K.; Han, Y. D.; Yoon, S.-J.; Joo, J.; Park, S. Y. Remarkable Mobility Increase and Threshold Voltage Reduction in Organic Field-Effect Transistors by Overlaying Discontinuous Nano-Patches of Charge-Transfer Doping Layer on Top of Semiconducting Film. *Adv. Mater.* **2013**, *25*, 719−724.
(275) Marchl, M.; Edler, M.; Haase, A.; Fian, A.; Trimmel, G.; Griesser, T.; Stadlober, B.; Zojer, E. Tuning the Threshold Voltage in Organic Thin-Film Transistors by Local Channel Doping Using Photoreactive Interfacial Layers. *Adv. Mater.* **2010**, *22*, 5361−5365.
(276) Pacher, P.; Lex, A.; Proschek, V.; Etschmaier, H.; Tchernychova, E.; Sezen, M.; Scherf, U.; Grogger, W.; Trimmel, G.; Slugovc, C.; Zojer, E. Chemical Control of Local Doping in Organic Thin-Film Transistors: From Depletion to Enhancement. *Adv. Mater.* **2008**, *20*, 3143−3148.
(277) Chen, W.; Gao, X. Y.; Qi, D. C.; Chen, S.; Chen, Z. K.; Wee, A. T. S. Surface-Transfer Doping of Organic Semiconductors Using Functionalized Self-Assembled Monolayers. *Adv. Funct. Mater.* **2007**, *17*, 1339−1344.
(278) Yamagishi, Y.; Noda, K.; Yamada, H.; Matsushige, K. Organic Field-Effect Transistors with Molecularly Doped Polymer Gate Buffer Layer. *Synth. Met.* **2012**, *162*, 1887−1893.
(279) Martinez Hardigree, J. F.; Katz, H. E. Through Thick and Thin: Tuning the Threshold Voltage in Organic Field-Effect Transistors. *Acc. Chem. Res.* **2014**, *47*, 1369−1377.
(280) Pernstich, K.; Haas, S.; Oberhoff, D.; Goldmann, C.; Gundlach, D.; Batlogg, B.; Rashid, A.; Schitter, G. Threshold Voltage Shift in Organic Field Effect Transistors by Dipole Monolayers on the Gate Insulator. *J. Appl. Phys.* **2004**, *96*, 6431−6438.
(281) Suemori, K.; Uemura, S.; Yoshida, M.; Hoshino, S.; Takada, N.; Kodzasa, T.; Kamata, T. Threshold Voltage Stability of Organic Field-Effect Transistors for Various Chemical Species in the Insulator Surface. *Appl. Phys. Lett.* **2007**, *91*, 2112.
(282) Salinas, M.; Jager, C. M.; Amin, A. Y.; Dral, P. O.; Meyer-Friedrichsen, T.; Hirsch, A.; Clark, T.; Halik, M. The Relationship Between Threshold Voltage and Dipolar Character of Self-Assembled Monolayers in Organic Thin-Film Transistors. *J. Am. Chem. Soc.* **2012**, *134*, 12648−12652.
(283) Jang, Y.; Cho, J. H.; Kim, D. H.; Park, Y. D.; Hwang, M.; Cho, K. Effects of the Permanent Dipoles of Self-Assembled Monolayer-Treated Insulator Surfaces on the Field-Effect Mobility of a Pentacene Thin-film Transistor. *Appl. Phys. Lett.* **2007**, *90*, 132104.
(284) Possanner, S. K.; Zojer, K.; Pacher, P.; Zojer, E.; Schürrer, F. Threshold Voltage Shifts in Organic Thin-Film Transistors Due to Self-Assembled Monolayers at the Dielectric Surface. *Adv. Funct. Mater.* **2009**, *19*, 958−967.
(285) Aghamohammadi, M.; Ro del, R.; Zschieschang, U.; Ocal, C.; Boschker, H.; Weitz, R. T.; Barrena, E.; Klauk, H. Threshold-Voltage Shifts in Organic Transistors Due to Self-Assembled Monolayers at the Dielectric: Evidence for Electronic Coupling and Dipolar Effects. *ACS Appl. Mater. Interfaces* **2015**, *7*, 22775−22785.
(286) Sze, S. M. *Physics of Semiconductor Devices*; Wiley: New York, 1981.
(287) Lim, E.; Jung, B.-J.; Chikamatsu, M.; Azumi, R.; Yoshida, Y.; Yase, K.; Do, L.-M.; Shim, H.-K. Doping Effect of Solution-Processed Thin-Film Transistors Based on Polyfluorene. *J. Mater. Chem.* **2007**, *17*, 1416−1420.
(288) Matsushima, T.; Adachi, C. Enhancing Hole Transports and Generating Hole Traps by Doping Organic Hole-Transport Layers with P-type Molecules of 2, 3, 5, 6-tetrafluoro-7, 7, 8, 8-tetracyanoquinodimethane. *Thin Solid Films* **2008**, *517*, 874−877.
(289) Lu, G.; Blakesley, J.; Himmelberger, S.; Pingel, P.; Frisch, J.; Lieberwirth, I.; Salzmann, I.; Oehzelt, M.; Di Pietro, R.; Salleo, A.; Koch, N.; Neher, D. Moderate Doping Leads to High Performance of Semiconductor/Insulator Polymer Blend Transistors. *Nat. Commun.* **2013**, *4*, 1588.
(290) Lüssem, B.; Kleemann, H.; Kasemann, D.; Ventsch, F.; Leo, K. Organic Junction Field-Effect Transistor. *Adv. Funct. Mater.* **2014**, *24*, 1011−1016.
(291) White, H. S.; Kittlesen, G. P.; Wrighton, M. S. Chemical Derivatization of an Array of Three Gold Microelectrodes with Polypyrrole: Fabrication of A Molecule-Based Transistor. *J. Am. Chem. Soc.* **1984**, *106*, 5375−5377.
(292) Bernards, D. A.; Malliaras, G. G. Steady-state and Transient Behavior of Organic Electrochemical Transistors. *Adv. Funct. Mater.* **2007**, *17*, 3538−3544.
(293) Khodagholy, D.; Rivnay, J.; Sessolo, M.; Gurfinkel, M.; Leleux, P.; Jimison, L. H.; Stavrinidou, E.; Herve, T.; Sanaur, S.; Owens, R. M.; Malliaras, G. High Transconductance Organic Electrochemical Transistors. *Nat. Commun.* **2013**, *4*, 2133.
(294) Malliaras, G. G. Organic Bioelectronics: A New Era for Organic Electronics. *Biochim. Biophys. Acta, Gen. Subj.* **2013**, *1830*, 4286−4287.
(295) Rivnay, J.; Owens, R. M.; Malliaras, G. G. The Rise of Organic Bioelectronics. *Chem. Mater.* **2014**, *26*, 679−685.
(296) Strakosas, X.; Bongo, M.; Owens, R. M. The Organic Electrochemical Transistor for Biological Applications. *J. Appl. Polym. Sci.* **2015**, *132*, 41735.

DOI: 10.1021/acs.chemrev.6b00329
Chem. Rev. 2016, 116, 13714−13751

Pictiva EX2009
Samsung v Pictiva
IPR2026-00129

(297) Kergoat, L.; Piro, B.; Berggren, M.; Horowitz, G.; Pham, M.-C. Advances in Organic Transistor-Based Biosensors: From Organic Electrochemical Transistors to Electrolyte-Gated Organic Field-Effect Transistors. *Anal. Bioanal. Chem.* **2012**, *402*, 1813−1826.
(298) Ates, M. A Review Study of (Bio) Sensor Systems Based on Conducting Polymers. *Mater. Sci. Eng., C* **2013**, *33*, 1853−1859.
(299) Sun, B.; Hong, W.; Thibau, E. S.; Aziz, H.; Lu, Z.-H.; Li, Y. Polyethylenimine (PEI) as an Effective Dopant to Conveniently Convert Ambipolar and P-type Polymers into Unipolar n-type Polymers. *ACS Appl. Mater. Interfaces* **2015**, *7*, 18662−18671.
(300) Lüssem, B.; Günther, A.; Fischer, A.; Kasemann, D.; Leo, K. Vertical Organic Transistors. *J. Phys.: Condens. Matter* **2015**, *27*, 443003.
(301) Lüssem, B.; Riede, M.; Leo, K. Doping of Organic Semiconductors. *Phys. Status Solidi A* **2013**, *210*, 9−43.

DOI: 10.1021/acs.chemrev.6b00329
Chem. Rev. 2016, 116, 13714−13751

Pictiva EX2009
Samsung v Pictiva
IPR2026-00129